

**PERIOCULAR REGION-BASED FACE RECOGNITION MODEL FOR IDENTIFYING MASKED
FACE**

**MOHD SAIF
LJMU MASTERS IN DATA SCIENCE**

Final Thesis Report

MARCH 2024

ABSTRACT

The most arising field of computer vision is facial recognition where the identification of existent has captured the interest of numerous scientists. For more than four decades the area of face recognition has surfaced as a wide metric for assessing human identification. Reliability of the being facial recognition systems still has a lot of challenges with respect to computer vision and pattern recognition irrespective of the colorful advancements made. The difficult part in recognizing faces occur mostly in scenarios like recognition of twins' face, different profile views of the face, having different accessories like beard, glasses, etc. The encircling environment conditions also plays a major part like light intensity, illumination condition, occlusion, etc. still, face recognition systems experience a decrease in accuracy when faces are partially obscured. Various scenarios involve partial coverage of the face, such as helmets, hair, glasses, or ski masks. In many instances, only the area around the eyes (periocular region) remains visible and can serve as a viable biometric identifier.

The primary goal of this study is to create a new and efficient framework for connecting people through the use of periocular biometric identification. Several periocular biometric discovery approaches were formerly developed earlier. But all the well-established approaches are not robust enough to handle variations in resolution, illuminated images, postures due to the inefficiency of hand-drafted texture descriptors, especially while working with periocular features. Therefore, periocular recognition still paves a way for a lot of exploration advancements in face recognition.

Table of Contents

ABSTRACT	2
LIST OF FIGURES	8
LIST OF TABLES	11
CHAPTER 1 INTRODUCTION	12
1.1 Background of the Study.....	13
1.2 Problem Statement	14
1.3 Aim and Objectives.....	15
1.4 Scope of the Study	16
1.5 Significance of the Study	16
1.6 Structure of the Study	17
CHAPTER 2 LITERATURE REVIEW	18
2.1 Introduction.....	18
2.2 Databases for Periocular Recognition Research	18
2.3 Segmentation of periocular image and preprocessing methods.....	19
2.4 Periocular Image Representation Methods	20
2.4.1 Global Periocular Features.....	20
2.4.1.1 Gabor Filters	20
2.4.1.2 Walsh Masks.....	21
2.4.1.3 Histogram of Gradients	21
2.4.1.4 GIST Descriptors	21
2.4.1.5 Phase Intensive Global Pattern.....	21
2.4.1.6 Laws' Masks	22
2.4.1.7 Local Phase Quantization.....	22
2.4.1.8 Force Field Transform	22
2.4.1.9 Discrete Wavelet Transform	22

2.4.1.10	Discrete Cosine Transform	22
2.4.1.11	Local Binary Patterns	23
2.4.1.12	Weber Local Descriptors.....	23
2.4.1.13	Local Color Histograms	23
2.4.1.14	Local Salient Patterns.....	23
2.4.1.15	Local Gradient Patterns	24
2.4.2	Local Periocular Features	24
2.4.2.1	Scale Invariant Feature	24
2.4.2.2	Speeded Up Robust Features	24
2.4.2.3	Symmetry Assessment.....	24
2.4.2.4	Binary Robust Invariant Scalable Key Points	24
2.4.2.5	Oriented FAST and Rotated BRIEF	25
2.4.2.6	Phase Intensive Local Pattern	25
2.5	Other Features for Periocular Recognition.....	25
2.6	Matching methods for periocular template matching.....	25
2.6.1	Distance Metrics	25
2.6.2	Other Classifiers	26
2.7	Convolutional Neural Networks, CNN-Based Periocular Recognition.....	26
2.8	Performance Indicators of Periocular Recognition Research	26
2.9	Summary	27
CHAPTER 3 RESEARCH METHODOLOGY	28
3.1	Introduction.....	28
3.2	Methodology	28
3.2.1	Data Selection	30
3.2.2	Data Pre-processing	30
3.2.3	Data Transformation	30
3.2.4	Algorithms & Techniques Description	32

3.2.4.1	An Analysis of Periocular Region Recognition	32
3.2.4.2	Extraction of neighbor gradient features based on region specificity and sub-image for resilient periocular recognition	32
3.2.4.3	Robust Periocular Recognition Using Modified Histogram of Gradient and Improved Accelerated KAZE.....	32
3.2.4.4	Training Strategy Using empirical multivariate mode and CNN for eye area Identification: An Ensemble Approach.	32
3.2.5	Evaluation	33
3.3	Logical flow of the system.....	33
3.4	Required Resources	34
3.4.1	Hardware requirements	34
3.4.2	Software requirements	34
3.5	Summary	35
	CHAPTER 4 ANALYSIS.....	36
4.1	Introduction.....	36
4.2	An Analysis of Periocular Region Recognition.....	37
4.2.1	Introduction.....	37
4.2.2	Proposed work	37
4.2.3	Deep Neural Network Algorithms	38
4.2.3.1	ReLU non-linearity	38
4.2.3.2	DeepIrisNet	38
4.2.3.3	FaceNet.....	39
4.2.3.4	Light CNN	39
4.2.3.5	Multimodal CNN.....	40
4.2.3.6	Deep CNN	41
4.2.3.7	RGB-OCLBCP	42
4.2.4	Result and analysis.....	44
4.2.4.1	Experiment No #1: Evaluation of UBIPr Databse	44
4.2.4.2	Experiment No #2: Evaluation of CASIA-Iris Dataset	45

4.2.4.3	Experiment No #3: Evaluation of AR	47
4.2.5	Conclusion	48
4.3	Extraction of sub-image based neighbor gradient features based on region specificity for robust periocular recognition	48
4.3.1	Introduction.....	48
4.3.2	Proposed Work	49
4.3.2.1	Pre-Processing	50
4.3.2.2	Corner of eye and eyebrow detection	51
4.3.2.3	Eyebrow Shape Feature Estimation	52
4.3.2.4	Segmentation of the fold of eye and corner of eye regions.....	53
4.3.2.5	HOG feature extraction	54
4.3.2.6	KAZE Feature Extraction.....	55
4.3.2.7	Feature matching	56
4.3.3	Result and analysis.....	56
4.3.3.1	Experimental images	56
4.3.3.2	Experimental results	57
4.3.3.3	Experimental results	60
4.3.4	Conclusion	64
4.4	Robust Periocular Recognition Using Modified Histogram of Gradient and Improved Accelerated KAZE.....	64
4.4.1	Introduction.....	65
4.4.2	Proposed Work	65
4.4.2.1	Pre-Processing	67
4.4.2.2	Improved HOG feature extraction.....	67
4.4.2.3	Improved Accelerated KAZE feature extraction.....	70
4.4.2.4	Feature Retrieval by Local Patterns of Gradient (LPOG)	72
4.4.3	Feature Retrieval by Local Patterns of Gradient (LPOG)	74
4.4.4	Result and analysis.....	75

4.4.4.1	Experimental Images	75
4.4.4.2	Experimental results	76
4.4.4.3	Experiment No #1: Performance Analysis of Classifiers.....	78
4.4.5	Conclusion	81
4.5	Training Strategy Using empirical multivariate mode and CNN for eye area Identification: An Ensemble Approach	82
4.5.1	Introduction.....	82
4.5.2	Proposed periocular recognition algorithm.....	83
4.5.3	Experimental Analysis	88
4.5.4	Conclusion	95
CHAPTER 5 RESULTS AND DISCUSSIONS		97
5.1	Introduction.....	97
5.2	Summary of proposed methodology	97
5.3	Experimental analysis	99
5.3.1	Analysis of Proposed Works.....	99
CHAPTER 6 CONCLUSIONS AND RECOMMENDATIONS		101
6.1	Introduction.....	101
6.2	Summary of the report	101
6.3	Discussion and conclusion.....	102
6.4	Strengths and Limitations	103
6.5	Future recommendations.....	103
REFERENCES.....		105
APPENDIX A : RESEARCH PROPOSAL.....		111

LIST OF FIGURES

Figure 1.1 General structure of biometric system	12
Figure 1.2 Major component of ocular region.....	13
Figure 1.3 Parts of periocular region	14
Figure 2.1 Example of periocular dataset	18
Figure 2.2 Phases of periocular biometric system	20
Figure 3.1 Periocular region of interest that was taken from a face image	30
Figure 3.2 General scales of human face image features	31
Figure 3.3 Flow diagram.....	34
Figure.4.1 Important Parts of Periocular Region Image.....	37
Figure.4.2 General Structure of Convolution Neural Network.....	38
Figure. 4.3 Preprocessing Stages of DeepIrisNet.....	38
Figure. 4.4 Common Flow Diagram of FaceNet.....	39
Figure.4.5 Diagram of Multimodel CNN.....	41
Figure.4.6 Detailed Diagram of Multimodel CNN Network.....	41
Figure 4.7 Flow Diagram of OCLBCP.....	43
Figure.4.8 dual-stream CNN's Flow Diagram.....	44
Figure.4.9 Rank-1 recognition rate comparison for UBIPr dataset.....	45
Figure.4.10 Rank-5 recognition rate comparison for UBIPr dataset.....	45
Figure.4.11 EER comparison for UBIPr dataset.....	45
Figure.4.12 ROC curve for UBIPr dataset.....	45
Figure.4.13 Rank-1 Recognition Rate Comparison For CASIAIris Dataset.....	46
Figure.4.14 Rank-5 Recognition Rate Comparison For CASIA-Iris Dataset.....	46
Figure.4.15 EER comparison for CASIA-Iris dataset.....	46
Figure.4.16 ROC curve for CASIA-Iris dataset.....	46
Figure.4.17 Rank-1 recognition rate comparison for AR dataset.....	47
Figure.4.18 Rank-5 recognition rate comparison for AR dataset.....	47
Figure.4.19 EER comparison for AR dataset.....	47
Figure.4.20 ROC curve for AR dataset.....	48
Figure.4.21 Features of Periocular Region Image.....	48
Figure.4.22 Procedure of Biometric Recognition System.....	49
Figure. 4.23 Proposed block diagram of periocular recognition.....	50
Figure.4.24 Process flow for unsharp mask filtering.....	51

Figure.4.25 Eye corner and eyebrow corner points are depicted	51
Figure.4.26 Illustration of shape of the eyebrow features.....	53
Figure.4.27 Segmentation Eye Fold and Eye Corner Region.....	53
Figure.4.28 Histogram Table of 9 bin.....	54
Figure.4.29 Diagram of HOG.....	55
Figure.4.30 Numerical Diagram of HOG.....	55
Figure. 4.31 Illustrative test images from various datasets	57
Figure. 4.32 Extraction of single eye periocular features.....	57
Figure.4.33 Extracting periocular features from the AR dataset	58
Figure. 4.34 The process of extracting periocular features	59
Figure. 4.35 Extracting periocular features from the dual eye	59
Figure.4.36 Comparison of the (ROC) curves	62
Figure. 4.37 Comparison of the Rank-1 recognition accuracy performance.....	64
Figure.4.38 Comparison of the Rank-5 recognition accuracy performance.....	64
Figure.4.39 Proposed block diagram for periocular recognition.....	66
Figure.4.40 Flow Diagram of Pre-processing.....	68
Figure.4.41 Structural Diagram of Improved HOG.....	69
Figure.4.42 Improved HOG Method's 3D Feature Extraction Process Diagram.....	72
Figure.4.43 Resultant Image	73
Figure.4.45 Examples of test images from various datasets.....	75
Figure.4.46 Extraction of periocular features from single-eye UBIPr dataset.....	76
Figure.4.47 Extraction of periocular features from the AR dataset	77
Figure.4.48 Feature extraction from the CASIA-Iris dataset	77
Figure. 4.49 Extracting features from the dual-eye periocular region in the UBIPr dataset.....	78
Figure.4.50 Comparison of rank-1 and rank-5 recognition accuracy performance.....	80
Figure.4.51 Comparison of rank-5 recognition accuracy performance.....	83
Figure.4.52 Few examples for periocular images.....	84
Figure.4.53 Schematic illustration of the suggested approach for periocular identification.....	85
Figure. 4.54 Illustration of DWT decomposition	87
Figure. 4.55 Training Ensemble Images in a Convolutional Neural Network.....	88
Figure. 4.56 Example images for testing from various collections.....	89
Figure.4.57 Experimental outcomes from the periocular recognition	90
Figure.4.58 Experimental findings from the periocular recognition system	92
Figure. 4.59 Experimental outcomes for the CASIA-Iris distance dataset	93

Figure. 4.60 Comparative graphical analysis	94
Figure. 4.61 Graphical comparison of rank-1 and rank-5 recognition.....	95
Figure. 4.63 Comparing the ROC curves for different datasets.....	96
Figure. 4.64 Graphical representation of testing time across varying values of K	97

LIST OF TABLES

Table4.1 Structural Diagram of The Light CNN-4.....	40
Table4.2 Detailed Layer Information of The Light CNN-4.....	40
Table 4.3 Layers Information of Multimodel Dataset.....	42
Table4.4 UBIPr dataset.....	44
Table4.5 CASIA-Iris dataset.....	46
Table4.6 AR dataset.....	47
Table4.7 Comparison of Equal Error Rate (EER) with conventional methods.....	60
Table 4.8 Comparison of Equal Error Rate (EER) with conventional.....	60
Table4.9 Comparison of Equal Error Rate (EER) with conventional methods.....	60
Table4.10 Comparison of AUC with the old method.....	61
Table4.11 Comparison of recognition accuracy metrics, including Rank-1 and Rank-5.....	63
Table4.12 Performance Evaluation of EER and AUC with the existing approaches.....	78
Table4.13 Comparison of recognition accuracy at Rank-1 and Rank-5 levels.....	79
Table4.14 Evaluation of area under curve and EER.....	81
Table4.15 Performance Evaluation of EER and AUC.....	90
Table 4.16 Contrasting the Equal Error Rate (EER) and Area under the Curve (AUC)	91
Table 4.17 Contrast in recognition accuracy across the UBIPr, AR, and CASIA-Iris datasets...	92
Table4.18 Rank-1 and Rank-5 recognition accuracy across varying numbers.....	95
Table4.19 Comparing time complexity for varying numbers of Intrinsic Mode Functions.....	99
Table 5.1 Comparison of EER and AUC with the traditional methods.....	99
Table 5.2 Comparison of Rank -1 and Rank-5 recognition accuracy.....	99

CHAPTER 1

INTRODUCTION

A person's distinctive physical and behavioral traits are measured and statistically analyzed in biometrics. The technology is mostly used to manage access and identify people who need to be watched, or it can be used to identify those who are being watched. The fundamental idea behind biometric authentication is that each individual can be reliably recognized by their inborn physical characteristics or behavioral characteristics (Alonso-Fernandez et al., 2020).

For several reasons, recognition-supported biometric features are preferred to traditional passwords and PIN-based procedures. In biometrics, recognition is verified by Fingerprints, retinal patterns, iris, hand geometry, vein patterns, voice passwords, and signature dynamics. A combination of both smart card and biometrics can be used to verify a user. The biometric scanner is used to read and scan biometric information of an individual through a smart card to determine whether the person is who they claim to be. This type of user validation is quick, exact, and very secure (Cascone, 2021).

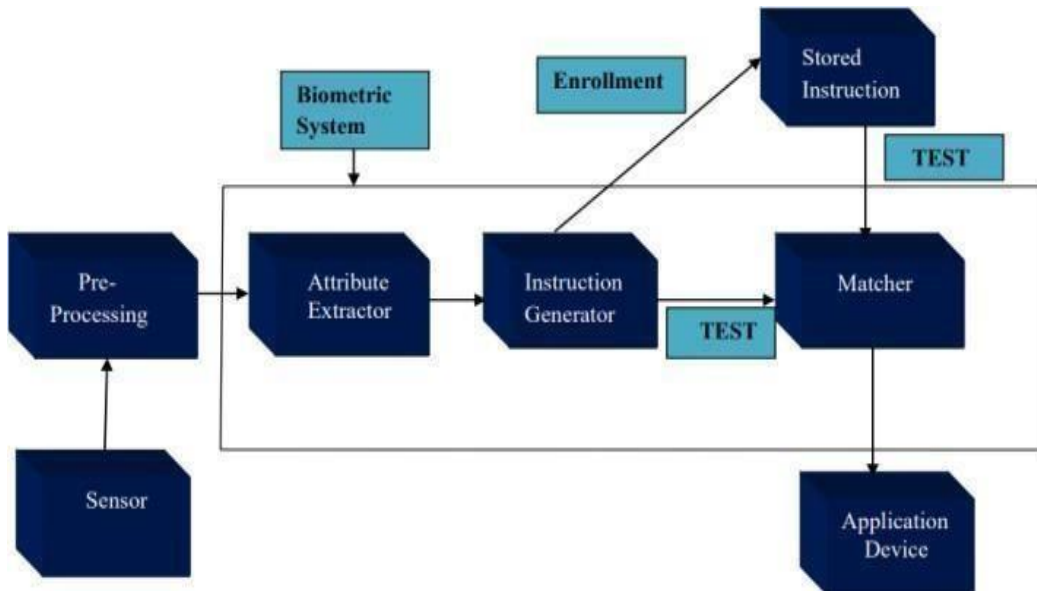


Figure. 1.1 General structure of biometric system

Without a doubt, the following factors can be utilized to recognize an individual's traits for biometrics:

- Absoluteness: Declare that each person must possess the qualities.
- Singleness refers to how well one can separate from another using biometrics.
- Collectability is the ability to add something to a calculation.
- Presentation - Discusses the accuracy, swiftness, and bravery of the technologies

deployed.

- The level of automated acceptance is called "correctness."
- A replacement's capability of use is the condition.
- Estimable - The object should be simple to gather the designated data quietly and should be appropriate for capture while we wait.
- Privacy - The procedure cannot infringe on the person's right to privacy.
- Unrepeatable by other means - the qualities must be unique.

1.1 Background of the Study

In face recognition biometrics with incomplete faces, automatically identifying people's identity is a difficult issue. Consequently, the goal of periocular recognition is to recognize a person based on characteristics that are taken from area encircling the eye. The area surrounded by top of the eyebrow, cheekbone, and nose midline is used for this periocular recognition. The periocular facial attribute comprises elements derived from the corners of the eyes, eyebrows, creases around the eyes, and the texture of the skin (Sujanthi et al., 2023).

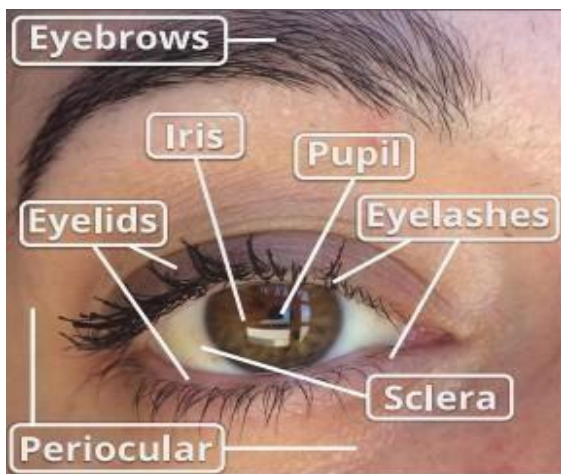


Figure. 1.2 Major component of ocular region

When faced with incomplete faces, that has hair, spectacles, a helmet, and a face mask on it, the face recognition system performs poorly. One of the periocular region's real-time applications is the recognition of offenders wearing masks on face in surveillance footage. Due to COVID-19 epidemic, wearing a face mask is now required. In situations like these, face recognition-based biometrics work poorly, necessitating the use of effective periocular-based biometric recognition. Expression variation also lowers the performance of facial biometrics. In contrast to the lower part of the face, the upper portion exhibits greater resilience to transitions. Periocular recognition proves more dependable than facial identification during expressions, as it encompasses a larger facial area. Ocular identification,

such as iris recognition, works well when faced with partial faces, but it necessitates intense eye focus. Unlike ocular biometrics, which require the camera to concentrate closely on the iris, retina, and sclera, periocular recognition does not require this (Almadan & Rattani, 2021). The proposed research contribution is as follows: (i) Hybrid approach for feature extraction that takes distinct features from various areas of the periocular facial picture. The goal of hybrid feature retrieval is to retrieve more crucial personality-differentiating descriptors. (ii) Utilizing a compatible feature extraction method to derive diverse area-based features from the periocular region can enhance the precision of periocular recognition. As a result, this technique employs several (region-specific) feature extraction algorithms depending on the periocular regions. (iii) The shape of the eyebrows plays a vital role, and recognition results can be obtained by extracting features related to the form along the upper and lower limits of the eyebrows, encompassing both width and height (Phillips & Karakaya, 2022). As a result, the three-layer structure predicted from the eyebrow regions is segmented into N points through the employed technique for extracting eyebrow shape features. The form variations throughout the N points are provided by this characteristic of the eyebrow. (iv) Study also suggests a SING feature extraction approach that can enhance recognition performance by being more resilient to rotation.

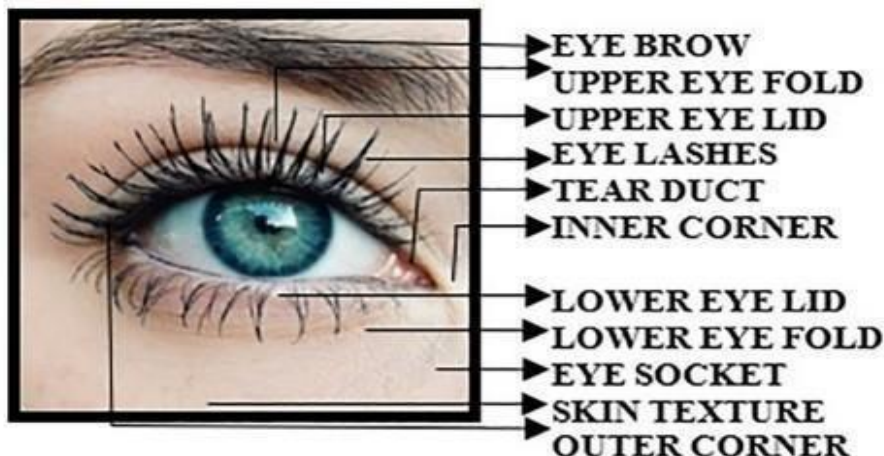


Figure. 1.3 Parts of periocular region

1.2 Problem Statement

The advent of face recognition technology has revolutionized various fields, but its effectiveness is compromised when faces are partially obscured, as is frequently the case in real-world scenarios such as surveillance footage, cultural practices, and the current widespread use of face masks due to the ongoing Covid-19 pandemic. In these situations, traditional face recognition(Ramachandra & Ramachandran, 2022) systems struggle to provide accurate

identification, prompting the need for alternative biometric identifiers. The periocular region, specifically the area around the eyes, emerges as a potential solution for reliable recognition in partially obscured face scenarios.

Despite the potential of periocular recognition, existing approaches face challenges in handling variations caused by factors like lighting conditions, pose changes, occlusions, and aesthetic alterations such as plastic surgery. Furthermore, the lack of databases and research focusing on periocular recognition in wild, uncontrolled environments poses a significant gap in the current literature. This research aims to bridge these gaps and proposes a comprehensive solution for periocular recognition in the wild(Cascone, 2021).

The primary objectives of this thesis are:

- Investigate and assess the complementarity between RGB periocular images and a novel texture-based retrieval method called SING for effective periocular detection in real-world scenarios.
- Introduce three distinct features (enhanced HOG, accelerated KAZE, and local gradient patterns) and employ a feature matching procedure to enhance recognition accuracy by combining RGB images and feature descriptors.
- Develop a new method for Eyebrow Shape Feature Estimation to improve the accuracy of periocular region recognition.
- Detect eyebrow and eye corner points in input face images to extract the periocular region for analysis.
- Propose a cumulative similarity score-based approach to match individuals based on periocular features.
- Perform an assessment to compare the suggested models by looking at their performance metrics to determine their efficiency.

1.3 Aim and Objectives

The initial aim of the thesis is to identify the most suitable machine learning technique for the recognition of periocular regions. The second aim of this thesis is to recognize a person with a periocular region using machine learning techniques.

Objectives:

- To implement a Sub image based neighbor gradient (SING) feature's extraction(Ramachandra & Ramachandran, 2022) for recognizing a person.
- To improve the recognition accuracy using improved HOG and accelerated KAZE

feature descriptor.

- To reduce the error rate by using a newly developed feature extraction technique.
- To develop a new method for Eyebrow Shape Feature Estimation that could make accurate recognition of the periocular region.
- To detect eyebrow and eye's corner point from input face images to extract the periocular region.
- To match the person based on features using a cumulative similarity score.
- To comparatively analyze the proposed models in terms of performance measures.

1.4 Scope of the Study

This thesis outlines its boundaries as follows:

- It is anticipated that the thesis will be finished 17 weeks after the research proposal has been submitted.
- The experimentation will take place utilizing freely available software and models.
- Feature Extraction Methods: Evaluate and enhance the performance of feature extraction methods such as KAZE, HOG, and SING in capturing diverse characteristics of periocular regions. Specifically, focus on the unique challenges posed by eyebrows, eye corners, and top eye fold region.

Scalability and Robustness: Investigate the scalability of the algorithm to handle a variety of periocular images and its robustness to factors like variations in expression, lighting conditions, and partial occlusions.

1.5 Significance of the Study

The significance of the proposed research is as follows:

- The proposed feature descriptor considers intensity variations in eight directions and can, therefore, detect the significant shapes clearly.
- In face images given that periocular region is visually different from non- periocular region, the proposed segmentation approach is most suitable to identify the difference between those regions.
- Ambiguous pixels in periocular region points are cleverly handled by the proposed feature extraction method.
- The proposed texture feature extraction technique possesses rotational and illumination

invariance properties.

1.6 Structure of the Study

This interim thesis is structured into three chapters.

In **Chapter 1**, an introductory overview of the research problem is presented. Following a concise introduction, the chapter delves into the topic's background, offering insights into prior research on the subject.

Chapter 2 offers an in-depth analysis of existing literature on human identification and recognition through periocular characteristics. The techniques used to extract the features for periocular recognition are also introduced, as well as the literature related to machine learning and implementations of deep learning in the periocular biometric system.

In **Chapter 3**, the methodology employed in this research is elucidated. Section 3.1 initiates with an introduction to the overarching theme, model, and metrics utilized for evaluation. Expanding on this, Section 3.2 delves deeply into the subject, with Section 3.1.1 presenting thorough details on the datasets, fields, and amount of data used. The following section provides a concise summary of the pre-processing techniques applied to the data prior to its incorporation into the model. Furthermore, Sub-section 3.2.3 provides a detailed description of the architecture of the employed recognition technique. The subsequent two sub-sections explain on the methods and metrics adopted to achieve each predefined aim and evaluate fairness using these metrics. The summary of our procedural steps is encapsulated in Section 3.4.

CHAPTER 2

LITERATURE REVIEW

2.1 Introduction

Periocular recognition has been the subject of numerous studies, with positive and encouraging outcomes and growing interest. Even in unrestricted situations, periocular biometrics has been used successfully for soft biometrics analyses such as gender and ethnicity classification. The application of periocular biometric systems and recognition techniques on diverse datasets is covered in detail in this section as well (Zabin & Bourlai, 2020).

2.2 Databases for Periocular Recognition Research

The CSIP (Cross-Sensor Iris and Periocular) database contains 2,004 images from various capturing conditions using different smartphones. Meanwhile, the UBIPr (UBI periocular recognition) database holds 10,950 images that are unconstrained, including 522 images focusing on the periocular area, showcasing variances in pose, scale, lighting, and other aspects. The FOCS (Face and Ocular Challenge Series) database provides access to 9,581 photos from 136 people, featuring varying levels of light and obstructions (Barcellos & Gonzaga, 2022).

In addition, the IMP (Multispectral Periocular) database offers imagery across three spectrums, encompassing detailed iris scans and images suitable for night vision. The BATH database specializes in grayscale NIR (Near-Infrared) photographs. The CASIA database (IRISv3-Lamp version) includes 16,212 NIR images captured under various lighting settings. Lastly, the UBIRIS database, created by the University of Beira, is available in two versions: the first focusing on the visible spectrum and the second on unconstrained imagery (Kirchgasser et al., 2020).

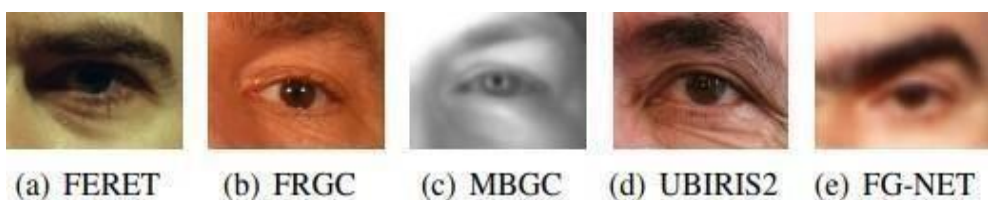


Figure. 2.1 Example of periocular dataset

The FERETv4 database by NIST includes 14,126 visible spectrum photos with diverse expressions and orientations. The Mobile Iris Challenge Evaluation (MICHE) database features annotated samples from smartphones, and CASIA 3D FV1 integrates 3D facial

models with 2D color photos. The FRGC (Face Recognition Grand Challenge) database comprises 44,278 high-resolution photos of faces within the visible spectrum. (Toledo Ferraz et al., 2021). The v2 of the Multiple Biometrics Grand Challenge (MBGC) features a collection of visible spectrum photographs and NIR (Near-Infrared) video sequences, documenting a variety of lighting conditions, obstructions, and instances of motion blur. The CMU Hyperspectral (CMU-H) database holds 764 films across 65 spectral bands. The ND 2004–2005 iris dataset presents 64,980 images of 356 individuals' irises, and the BioSec database includes 3,200 infrared iris images. (Agrawal et al., 2021).

The MobBIO dataset showcases 1,680 iris images taken in the visible spectrum, while the Photos of Groups (IoG) database captures 28,231 faces in natural settings. The Cross-Spectral Iris/Periocular Dataset (Cross-Eyed DB) features a compilation of 5,600 photographs aimed at supporting research in periocular and iris recognition. Lastly, the Visible Light Mobile Ocular Biometric (VISOB) dataset is made up of 77,942 images for validation and 80,194 for enrollment, all captured under a variety of lighting conditions. (Wang et al., 2022).

2.3 Segmentation of periocular image and preprocessing methods

In many studies focusing on biometrics within uncontrolled settings, it is essential to first separate the periocular area from the entire facial region. There are primarily two techniques for segmentation: manual and automatic. Several scholars rely on the database-provided actual eye center coordinates to segment the periocular area manually. Alternatively, the periocular zone can be detected or segmented automatically using three commonly employed approaches in academic writings. Initially, a facial recognition algorithm such as the Viola-Jones (VJ) method is applied to locate the face, where the accuracy of this detector significantly influences the success of specific recognition tasks. The second approach focuses on detecting the eye within the image, pinpointing features like the iris, pupil, or eye corners (Ambika et al., 2020). Similarly, canny edge detection, morphological techniques, and the Harris corner detection method have shown success in identifying eye corners. The iris segmentation method, which determines the periocular area based on the iris's position, represents the third strategy. To locate the eye center, correlation filters are used. Gabor filters and convolutions with 1D filters tailored to identify circular symmetries could also be used to detect eyes. Last but not least, sub face parts like the sclera, eyebrow, or VJ sub-part detectors could be used to identify the periocular region (Boutros, Damer, Raja, et al., 2020c). Using the Local Eyebrow Active Shape Model (LE-ASM) and graph based separation, the eyebrow may be identified immediately from a facial image. After iris segmentation, the sclera region was found using the HSV/YCbCr color spaces (Ogawa & Kameyama, 2021).



Figure. 2.2 Phases of periocular biometric system

Following the segmentation of the iris, the sclera area was identified utilizing the HSV and YCbCr color models. A common preliminary step involves dividing the region of periocular into smaller sections, arranged in rows and columns, to facilitate the examination of global features; this can take various configurations such as 6x8, 7x5, among others. The process includes cropping, padding, and resizing images to specified dimensions like 100x160 [18], 128x168 [3], 49x19 [8], 20x30 [6], and 32x49 [40]. This is accompanied by adjustments in grayscale and color balance, including the conversion between color spaces. Techniques are applied to normalize or equalize the histogram. An automated process is employed to exclude low-quality images from the dataset based on global or mean intensity thresholds. Furthermore, any rotational discrepancies are corrected by aligning the images horizontally, focusing on the eyes' centers or corners.

Photometric normalization or illumination variance correction (Rot et al., 2020). To smooth out the fluctuation among local pixel intensities, Gaussian blurring is used and short line edges in images, such as eyelashes, can be removed using morphological procedures or 1D rank filters (Khellat-Kihel et al., 2022).

2.4 Periocular Image Representation Methods

Global features and local characteristics can be used to categorize the features used for periocular recognition. The local method initially identifies significant points within the image, known as key spots, while the global method focuses on capturing features that describe the whole region of interest (ROI) and conducts an overall analysis of the image. Following a local examination of these critical points, the characteristics of the adjacent pixels are deduced. Other feature extraction techniques that do not fit into either of these two categories are covered in a different section of this article.

2.4.1 Global Periocular Features

2.4.1.1 Gabor Filters

Gabor filters are key in analyzing textures as they identify distinct frequencies and directions within images. For tasks involving a variety of frequencies and directions, scholars have applied a combination of five frequency channels and six orientations spaced evenly. This is

sampled at every section point near the center of eye, and these sampled grid results are combined to create a feature vector. Gabor filters with four scales and eight orientations to create the spatial envelope for their normalized image, emphasizing the effectiveness of Gabor filters in texture representation and differentiation (Kumari & R, 2020).

2.4.1.2 Walsh Masks

Walsh masks, constructed with +1 and -1 elements, function as convolution filters to detect local image features like contrast. These filters, organized in $N^2 \times N$ sets, encapsulate the discrete Walsh function pairs ($N=3,5,7,9$, etc.). Employed for age-invariant periocular biometrics and for periocular identification, these masks approximate the Walsh-Hadamard transform in capturing distinctive image characteristics (Lohith et al., 2023).

2.4.1.3 Histogram of Gradients

The Histogram of Oriented Gradients (HOG) is a technique for detecting objects based on their appearance, which depends on the distribution of direction gradients and intensity levels in images. This method splits the image into several grid cells and calculates the direction and strength of gradients for each pixel in those cells, subsequently assembling these calculations into histograms. In studies, HOG outperformed other descriptors, providing optimal results with a 7×6 cell grid. Moreover, it was utilized by various researchers and Halmstad University competitors in the Cross-Eyed 2017 competition (P. Kaur & Kumar, 2023).

2.4.1.4 GIST Descriptors

The five GIST descriptors, encompassing naturalness, roughness, ruggedness, openness, and expansion, serve to represent images in a compact form for scene identification. Image convolution with filters of N Gabor of varying dimension and arrangement generates feature maps, which are then aggregated to form a feature vector. Notably, GIST descriptors exhibit superior computational efficiency and performance advantages. In a related study a score-level fusion of local circular LBP and global GIST (1536 length) was employed (Reddy & Derakhshani, 2020).

2.4.1.5 Phase Intensive Global Pattern

The Phase Intensive Global Pattern (PIGP) technique enhances periocular recognition by convolving an image with kernels at four different phase-tilt angles to capture variations in intensity among neighboring pixels. This method effectively captures nuanced intensity changes for improved recognition (Prasanth et al., 2023).

2.4.1.6 Laws' Masks

Laws' energy filters consist of a collection of 2D kernels, created from five vectors that each contain five elements. By applying these kernels to an image through convolution, it becomes possible to extract various textural characteristics, including spots, levels, ripples, edges, and waves. (Rao et al., 2022).

2.4.1.7 Local Phase Quantization

Local phase quantization (LPQ) is a method designed for effective texture classification that proves particularly resilient against centrally symmetric blurs, such as those caused by motion, out-of-focus, or atmospheric disturbances. This technique uses the spectrum obtained from the discrete Fourier transform (DFT) of an image. By calculating the four low-frequency coefficients from both the real and imaginary parts of the DFT, an 8-bit binary LPQ code is created through their concatenation. This process is performed over the image using a 2-D DFT applied within an NxN window kernel (where N can be 3, 5, etc.). The collection of these LPQ codes from each pixel forms a histogram, a method notably applied in the Cross-Eyed2017 contest by the Indian Institute of Technology (IIT) Indore. (Tripathi & Jalal, 2022).

2.4.1.8 Force Field Transform

The Force Field Transform (FFT) treats image pixels as a particle array, akin to the gravitational force's inverse square law. It calculates the total force on a unit-intensity pixel at a given position, summing forces from surrounding pixels. This resultant force, viewed as a vector based on intensity and position, serves as a powerful noise reduction method in image processing. Conducted experiments leveraging this transformative approach (Mon et al., 2020).

2.4.1.9 Discrete Wavelet Transform

Utilizing the Haar wavelet through a non-continuous single-level 2D Discrete Wavelet Transform (DWT), this method extracts features from data by decomposing approximation coefficients into four components. These components represent both the next level's approximation and specific details in vertical, horizontal, and diagonal orientations, serving as distinctive features (Han et al., 2021).

2.4.1.10 Discrete Cosine Transform

Applying a 2D mask of size NxN (where N is an odd number) to an image using the discrete cosine transform (DCT) yields N^2 coefficients that amalgamate vertical and horizontal frequencies. The linear blending of these coefficients with the original mask produces features

representing the image. In few research, DCT was employed for classifying soft biometric data, specifically focusing on the periocular area and Local Binary Pattern (LBP) characteristics (Vitek et al., 2020).

2.4.1.11 Local Binary Patterns

Local Binary Patterns (LBP) are effective for texture classification, discerning edges, corners, and other patterns by considering a pixel's 3x3 neighborhood. This involves encoding the binary values of a pixel's eight neighbors based on intensity comparisons with the reference pixel, resulting in an 8-bit string. With 256 potential values, these strings are quantized into an 8-bin histogram for a region of interest. Variations like Circular LBP (CLBP) consider neighbors up to distance R, while Uniform LBP (ULBP) reduces values to 59 by assigning unique labels to uniform patterns. Local Ternary Pattern (LTP) uses three coding values to lower sensitivity to noise, and Median Binary Pattern employs thresholding against median values for noise resistance. Various studies utilize LBP, while CLBP and other variants, like MB-TLBP with bicubic interpolation, are employed in different contexts (Nascimeno & Souza, 2023).

2.4.1.12 Weber Local Descriptors

Derived from the theory of human perception, Weber's local descriptor (WLD) is inspired by the relationship between perception and the size or intensity of the initial input and its change. The Weber constant, representing the ratio of changed intensity to initial intensity, is a key element in WLD, serving as an indicator of intensity change concerning a central pixel and gradient orientation. Many researchers have employed WLD in their work (da Silva et al., 2020).

2.4.1.13 Local Color Histograms

The Local Color Histogram (LCH) represents color distribution in an image by discretizing color dimensions into bins and counting pixels within each range. LCH is applicable to subsets of an image, while Global Color Histogram (GCH) considers the entire image. Woodard et al found the RG color space with a 4x4 bin configuration yielded optimal results. Ahmed et al converted RGB images to HSI for 2D color histogram computation, while LOSIB, refines the LBP concept by calculating mean absolute differences between a reference pixel and its 8 neighbors using a 3x3 window for local oriented statistical content (Tripathi & Jalal, 2021).

2.4.1.14 Local Salient Patterns

Local Salient Patterns (LSP), akin to LBP, extract features by taking into account the largest absolute discrepancy between the central pixel and its eight surrounding pixels in a 3x3 grid, aiming to mitigate the influence of noise (Saad Shakeel & Lam, 2022).

2.4.1.15 Local Gradient Patterns

Local Gradient Patterns (LGP), akin to LBP, derive features based on gradient information instead of pixel values for enhanced texture analysis (Umer et al., 2023).

2.4.2 Local Periocular Features

Identifying highlighted image areas and tagging key points involves algorithms for local information extraction. Through local analysis of these key sites, properties in the surrounding pixels are then reconstructed (Seha et al., 2021).

2.4.2.1 Scale Invariant Feature

Utilizing a Difference of Gaussian (DoG) function across distinct scales and octaves, Scale Invariant Feature Transformation (SIFT) identifies critical image locations invariant to scaling, translation, and rotation. Extracted points' coordinates, scale, and orientation form their representation, normalized through an affine transformation. Adaptive thresholding is iteratively applied to limit key points to a maximum of 200, generating descriptors for key points. (Kumari & Seeja, 2020).

2.4.2.2 Speeded Up Robust Features

Speeded Up Robust Features (SURF) employs the Hessian matrix to detect key locations in an input image, creating an axis-aligned box and applying an affine transformation. Features are then extracted from a 4x4 sub-region using Haar wavelet responses. In a comparative study, SURF and PILP were evaluated, with SURF. (Shao et al., 2021).

2.4.2.3 Symmetry Assessment

Symmetry Assessment by Feature Expansion (SAFE) identifies key locations in an image and assesses the presence of symmetric curves in their vicinity, utilizing harmonic functions for feature expansion. The neighborhoods surrounding key points are described within concentric circles of varying radii using these highly symmetric curve functions. Periocular recognition, employing SAFE, was applied in and by participants from Halmstad University in the Cross-Eyed2017 competition (Y. W. Lee et al., 2022).

2.4.2.4 Binary Robust Invariant Scalable Key Points

BRISK, a descriptor, is formed by concatenating results from various bright tests performed on

a pattern of 60 evenly spaced points around key locations on concentric rings. Achieving rotation invariance involves rotating the sample pattern relative to the gradient angle at its origin. Intensity comparisons between short-distance pixel pairs in the pattern generate a 512-bit feature vector for each key point, applied in periocular recognition (Zanlorensi et al., 2020).

2.4.2.5 Oriented FAST and Rotated BRIEF

To address BRIEF's vulnerability to rotation, Oriented FAST and Rotated BRIEF (ORB) enhances feature retrieval by integrating BRIEF with the FAST corner detector. Initially, first-order moments identify the dominant rotation of the key point, guiding the subsequent orientation of the BRIEF descriptor (Liu et al., 2022).

2.4.2.6 Phase Intensive Local Pattern

Phase Intensive Local Pattern (PILP) identifies crucial locations in an image by convolving it with filters of varying sizes (3x3, 5x5, 7x7, and 9x9) at four phase-tilt angles. Extrema detection is performed on the resulting four filtered images per kernel, and the feature vector is constructed by concatenating the gradient orientation histograms generated for each key point (Vyas et al., 2020).

2.5 Other Features for Periocular Recognition

Researchers have explored various periocular features beyond global and local characteristics, including facial marks like freckles, scars, and moles. Derived from triangular mesh analysis, to obtain periocular Eigen spectrum for biometric purposes. Additionally, eyelid shape descriptors, integrated with Local Binary Patterns (LBP), were explored, incorporating features like accumulated curvature and Elliptical Fourier Descriptors (EFD) for periocular recognition (Boutros, Damer, Fang, et al., 2020).

2.6 Matching methods for periocular template matching

Periocular biometrics employ diverse distance metrics like Euclidean, X2, and Chi-square distances for matching feature vectors. Common classifiers, broadly categorized as Distance metrics, CNN, and others, include SVM, K-NN, Bagging, ANN, CNN, Bayesian Networks, etc., facilitating effective classification and matching processes (Y. Chen et al., 2023).

2.6.1 Distance Metrics

During the matching phase in periocular biometrics, various distance metrics were employed. X2 distance for concatenated feature vectors, used it to match GIST and CLBP features, combining results through the weighted sum rule. Euclidean distance was applied for

classifiers, including HOG and LBP features. Verification involved computing Euclidean distance between shape descriptors, with positive authentication determined by falling within a specified threshold. Woodard found city block distance and Bhattacharya coefficient performed best for LBP and color histograms, respectively, and used Hamming and Chi-Square distances for iris and periocular matching, with fused results using experimentally determined weights (Wazirali & Ahmed, 2022).

2.6.2 Other Classifiers

The Support Vector Machine (SVM) maximizes sample classification accuracy by identifying the optimal hyperplane. SVM for recognition and gender classification using brow features, and used it for gender classification based on periocular features and applied SVM for gender and ethnicity classification. Other methods included Joint Bayesian, with a single hidden layer, and used a two-hidden-layer ANN for periocular recognition (Morris et al., 2022).

2.7 Convolutional Neural Networks, CNN-Based Periocular Recognition

Recent advancements in periocular recognition involve the adoption of end-to-end Convolutional Neural Network (CNN) frameworks with diverse architectures. CNN with both primary and branch structures for classification, incorporating gender and eye location information. In their latest work, they focused on the eyebrow and eye region using an attention-based CNN with multiple-glance structure and an attention mechanism CNN (AttNet). Combining two CNN models for verification, integrating periocular and iris characteristics through a fusion of features obtained from different layers and methodologies, including transfer learning and Root SIFT feature descriptors (K. M, 2021).

2.8 Performance Indicators of Periocular Recognition Research

Research on periocular-based recognition has shown promising results, particularly when combined with other modalities. The accuracy varies across datasets, with impressive F-Measure accuracy of 99.4% on the MBGC database for eyebrow segmentation. Recognizing gender on the MBGC and FRGC databases achieved 96% and 97% accuracy, respectively. Various descriptors like GIST, CLBP, and PILP were employed, yielding recognition rates ranging from 54.30% to 91.07%. Convolutional Neural Networks (CNNs) proved effective, achieving verification accuracies of up to 98.90%. Attention-based CNNs on multiple databases produced low Equal Error Rates (EERs), and a hybrid CNN model demonstrated excellent performance with an AUROC of 0.986 and an EER of 0.053. Overall, periocular recognition, when combined with diverse techniques, exhibits high accuracy across different

datasets (M. B. Lee et al., 2021).

2.9 Summary

Periocular recognition techniques are gaining attention as an effective standalone method and a complement to face and iris recognition, especially in challenging situations. This field, though in its early stages, exhibits promise and is expected to attract continued research interest. Various segmentation techniques using eye centers, corners, and brows have been explored, along with descriptors and classification methods, showcasing remarkable performance accuracies. Fusion of multiple feature descriptors is a common trend, contributing to enhanced recognition. Despite the potential for development, some periocular characteristics, such as eyelash features and tear duct texture, remain understudied. Future research aims to incorporate these characteristics for improved age estimation and classification. Stable eye corners offer potential for more precise periocular segmentation, benefiting mobile-based recognition systems. Research emphasis on reliable descriptors, classifiers, and low-computation-cost fusion algorithms is crucial for on-the-go subject recognition. Additionally, the creation of diverse image databases reflecting real-world scenarios with various sensors will facilitate further advancements.

CHAPTER 3

RESEARCH METHODOLOGY

3.1 Introduction

A typical identification method for a periocular region consists of the following steps: obtaining an image, pre-processing it, matching two feature sets, localizing the ROI, extracting the feature, and post-processing the extracted feature. During the acquisition stage, a sensor or camera records the periocular image. Benchmark datasets are also utilized by the periocular recognition system in other cases (Agrawal & Christopher, 2020).

3.2 Methodology

In the initial investigation, the suggested algorithm for periocular recognition was assessed utilizing the UBIPr, AR, and CASIA-Iris distance datasets. Enhancing an image's aesthetic appeal is the goal of the following step in the preprocessing procedure. Pre-processing techniques are often employed to normalize lighting variations. In our work, we use the unsharp mask filtering algorithm for this. After the pre-processing phase is finished, the localization process is applied. The periocular region is extracted in the localization step using the acquired or previously processed picture. Within our research, the periocular area is subdivided into four segments: the eyebrow region, eye side areas, top and down eye fold sections, and points corresponding to the left and right corners of the eyes (Behera & Puhan, 2023).

After extracting all the points required to identify the periocular region, the characteristics are derived. In the feature extraction stage, robust and distinctive attributes are derived from the delimited periocular area. The feature extraction procedures employ a combination of global and local approaches. Unlike global features, which are derived from the entire image or the region of interest (ROI), local features are specifically acquired from distinct areas known as key points. Our task is to extract the feature, not the complete image, from the key derived points. Thus, we used methods for extracting local features. From a range of existing local extraction strategies, including Histogram of Oriented Gradients (HOG) and KAZE, we select two approaches. Either of these two approaches is employed by HOG to extract the color features from the key spots. KAZE is used to derive the form properties from the key points. An approach for extraction of feature: Sub-image-based Neighbor gradient (SING). Texture features can be extracted using a variety of techniques, such as Wavelet, Local Binary Pattern (LBP), and Local Ternary Pattern (LTP) (Ramaraj, 2021).

However, because handcrafted texture descriptors are too rigid and insufficient to accurately capture periocular properties, the methods are less robust against "in wild" variables including resolution, illuminating degrees, postures, and occlusion. Consequently, it remains challenging to identify periocular in the field. To solve this issue, a unique texture feature extraction technique was presented in this paper. A neighbor gradient based on sub-images (SING) is what this is called. Then, using the extracted traits, it matches the algorithm for identity. The cumulative similarity score method is used to achieve it (Boutros, Damer, Raja, et al., 2020a).

The second proposed study establishes three features extraction techniques to retrieve the feature of color, design, and texture. In the first stage, HOG is used to extract the color feature. However, HOG's computation time is lengthy when attempting to locate objects in large-scale images since it uses a sliding window technique to extract attributes from each pixel of an image. This is why the accuracy is not particularly reliable when the input image is blurry. It computes slowly and produces low accuracy numbers as a result. To fix this issue, the second piece of work creates an updated HOG algorithm. Furthermore, an enhanced KAZE methodology takes the place of the first KAZE algorithm. The better version of the AKAZE-algorithm (SRP) is proposed in the second publication, using SIFT descriptors, and it is based on sparse random projection. Proposed approach maintains SIFT descriptor stability and the high feature detection efficiency advantage of the AKAZE algorithm. Furthermore, elevated dimensionality of the SIFT descriptor; nevertheless, the SRP approach considerably reduces the computational cost caused by this limitation(Boutros, Damer, Raja, et al., 2020b).

The SING approach is also replaced in the second work with the Local Patterns of Gradient (LPOG) approach. The SING operator's exhibit three drawbacks: firstly, they generate relatively lengthy histograms, causing delays in identification, particularly with extensive face databases; secondly, they may overlook local structures due to their disregard for the center pixel's impact; and thirdly, they yield noisy binary data. To address these issues, we suggest employing the LPOG operator. The LPOG operator offers the following benefits: firstly, it significantly reduces histogram dimensionality by comparing pairs of neighbors in the operator; secondly, it takes into account and assigns the highest weight to the central pixel point; thirdly, it reduces the impact of occlusion on facial images by altering the sign function of the current SING operator. Rather of employing a cumulative similarity score, an ensemble training strategy is proposed in the third paper. For periocular recognition in this work, a convolutional neural network and FA-MVEMD were employed. To increase the detection accuracy, a deep learning classifier was employed in this study (Srivika et al., 2023).

3.2.1 Data Selection

This work makes use of three datasets:

- UBIPr: A variation of the UBIRIS.v2 set, called UBIPr, has images trimmed to cover a larger area of the ocular region than the original UBIRIS.v2 data. It works very well for periocular recognition trials.
- CASIA-Iris-Distance: The dataset originates from the Institute of Automation at the Chinese Academy of Sciences. The image region of interest encompasses dual eye iris and face patterns due to the high-resolution camera used to capture iris images in CASIA-Iris-Distance. Additionally, the fusion of multi-modal biometric information enables the observation of detailed facial characteristics, such as skin patterns.
- AR Dataset: The AR Face Database contains over 3000 mug shots of 130 individuals exhibiting various facial expressions.

3.2.2 Data Pre-processing

Preprocessing steps involve grayscale and color correction, color space conversion, histogram normalization or equivalence, and Low-quality images are automatically filtered out through the use of global or mean intensity thresholding techniques. To correct for rotation, images are aligned horizontally based on the position of the eyes' centers or corners. Additionally, variations in lighting are addressed through photometric normalization. (Lionnie et al., 2022). Finally, Gaussian blurring is employed to smooth out fluctuations among local pixel intensities, and morphological procedures or 1D rank filters can remove short line edges like eyelashes.

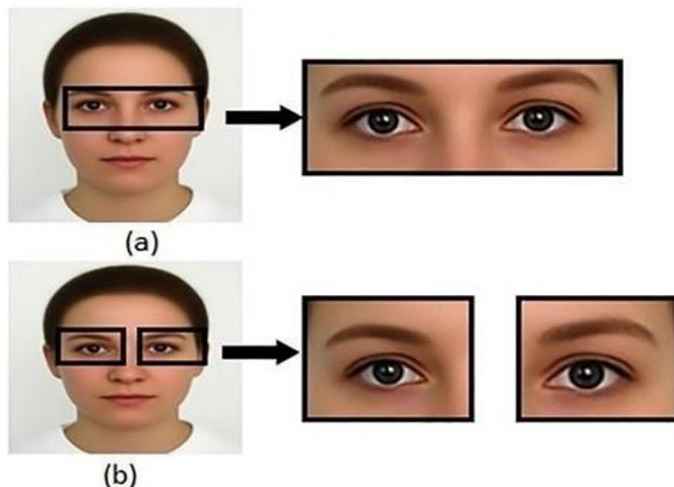


Figure. 3.1 Periocular region of interest that was taken from a face image

3.2.3 Data Transformation

The effectiveness of our proposed approach relies significantly on the careful curation and transformation of the diverse datasets employed in this study (Hernandez V et al., 2022). The AR Dataset, CASIA-Iris-Distance and UBIPr(Ramachandra & Ramachandran, 2022), each possess distinct characteristics that set them apart, when harnessed appropriately, contribute to the robustness and generalization of our periocular recognition system.

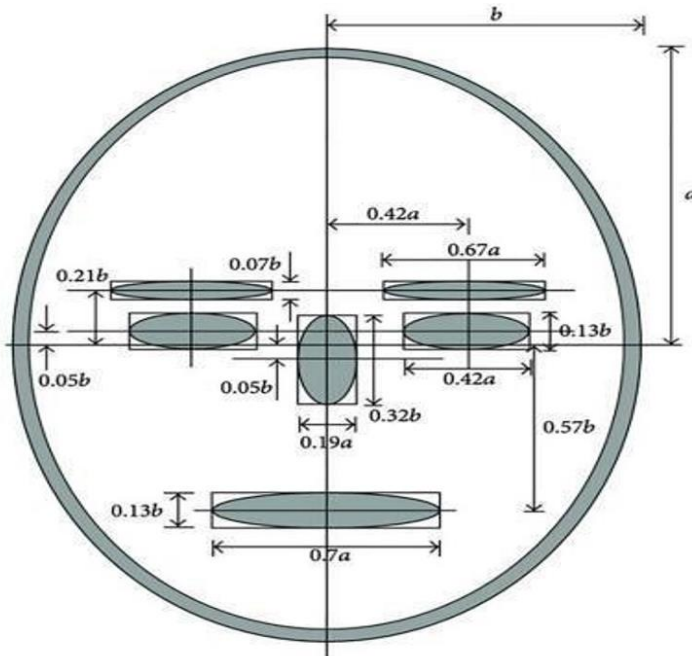


Figure 3.2 General scales of human face image features

The UBIPr dataset, a refined version of the UBIRIS.v2 set, is tailored for periocular recognition trials. To enhance its utility, we employ image trimming techniques, focusing on expanding the coverage of the ocular region compared to the original UBIRIS.v2 data. In pursuit of enhancing periocular feature extraction, a strategic refinement has been implemented to optimize the dataset. The CASIA-Iris-Distance dataset offers high-resolution images that encompass both dual eye iris and facial patterns. By capitalizing on the strengths of this dataset, we execute preprocessing procedures, including grayscale and color correction, conversion of color spaces, and histogram normalization. The fusion of multi-modal biometric information facilitates detailed observation of facial characteristics, such as skin patterns, contributing to a comprehensive periocular recognition framework (B. Kaur, 2023). Comprising over 3000 mug shots of 130 individuals displaying diverse facial expressions, the AR Face Database offers a rich source of facial data. During data pre-processing, we apply techniques such as rotation correction, photometric normalization, and Gaussian blurring to address various challenges. Correction of rotation achieves horizontal alignment by utilizing the centers or corners of the eyes, while photometric normalization mitigates illumination

variance (Hernandez-Diaz et al., 2020).

3.2.4 Algorithms & Techniques Description

3.2.4.1 An Analysis of Periocular Region Recognition

This study assesses the effectiveness of seven varied periocular recognition approaches, including ReLU non-linearity, Deep-Iris-Net, Face-Net, Light CNN, Multimodal CNN, Deep CNN, and RGB-OCLBCP. These methodologies are tested on three distinct image datasets, namely CASIA-Iris, UBIPr and AR. The comparison of these approaches reveals that, depending on the real-world application for which a system is designed, each algorithm exhibits its benefits and drawbacks in different ways. From this deep evaluation of their performance, we found that the RGB-OCLBCP technique gives many promising outcomes when compared with other techniques (Boutros et al., 2022).

3.2.4.2 Extraction of neighbor gradient features based on region specificity and sub-image for resilient periocular recognition

A periocular recognition approach is implemented to capture periocular features from four distinct regions: the brow, upper and lower eye folds, and eye corners. Conventional HOG and KAZE featuring retrieving techniques are applied to the eyebrows, top eye folds, and eye sidelines areas to retrieve feature. Facilitating the retrieval of eyebrow size involves estimating height and width features along(Ramachandra & Ramachandran, 2022) both the top and bottom boundaries of the eyebrows. (Ramachandra & Ramachandran, 2022).

3.2.4.3 Robust Periocular Recognition Using Modified Histogram of Gradient and Improved Accelerated KAZE

An approach to periocular recognition gathers data from four distinct regions, encompassing the eyebrow, top and down eye folds, and the eye corner. Employing enhanced accelerated KAZE feature extraction techniques and updated HOG feature retrieval methods, features are retrieved from the brow, upper eye lid, and eye sideline regions. Extraction of eyebrow features involves predicting breadth and height characteristics along both the up and down boundaries of the eyebrows (Ramachandra & Ramachandran, 2022).

3.2.4.4 Training Strategy Using empirical multivariate mode and CNN for eye area Identification: An Ensemble Approach

The approach to enhance a CNN classifier's performance involves producing $K+2$ unique ensemble images from a singular periocular picture. This technique broadens the dataset by generating additional, varied images from each original one, providing a richer training set for the classifier. Initially, the image is subjected to a Discrete Wavelet Transform (DWT) which splits it into four frequency bands: low-low (LL), low-high (LH), high-low (HL), and high-high

(HH). The LL band is further processed using the FA-MVEMD method, resulting in K -level Intrinsic Mode Functions (IMFs) along with a residual component. These K -level IMFs, the residual, and the HH band from the DWT are then utilized to form the ensemble images. These images are subsequently used to train the CNN model.

3.2.5 Evaluation

The evaluation will be achieved using metrics such as rank-2, rank-1, AUC, and EER for dataset UBPIr, AR, and CASIA-Iris datasets.

The proposed metrics for evaluation are:

- Equal error rate (EER) - The Error Equal Rate is a point on the Receiver Operating Characteristic (ROC) curve where the false acceptance rate (FAR) is equal's to the false rejection rate (FRR).
- Area Under the Curve (AUC) - The region below the ROC Curve quantifies the overall performances of a binary classification model across various decision thresholds.
- Rank-1 Recognition Accuracy – Rank-1 accuracy measures the percentage of cases where the correct match is ranked first among all possible matches.
- Rank-5 Recognition Accuracy – Rank-5 accuracy is similar to Rank-1, but it considers whether the correct match is present within the top 5 ranked choices.

3.3 Logical flow of the system

The algorithm employs a novel approach of area specific and the sub image based neighbor gradient(Ramachandra & Ramachandran, 2022) features retrieval to enhance identification accuracy. It begins by segmenting the periocular region into 4 sub-region: eyebrows, eye-corner regions, top and bottom eye fold region. Different feature extraction algorithms, such as KAZE for upper eye fold and HOG for eyebrow and eye corner regions, are utilized to capture diverse characteristics (Ipe & Thomas, 2021).

Additionally, the algorithm estimate size of eyebrows by analyzing distances from N point on eyebrows regions to eye-side mid-point. This eyebrow shape and size feature includes breadth and length measure, providing valuable information for effective recognition. Proposing a sub-image-based neighbor's gradient (SING) feature retrieval method to enhance robustness against rotation. Subsequently, the extracted features are trained using a Naïve Bayes classifier (Ramachandra & Ramachandran, 2022).

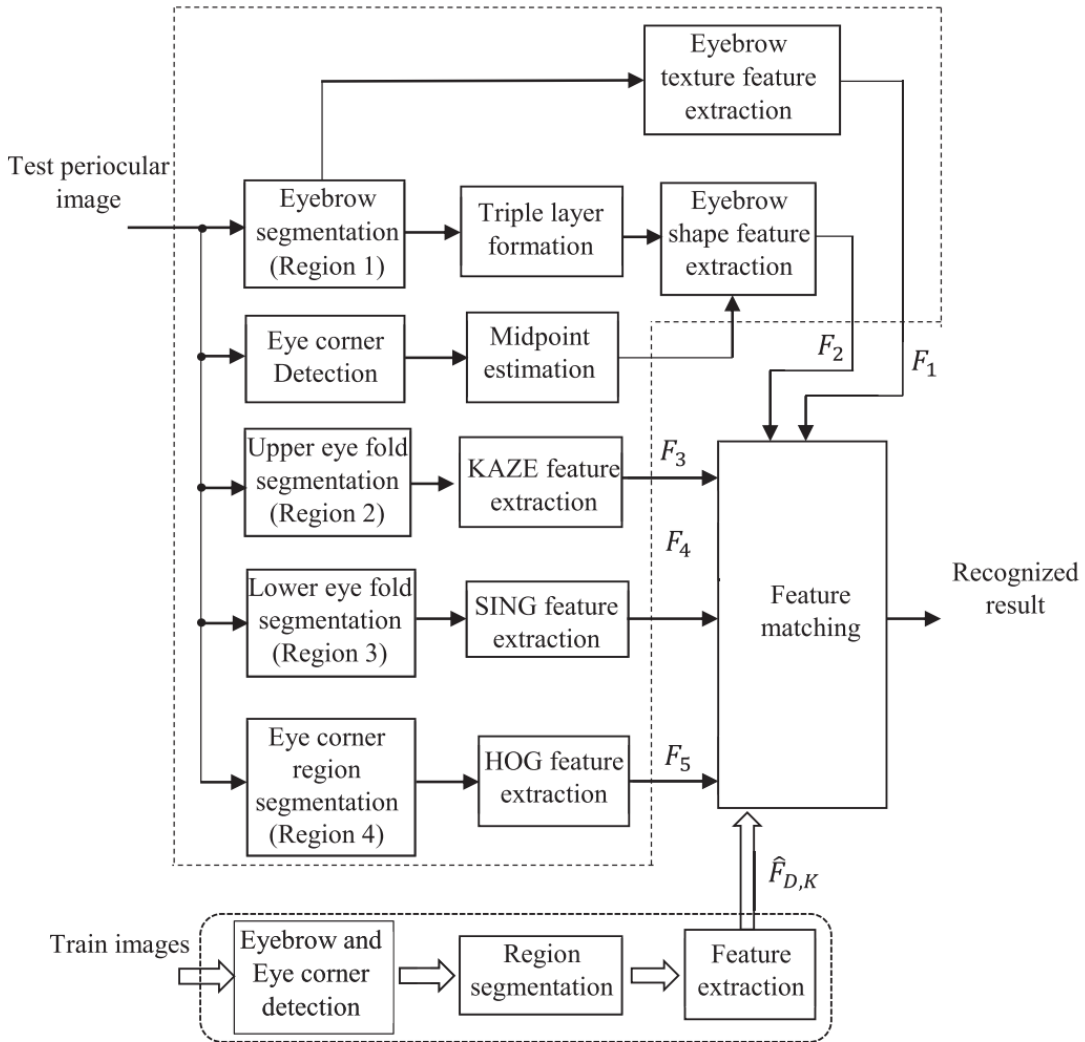


Figure 3.3 Flow diagram

3.4 Required Resources

3.4.1 Hardware requirements

For the successful completion of this research, certain hardware prerequisites need to be satisfied:

- A laptop or desktop computer equipped with internet connectivity, capable of browsing, document creation, and code compilation/execution is essential for this research.
- RAM (Random Access Memory): A minimum of 16GB RAM is recommended.

3.4.2 Software requirements

For the successful completion of this research, certain software prerequisites need to be satisfied:

- Web-browser

- Coding IDE Python 3.7+
- PIL (Pillow)
- Deep Learning libraries such as TensorFlow, PyTorch and Keras (which can be integrated with TensorFlow)
- Libraries required: Pandas, Numpy, OpenCV, etc.

3.5 Summary

This segment begins by introducing the technique for identifying the periocular region in section 3.1. Following this, in section 3.2, we present our datasets, offer a comprehensive overview of them, and detail the data we intend to use. The subsequent sections delve into the steps for preprocessing the data and provide a detailed architectural overview of the recognition model employed. Section 3.3 outlines the system's logical progression. In section 3.4, we enumerate the tools necessary for our research, concluding with a summary of our methodology in section 3.5.

CHAPTER 4

ANALYSIS

4.1 Introduction

In our comprehensive study on periocular recognition systems, we delve into the intricacies of identifying individuals through the unique characteristics of the periocular region. Our investigation begins with the crucial step of image acquisition, utilizing both high-resolution sensors and benchmark datasets like CASIA-Iris distance, UBIPr and the AR(Ramachandra & Ramachandran, 2022) to evaluate the efficacy of our proposed algorithms. We advance through the stages of pre-processing, employing techniques like unsharp mask filtering to enhance image quality and normalization to address variations in illumination. The pivotal localization process then identifies specific regions around the eyes, segmenting the area into detailed sub-regions for further analysis. Our research meticulously explores the extraction of distinctive features, focusing on local feature extraction methods like Histogram of Oriented Gradients (HOG) and KAZE for capturing color and shape details, respectively.

Additionally, we introduce a novel texture feature extraction method, Sub-image-based Neighbor Gradient (SING), to overcome the limitations of traditional handcrafted descriptors in varying environmental conditions. Through the advancement of algorithms and the incorporation of ensemble training methods and deep learning classifiers, our study aims to significantly enhance the accuracy and efficiency of periocular recognition systems, offering promising improvements for real-world applications.

Algorithms & Techniques used for analysis:

- An Analysis of Periocular Region Recognition.
- Extraction of sub-image based neighbor gradient features based on region specificity for robust periocular recognition.
- Robust Periocular Recognition Using Modified Histogram of Gradient and Improved Accelerated KAZE.
- Training Strategy Using empirical multivariate mode and CNN for eye area Identification: An Ensemble Approach.

4.2 An Analysis of Periocular Region Recognition

4.2.1 Introduction

Periocular biometrics is an emerging field in personal identification technology, focusing on the unique features surrounding the human eye, including the eyebrows, eyelids, sclera, skin texture, and blood vessels. This method has gained prominence due to its ability to offer reliable identification even in challenging conditions, such as when the face is partially obscured or in poor lighting. Periocular recognition systems measure various attributes like eyebrow shape, eyelash density, and the structure of blood vessels, providing a non-invasive and efficient alternative to traditional biometric systems like facial and iris recognition. Its resilience against occlusion and minimal requirement for user cooperation make it particularly suited for security applications in access control and financial systems.

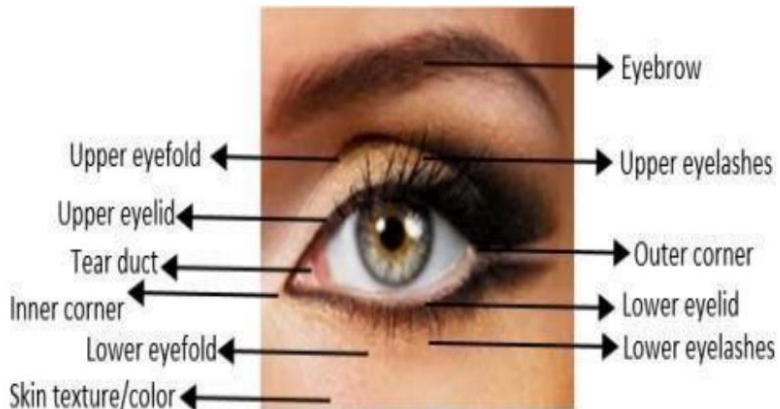


Figure. 4.1 Important Parts of Periocular Region Image

This technology leverages existing facial or iris images, eliminating the need for specialized equipment or extensive user interaction. With its potential for integration with other biometric modalities for enhanced accuracy, periocular biometrics represents a significant advancement in the field of secure personal identification.

4.2.2 Proposed work

Deep learning, especially Convolutional Neural Networks (CNNs), has significantly advanced periocular recognition by learning feature representations directly from data, surpassing traditional methods based on human assumptions. Proenca et al. enhanced feature learning with a four-layer CNN, focusing on crucial image areas, while Zhao et al. proposed emphasizing vital regions with higher weights for improved recognition accuracy. This approach has shown positive outcomes in periocular biometrics, even though challenges like scale, translation,

rotation, and lighting variations remain. The integration of a second neural network to learn cross-spectral variability represents an innovative step towards addressing these challenges, expanding the utility of periocular biometrics in real-world applications.

4.2.3 Deep Neural Network Algorithms

4.2.3.1 ReLu non-linearity

Figure below provides a summary of our network's architecture. It has eight learned layers: three fully linked and five convolutional.

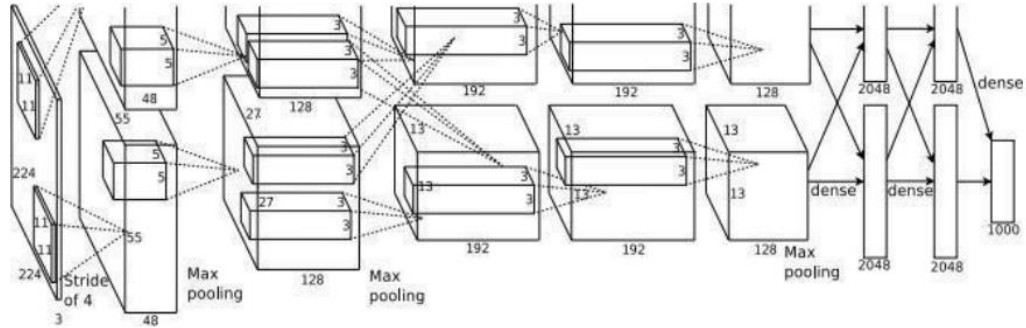


Figure 4.2 General Structure of Convolution Neural Network

The net is composed of eight weighted layers,: five convolutional followed by three fully connected layers, leading to a 1000-class softmax output for classification. It employs a multinomial logistic regression goal, optimizing by averaging log probabilities of correct labels. Convolutional layers are connected based on specific GPU kernel mappings, with unique couplings in the third layer to enhance feature learning. Response-normalization and max-pooling layers are strategically placed to improve signal clarity and reduce dimensionality, while ReLU non-linearity is applied across all layers for activation.

4.2.3.2 DeepIrisNet

DeepIrisNet-A and DeepIrisNet-B are CNN architectures for iris recognition, with the former using traditional convolutional layers followed by batch normalization and pooling, and the latter incorporating inception layers. DeepIrisNet-A has eight convolutional layers, while DeepIrisNet-B stacks five convolutional layers before adding two inception layers, both using 3x3 convolution kernels and 5x5 filters in specific layers.

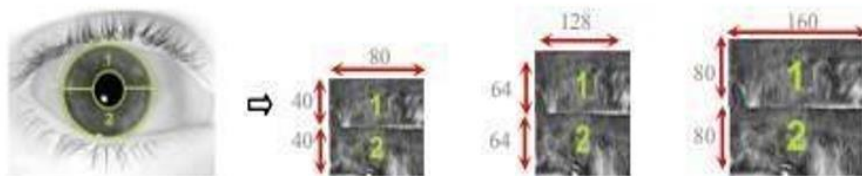


Figure. 4.3 Preprocessing Stages of DeepIrisNet

Max-pooling with a stride of 2 over a 2x2 window is used in both networks, which also share a fully connected layer configuration and employ the ReLU activation function. Training uses SGD with a momentum of 0.9, without data augmentation, on a 128x128 gray iris image from the ND-0405 database, selecting the model with the lowest validation error for testing, where the softmax layer is removed.

4.2.3.3 FaceNet

FaceNet employs a deep convolutional network and triplet loss to distinguish faces by projecting similar identities close together while keeping distinct identities apart in the embedding space.

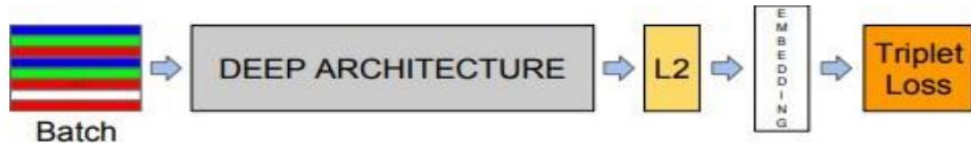


Figure 4.4 Common Flow Diagram of FaceNet

It uses Stochastic Gradient Descent (SGD), AdaGrad, and a margin value of 0.2 for training. The network architectures vary, with one having 22 layers and 1.6 billion FLOPS, and the other based on the Inception models with up to 5 billion FLOPS. To accommodate mobile devices, models like NNS1 and NNS2 have been optimized for reduced depth and computational requirements. The largest network, NN2, and its variants, focus on balancing input size and computational efficiency without compromising accuracy, specifically by omitting 5x5 convolutions in smaller models.

4.2.3.4 Light CNN

The MFM function in CNN serves a similar purpose to local feature selection in biometrics by choosing the best feature at each place learned by various filters. Back propagation causes a binary gradient (1 or 0) to activate or inhibit a neuron, similar to the famous ordinal measure in biometrics. These findings show MFM's ability to perform feature selection and create sparse connections, which are valuable qualities.

Table 4.1 Structural Diagram of The Light CNN-4

Type	Filter Size /Stride	Output Size	#Params
Conv1	$9 \times 9/1$	$120 \times 120 \times 96$	7.7K
MFM1	-	$120 \times 120 \times 48$	-
Pool1	$2 \times 2/2$	$60 \times 60 \times 48$	-
Conv2	$5 \times 5/1$	$56 \times 56 \times 192$	230.4K
MFM2	-	$56 \times 56 \times 96$	-
Pool2	$2 \times 2/2$	$28 \times 28 \times 96$	-
Conv3	$5 \times 5/1$	$24 \times 24 \times 256$	614K
MFM3	-	$24 \times 24 \times 128$	-
Pool3	$2 \times 2/2$	$12 \times 12 \times 128$	-
Conv4	$4 \times 4/1$	$9 \times 9 \times 384$	786K
MFM4	-	$9 \times 9 \times 192$	-
Pool4	$2 \times 2/2$	$5 \times 5 \times 192$	-
fc1	-	512	2,457K
MFM_fc1	-	256	-
Total	-	-	4,095K

This section covers three architectures for our Light CNN framework. The first architecture uses four convolution layers with maximum feature map operations and four maximum pooling layers, similar to Alexnet, with approximately 4,095K parameters and 1.5G FLOPS.

Table 4.2 Detailed Layer Information of The Light CNN-4

Type	Filter Size /Stride, Pad	Output Size	#Params
Conv1	$5 \times 5/1, 2$	$128 \times 128 \times 96$	2.4K
MFM1	-	$128 \times 128 \times 48$	-
Pool1	$2 \times 2/2$	$64 \times 64 \times 48$	-
Conv2a	$1 \times 1/1$	$64 \times 64 \times 96$	4.6K
MFM2a	-	$64 \times 64 \times 48$	-
Conv2	$3 \times 3/1, 1$	$64 \times 64 \times 192$	165K
MFM2	-	$64 \times 64 \times 96$	-
Pool2	$2 \times 2/2$	$32 \times 32 \times 96$	-
Conv3a	$1 \times 1/1$	$32 \times 32 \times 192$	18K
MFM3a	-	$32 \times 32 \times 96$	-
Conv3	$3 \times 3/1, 1$	$32 \times 32 \times 384$	331K
MFM3	-	$32 \times 32 \times 192$	-
Pool3	$2 \times 2/2$	$16 \times 16 \times 192$	-
Conv4a	$1 \times 1/1$	$16 \times 16 \times 384$	73K
MFM4a	-	$16 \times 16 \times 192$	-
Conv4	$3 \times 3/1, 1$	$16 \times 16 \times 256$	442K
MFM4	-	$16 \times 16 \times 128$	-
Conv5a	$1 \times 1/1$	$16 \times 16 \times 256$	32K
MFM5a	-	$16 \times 16 \times 128$	-
Conv5	$3 \times 3/1, 1$	$16 \times 16 \times 256$	294K
MFM5	-	$16 \times 16 \times 128$	-
Pool4	$2 \times 2/2$	$8 \times 8 \times 128$	-
fc1	-	512	4,194K
MFM_fc1	-	256	-
Total	-	-	5,556K

We incorporate Network in Network (NIN) and a small convolution kernel size into the network using MFM, making this model faster and deeper than the Light CNN-4, with a total of 1G FLOPS and around 5,556K parameters.

4.2.3.5 Multimodal CNN

This suggested multimodal architecture consists of a shared representation layer and several CNN-based modalities-dedicated networks that are jointly optimized. A combined model is educated to investigate and enforce dependence across various modalities.

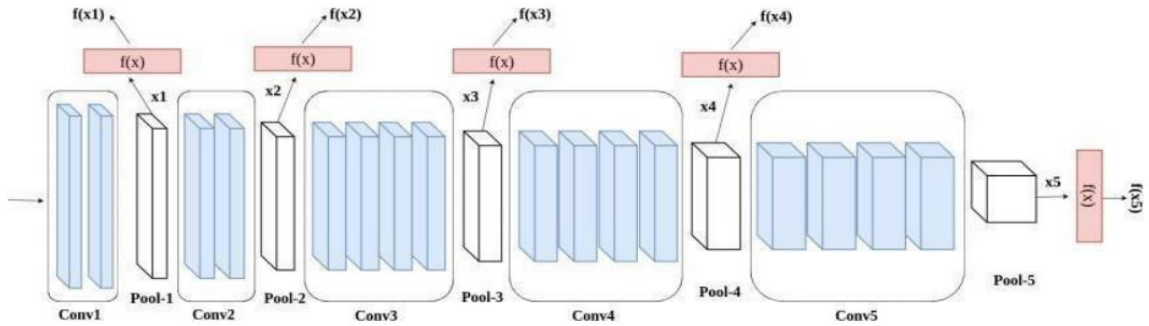


Figure. 4.5 Diagram of Multimodel CNN

In the CNN architecture, the input is represented by layers, each representing a different abstract feature representation, with deeper levels providing more abstract and complicated features. General illustration of this strategy, with deep and shallow level feature maps contributing to the classification method.

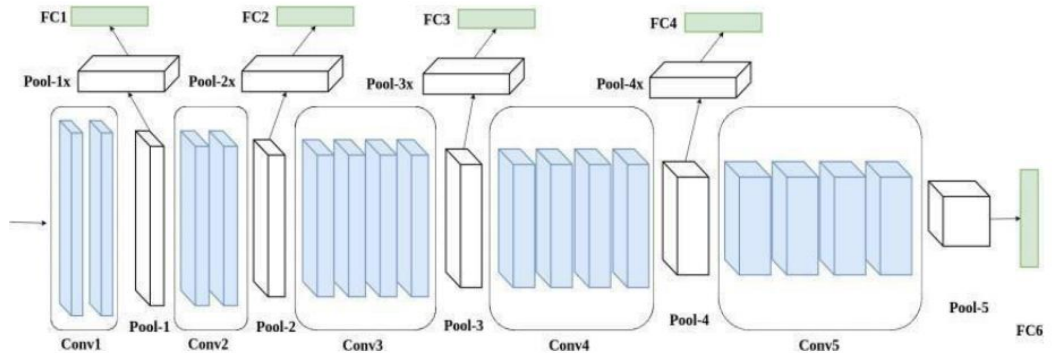


Figure. 4.6 Detailed Diagram of Multimodel CNN Network

In this study, we concentrate on the first scenario, as shown in Figure 4.6. Different levels of abstraction from each modality are used in the proposed multi-stream CNN to help in decision-making. One example of a multistream multimodal CNN architecture is shown in Table 4.1, where each modality is represented by both feature maps in the decision-making approach. Layers Structure of Deep CNN. For this application, the typical VGG19 networks are impractical because of the enormous number of parameters that must be trained, making it almost impossible to optimize all of the networks that are specific to each modality at the same time as the joint representation. Layers Information of Different Dataset Large feature dimensionality and resource constraints lead to a variety of training phase complications that call for solutions. Consequently, the fully connected layer's (FC6) number of kernels is 1024 instead of the usual VGG19.

4.2.3.6 Deep CNN

The Quality in Face and Iris Research Ensemble (Q-FIRE) dataset presents face and iris movies taken at various distances and quality levels—from 5 to 25 feet. It includes 195 participants

across two visits. This dataset primarily serves as a benchmark for assessing face and iris recognition algorithms in suboptimal conditions. It compares multimodal datasets similar to it and doubles the number of face images for subjects wearing glasses, resulting in 20 photos with and without spectacles. The background for face photos is adjusted using a grey color with 18% reflectivity.

TABLE 4.3 Layers Information of Multimodel Dataset

Dataset	Number of Subjects	Number of Sessions	Modalities	Data Type
XM2VTS [4]	295	4	Face, Voice	Video Audio
BiosecurID [13]	400	4	Face, Iris, Fingerprint, Voice, Hand, Hand Writing, Signature, Keystroke	Image Audio
BioSec [14]	250	2	Face, Iris, Voice	Image Audio
BIOMET [15]	91	3	Face, Fingerprint, Voice, Hand, Signature	Image, Audio
MCYT [16]	330	2	Fingerprint, Hand Writing	Image

The dataset compares an unconstrained set with a constrained set from a commercially available system, showcasing a range of high- to low-quality videos selected according to established standards. Each of the two sessions per participant includes 28 face videos and 27 iris videos, totaling about 16 terabytes per session. Videos were recorded at five distances: 5, 7, 11, 15, and 25 feet, with six seconds of footage at approximately 25 frames per second, capturing motion blur and variations in illumination to assess contrast concurrently for face and iris.

4.2.3.7 RGB-OCLBCP

The Orthogonal Combination—Local Binary Coded Pattern (OCLBCP) is a new color-based texture descriptor.

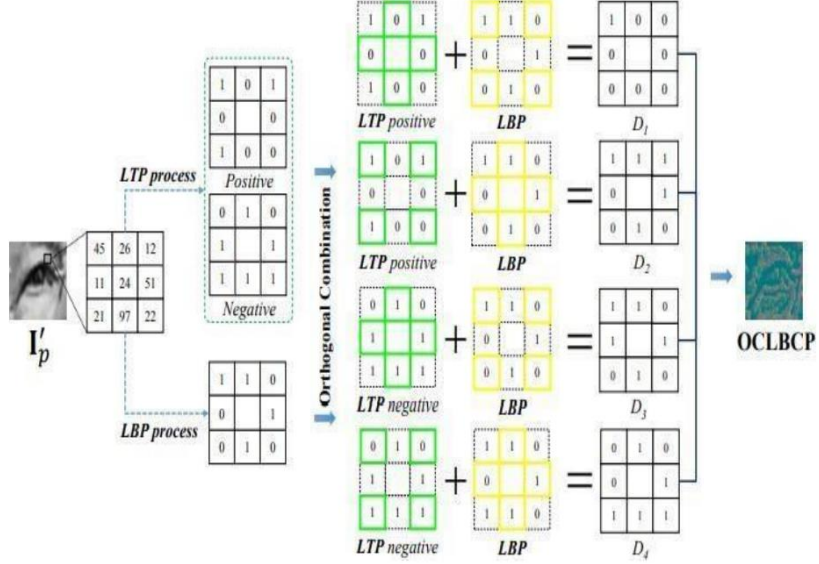


Figure.4.7 Flow Diagram of OCLBCP

It is derived from an image processed through inverse Fourier transform and analyzed using Local Binary Patterns (LBP) and Local Ternary Patterns (LTP) for summarizing local image structures. The OCLBCP descriptor divides the image into 3×3 submatrices, binarizes them based on a central threshold value, and categorizes them into four orthogonal groups (D_1, D_2, D_3, D_4). A dual-stream Convolutional Neural Network (CNN) utilizes both RGB periocular images and OCLBCP descriptors for ocular recognition, combining them through feature fusion layers for enhanced feature extraction.

Algorithm 1 provides a summary of the OCLBCP generation procedure.

Algorithm 1 Creating colour-based texture description OCLBCP.

Input: $I_p \in \mathbb{R}^{x \times y}$

Output: OCLBCP

- 1: Perform preprocessing to I_p and obtain the filtered image I'_p
 - 2: Construct LBP and LTP process on I'_p
 - 3: Perform Equation (1) with the LBP, LTP positive and LTP negative matrices to obtain θ
 - 4: Construct distance pattern matrix Δ using Equation (2)
 - 5: Generate the colour-based pattern matrix M with δ by using Equations (3) and (4)
 - 6: Map θ with M to generate OCLBCP
-

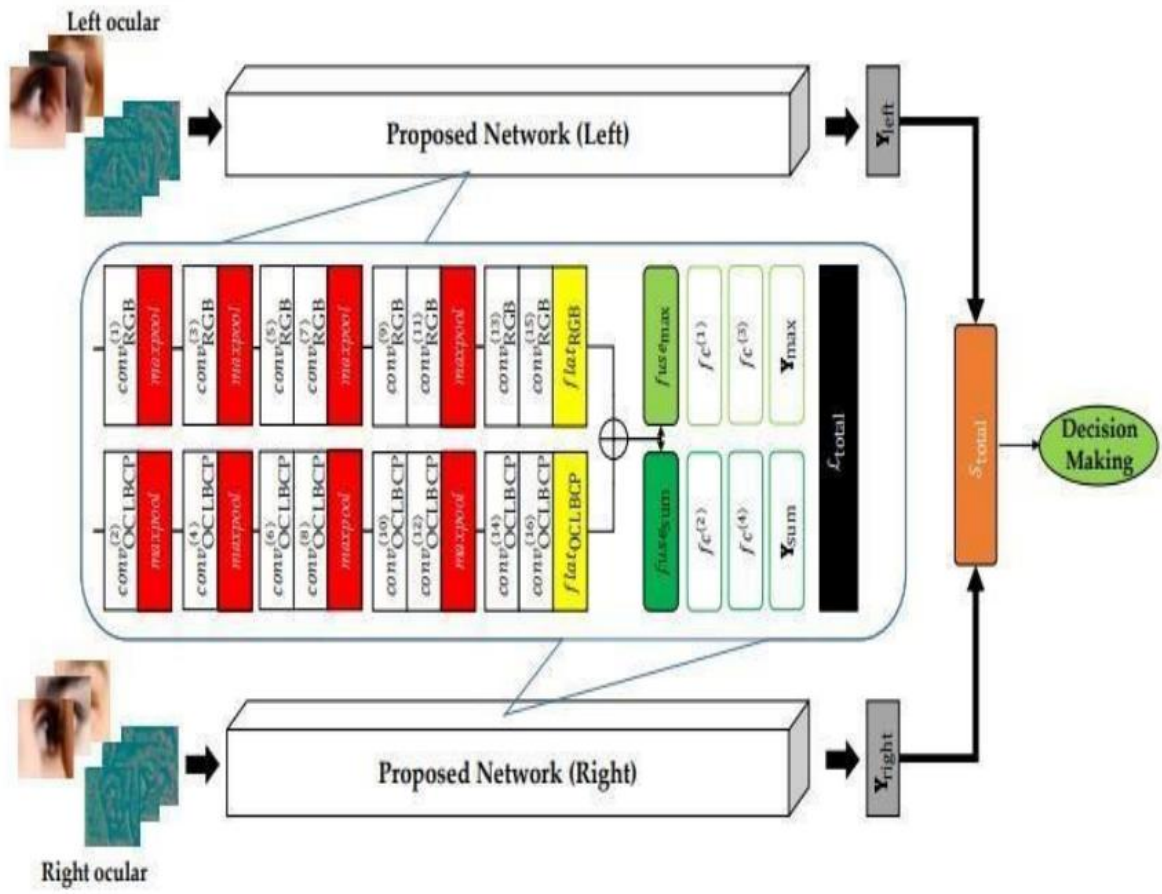


Figure 4.8 dual-stream CNN's Flow Diagram

This network architecture includes 16 convolutional layers and 8 max-pooling layers, designed to capture and correlate features from both input streams for accurate recognition.

4.2.4 RESULT AND ANALYSIS

4.2.4.1 Experiment No #1: Evaluation of UBIPr Dataset

Table 4.4 UBIPr dataset

Schemes/Methods	Rank-1 recognition rate (%)	Rank-5 recognition rate (%)	EER (%)
Method 1	84.88	96.01	7.11
Method 2	90.3	97.41	5.07
Method 3	90.24	97.36	5.46
Method 4	90.28	97.18	6.34
Method 5	90.75	97.44	4.09
Method 6	90.24	97.09	4.38
Method 7	91.28	98.59	3.41

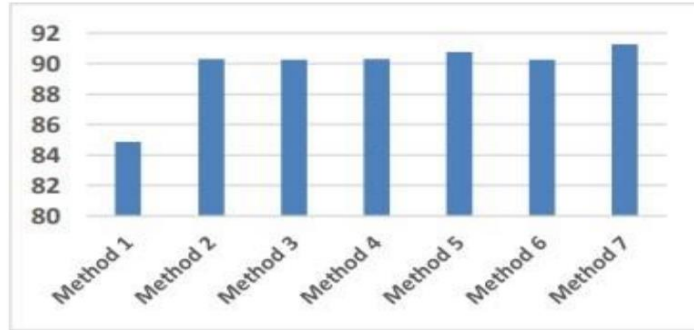


Fig 4.9 Rank-1 recognition rate comparison for UBIPr dataset

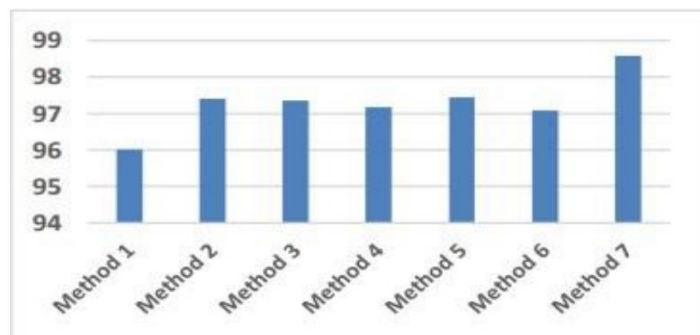


Figure. 4.10 Rank-5 recognition rate comparison for UBIPr dataset

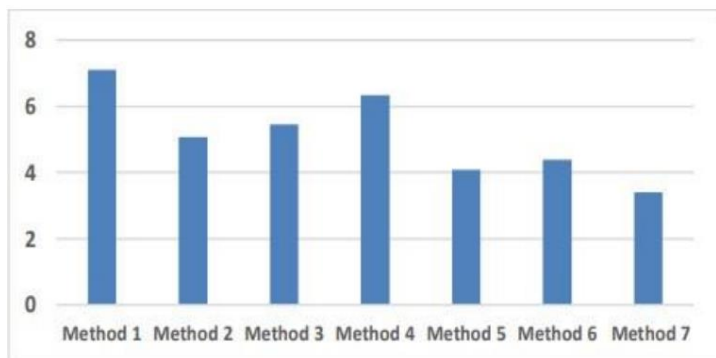


Figure. 4.11 EER comparison for UBIPr dataset

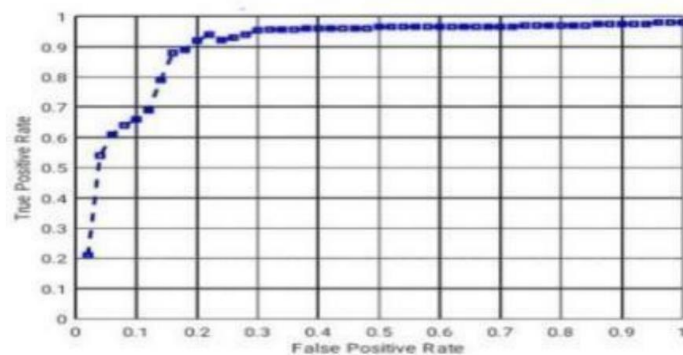


Figure. 4.12 ROC curve for UBIPr dataset

4.2.4.2 Experiment No #2: Evaluation of CASIA-Iris Dataset

Table 4.5 CASIA-Iris dataset

Schemes/Methods	Rank-1 recognition rate (%)	Rank-5 recognition rate (%)	EER (%)
Method 1	95	96.98	8.06
Method 2	95.95	98.15	7.51
Method 3	96.09	98.1	6.1
Method 4	96.01	97.85	6.34
Method 5	95.81	97.67	8.69
Method 6	95.88	97.99	7.42
Method 7	96.62	98.45	4.35

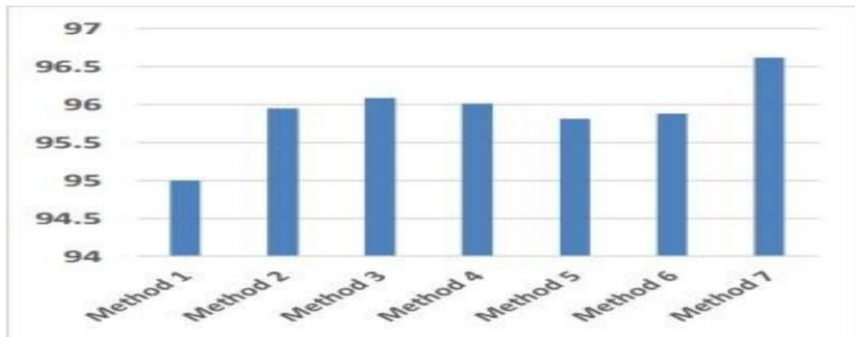


Figure. 4.13 Rank-1 Recognition Rate Comparison For CASIAIris Dataset

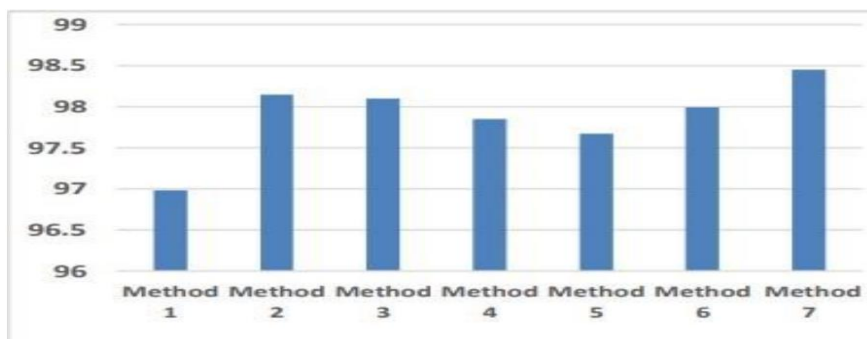


Figure. 4.14 Rank-5 Recognition Rate Comparison For CASIA-Iris Dataset

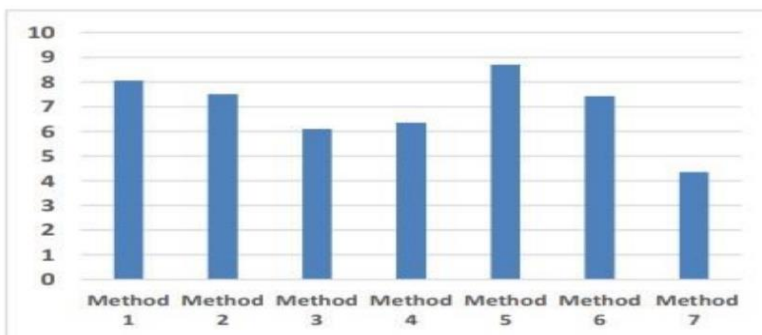


Figure. 4.15 EER comparison for CASIA-Iris dataset

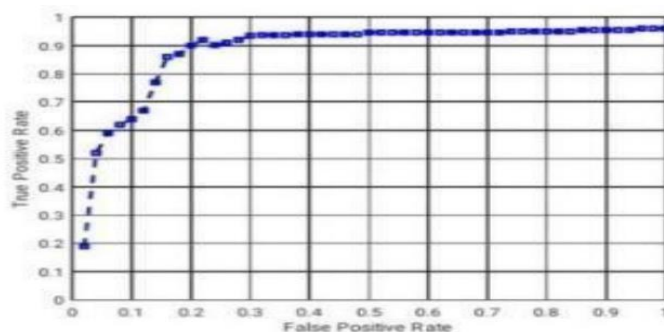


Figure. 4.16 ROC curve for CASIA-Iris dataset

4.2.4.3 Experiment No #3: Evaluation of AR

Table 4.6 AR dataset

Schemes/Methods	Rank-1 recognition rate (%)	Rank-5 recognition rate (%)	EER (%)
Method 1	93.59	96.75	14.53
Method 2	95.24	98.38	7.69
Method 3	94.19	97.75	9.4
Method 4	94.27	97.52	9.39
Method 5	96.07	98.71	7.69
Method 6	94.2	97.61	7.69
Method 7	96.32	98.8	5.13

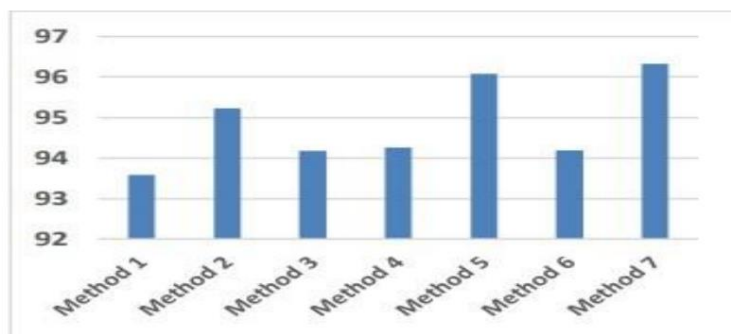


Figure. 4.17 Rank-1 recognition rate comparison for AR dataset

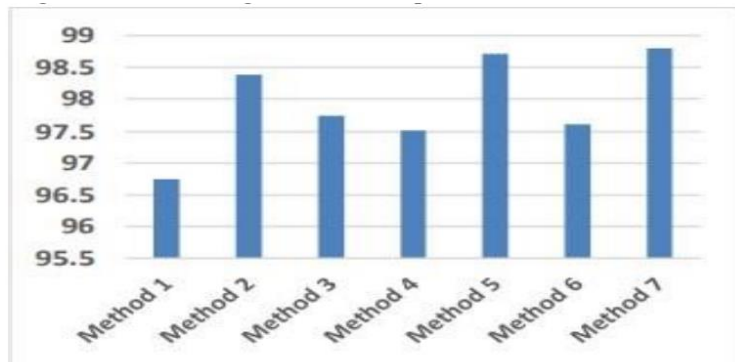


Figure. 4.18 Rank-5 recognition rate comparison for AR dataset

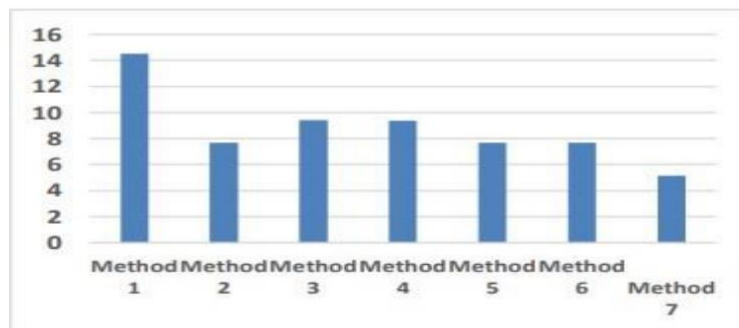


Figure. 4.19 EER comparison for AR dataset

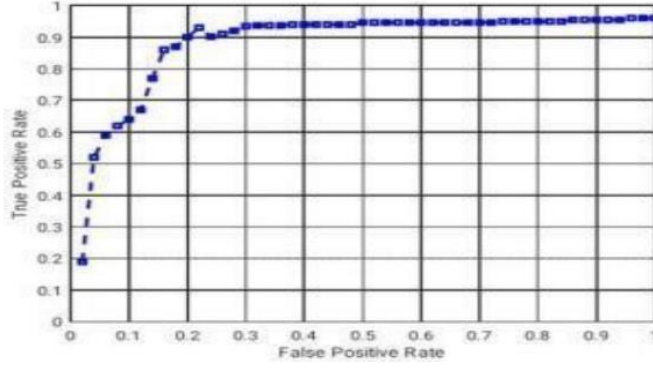


Figure. 4.20 ROC curve for AR dataset

4.2.5 CONCLUSION

This study evaluates the performance of seven periocular recognition methods: ReLU non-linearity, DeepIrisNet, FaceNet, Light CNN, Multimodal CNN, Deep CNN, and RGB-OCLBCP, across three datasets: UBIPr, CASIA-Iris, and AR. Each technique's benefits and drawbacks vary by the intended real-world application. The comparative analysis shows that while each method has its unique advantages, RGB-OCLBCP stands out with promising results in comparison to the others. This evaluation highlights the importance of selecting the appropriate algorithm based on specific application needs.

4.3 Extraction of sub-image based neighbor gradient features based on region specificity for robust periocular recognition

4.3.1 Introduction

The increasing use of biometric data for authentication, such as fingerprint scanners, has been further emphasized by the need for contactless methods during the Covid-19 pandemic, leading to challenges for systems like facial recognition due to mask-wearing. Researchers have turned to periocular biometrics, which focus on the eye's surrounding area, using only about 10% of the facial information yet achieving high accuracy in identification.

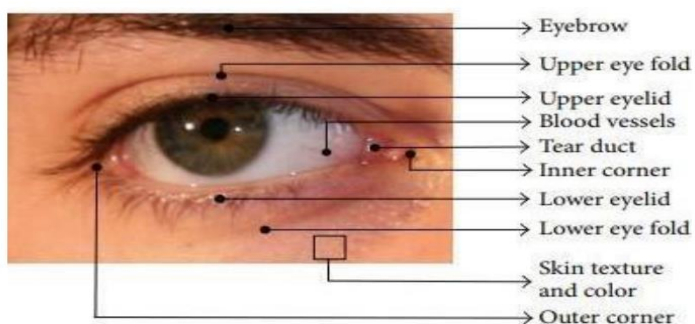


Figure.4.21 Features of Periocular Region Image

This approach leverages the uniqueness of the periocular region, including eyebrows and lower

eyelids, to address the limitations faced by full facial recognition, such as changes due to age or emotions. Periocular biometrics offer a cost-effective solution since they don't require additional data storage and can complement iris data, especially in cases of poor image quality.

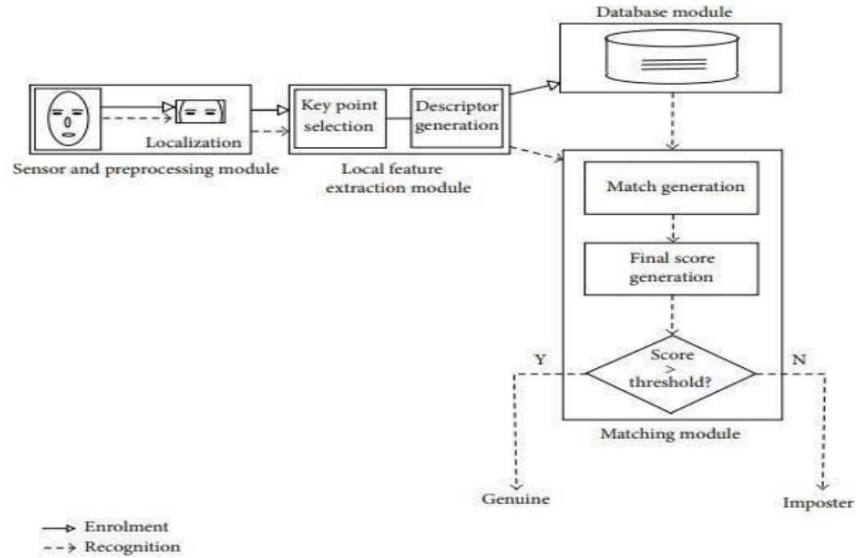


Figure 4.22 Procedure of Biometric Recognition System

This study explores defining an ideal boundary for the periocular region that doesn't rely on edge information but on the area's distinctive pixel intensity patterns, aiming to create a reliable identification template that could potentially be used for official documents like biometric passports.

4.3.2 Proposed Work

The proposed periocular recognition algorithm is presented in both a block diagram (Fig 3) and Algorithm 1. This technique is divided into two main phases: testing and training. Throughout both phase, 5 distinct features types labeled F_1, F_2, F_3, F_4 , and F_5 are extracted.

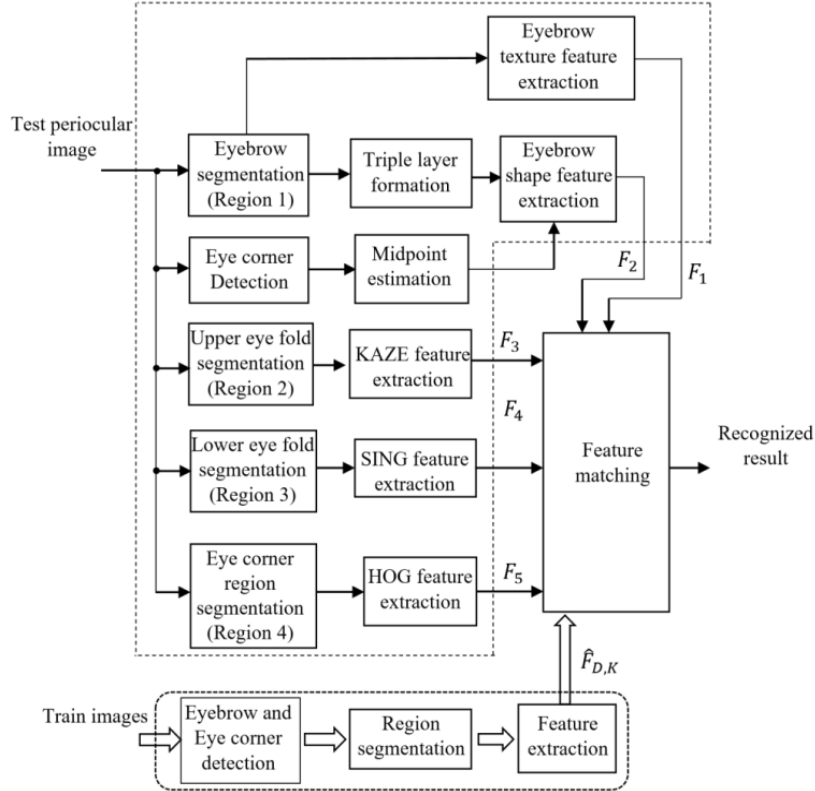


Figure. 4.23 Proposed diagram for recognition of periocular

Following the segmentation of the region of periocular into four distinct small regions, five unique features are retrieved. These regions encompass the brow, upper eye lid, lower eye lid, and corner of eye. Additionally, eyebrow form features are retrieved alongside the features retrieved from the four regions(Ramachandra & Ramachandran, 2022).

The total number of features present in V_1 , V_2 , V_3 , V_4 , and V_5 is denoted as N_1 , N_2 , N_3 , N_4 , and N_5 . Consequently, the number of characteristics collected from the region of periocular of a single eye is calculated(Ramachandra & Ramachandran, 2022).

$$NT = N_1 + N_2 + N_3 + N_4 + N_5 \quad (1)$$

The number of characteristics extracted for a two-eyed periocular area is $2NT$.

The proposed work is divided into five steps. They are

1. Pre-processing
2. Segmentation
3. Feature Extraction
4. Matching

4.3.2.1 Pre-Processing

To mitigate the blurring effect originating from the camera, the facial image is initially refined

through a technique called unsharp masking. This traditional technique, familiar to photographers, adjusts the image's high-frequency elements by subtracting a version of the image that has been blurred (processed with low pass filtering). Optically, this is achieved by first creating a less sharp version on negative film, which is then utilized as a mask in a later stage of development. Mathematically, unsharp masking can be explained as

$$\hat{f} = \alpha f - \beta f_{LP} \quad (1)$$

Where α and β are positive values, with α being greater than or equal to β . It is advantageous to maintain the local average of the image when handling digital imagery. The subsequent expression of unsharp masking ensures the local average within the image remains constant, provided that the coefficients in the low-pass filter f_{LP} are standardized, meaning their sum amounts to 1.

The image forthcoming illustrates the workflow for filtering via an unsharp mask

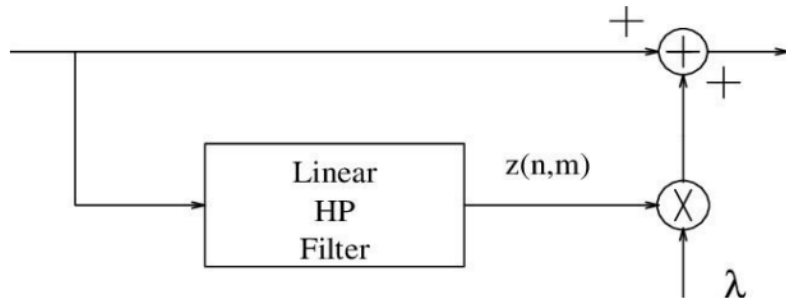


Figure 4.24 Process flow for unsharp mask filtering

4.3.2.2 Corner of eye and eyebrow detection

Following preprocessing, corner of eye points and brow of the face are recognized. The Local Eyebrow Active Shape Model algorithm is employed to recognize the eyebrow, determining both its lower and upper boundaries. Additionally, the corner of eye locations are identified using algorithm (Ramachandra & Ramachandran, 2022). Figure 4.25 (a) Illustrates the depiction of the brow and eye corner points.

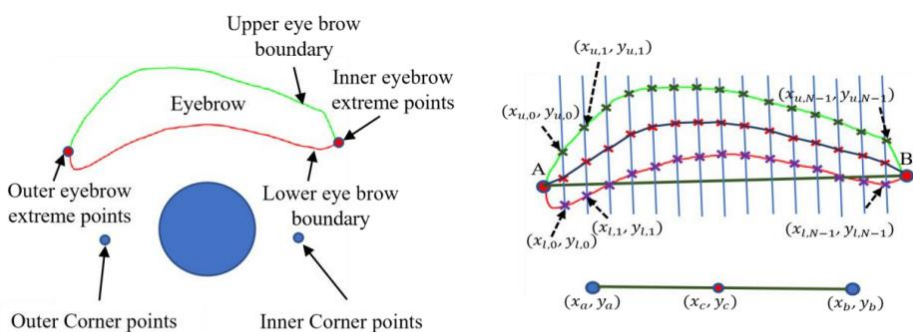


Figure. 4.25 (A) Eye corner and eyebrow corner points are depicted in the illustration. (B) Derivation of eyebrow shape features via triple eyebrow layers.

The remaining regions are divided using the eye corner points as markers, as demonstrated in the illustration.

4.3.2.3 Eyebrow Shape Feature Estimation

The eye corner point detection technique identifies both inner and outer corner points, and the line connecting these points has a midway(Ramachandra & Ramachandran, 2022), represented by the formula:

$$= (xa+2xb \ ya+2yb) \quad (2)$$

The eyebrow detection technique is utilized to identify the upper and lower limits of the eyebrow. Following this, the line joining the brow's extreme points is sectioned into N uniform segments, with N lines perpendicular to line AB being constructed. These perpendicular lines, marked as (i) and (i) , cross the eyebrow's upper and lower edges, as demonstrated in Fig 4.26(b). The midpoints on these boundaries are estimated to be (i) and (i) , for the N points at the upper and lower edges respectively, as derived from the calculation:

$$(m_i m_i) = (x_{u,i} + x_{l,i}) / 2 \quad i = 0, 1, 2, \dots, N-1 \quad (3)$$

Connecting the center point of the corners of eye points ($mimi$) and extending outward to intersect the upper and lower eyebrow borders results in points ($UiUi$) and ($LiLi$), respectively. The extraction of eyebrow shape features involves utilizing a triple layer approach comprising the eyebrow upper layer, eyebrow lower layer, and middle layer. Illustrated in Figure. 5, the distances between the centroid and points ($LiLi$), ($mimi$), and ($UiUi$) are denoted as SLi , Smi , and SUi , respectively. SLi is computed using equation (4), while the distances Smi and SUi are determined using the Euclidean distance method(Ramachandra & Ramachandran, 2022) outlined in equation (4).

$$SLi = \sqrt{(x_{L,i} - x_c)^2 + (y_{L,i} - y_c)^2} \quad (4)$$

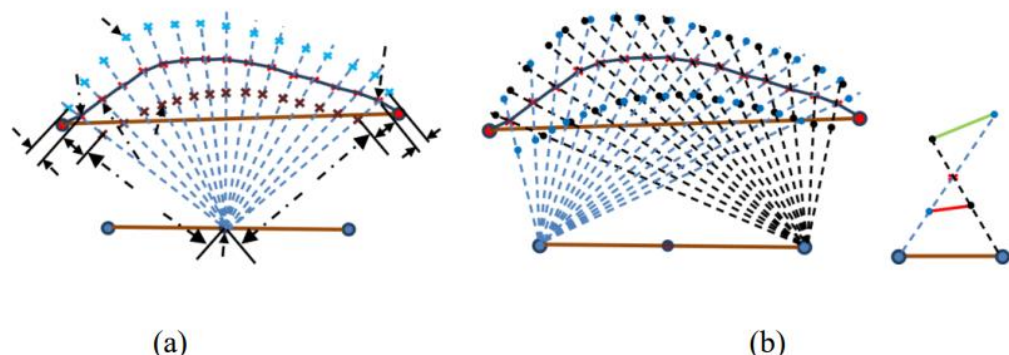


Figure. 4.26 Illustration of shape of the eyebrow features :(a) Height of eyebrow

feature(b) Width of eyebrow feature

The features SLi , Smi , and SUi provide information regarding eyebrow height, while the features dUi and dLi offer insights into eyebrow width. Extending the line connecting the points and $mimi$ to the top edge of the eyebrow results in points $(U'iU'i)$ and $(L'iL'i)$, which connect the upper and lower eyebrows, in the Figure. 4.26 (b). Similarly, connected lines points and $(mimi)$ to the boundary of upper eyebrow yields points $(U'iU'i)$ and $(L'iL'i)$, linking the upper and lower eyebrows. The distance between $(U'iU'i)$ and $(L'iL'i)$ is calculated using relation of Euclidean distance (Ramachandra & Ramachandran, 2022).

$$dui = \sqrt{dU' i' i U' i' i U' i} \quad (5)$$

The distance between $(U'iU'i)$ and $(L'iL'i)$ is represented as dLi . S , comprising SLi , Smi , SUi , dUi , and dLi , signifies the $N2$ number of brow characteristics(Ramachandra & Ramachandran, 2022), where $N2$ equals $5N$.

4.3.2.4 Segmentation of the fold of eye and corner of eye regions.

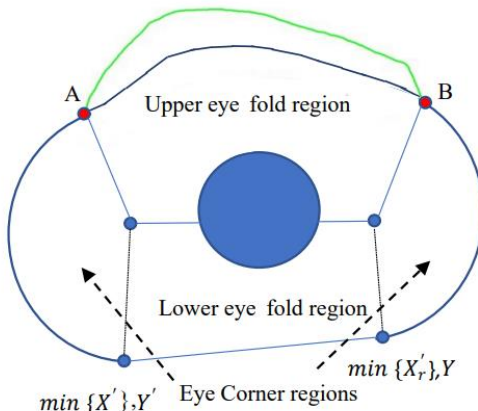


Figure. 4.27 Segmentation of fold of eye and corner of eye

The area between the two eye corner points and the mid-layer of the eyebrow constitutes the upper eye fold. To delineate this region, a semi-circle is constructed with the left eye corner as the center and the distance between point A and point B as the radius. This semi-circle extends until reaching the point $(\min\{X'\}Y')$, where $X'Y'$ denotes the location of boundary pixels enclosed by the circle whose center is at the left eye corner and whose diameter is the distance between points A and B. The region bounded by points A, $(\min\{X'\}Y')$, and the left semi-circular border is identified as the left eye corner region. Similarly, the right eye corner region is determined using a comparable method(Ramachandra & Ramachandran, 2022). As depicted in Figure. 4.27, the lower eye fold region is approximated by connecting the points $(\min\{Xr'\}Yr')$ and $(\min\{X'\}Y')$.

4.3.2.5 HOG feature extraction

The Histogram of Oriented Gradients (HOG) method is closely aligned with techniques like the Scale Invariant Feature Transformation (SIFT) and Edge Orientation Histograms (EOH), highlighting an object's geometry or form. Specifically, the HOG feature extraction process targets the eyebrow corners and the eyebrow zone $F5$ and $F1$, respectively (Ramachandra & Ramachandran, 2022). The utilization of HOG in the eyebrow area is due to its effectiveness in capturing the texture of eyebrow hairs, revealing key characteristics such as hair density and orientation. For the areas around the eyes, HOG is adept at delineating the nasal bridge's contour. This HOG procedure encompasses computing the direction of gradients within a specific analysis window, including steps like estimating gradients, categorizing orientations into bins, and summarizing the feature data. (Ramachandra & Ramachandran, 2022).

Value									
Bins	0	20	40	60	80	100	120	140	160

Figure.4.28 Histogram Table of 9 bin

Gradient estimation involves calculating the gradients in both the vertical and horizontal directions to estimate their magnitudes and angles(Ramachandra & Ramachandran, 2022).

Orientation binning subdivides the image into small regions called cells. Within each cell, the magnitude of every pixel is allocated to different orientations based on the gradient angle.

Feature description entails grouping adjacent cells to form blocks. These blocks are then normalized using the $L2$ -norm(Ramachandra & Ramachandran, 2022).

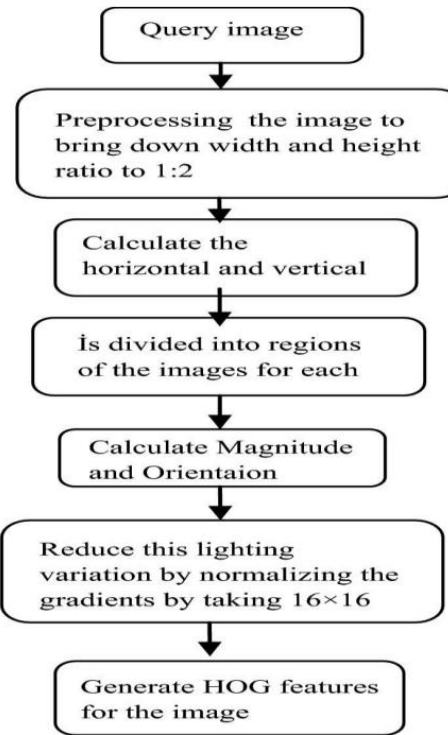


Figure.4.29 Diagram of HOG

Imagine that N_1 is the number of Histogram of Oriented Gradients (HOG) features derived from a singular eyebrow area, and N_5 indicates the quantity of HOG features obtained from the areas near both the left and right eye corners. Upon analysis, it becomes clear that the region adjacent to the nasal side of the eye contains a higher concentration of significant HOG features compared to the area near the ear side of the eye. (Ramachandra & Ramachandran, 2022).

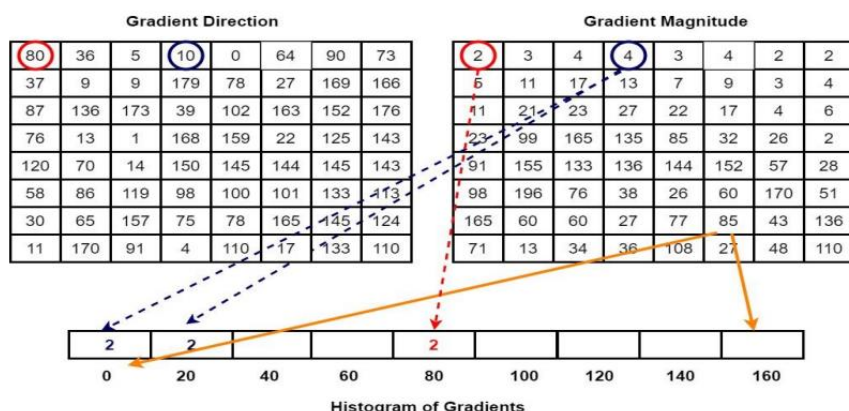


Figure.4.30 Numerical Diagram of HOG

4.3.2.6 KAZE Feature Extraction

A unique method for feature recognition and description, the KAZE Features algorithm is a member of the class of techniques that make use of the so called scale space. It differs from other approaches, like SIFT or SURF, in that it finds features in a nonlinear scale space instead

of the Gaussian scale space. The KAZE feature extraction technique involves three primary processes (Ramachandra & Ramachandran, 2022), which are as follows:

- 1)** Create a Nonlinear Scale space pyramid based on the first image.
- 2)** In the nonlinear scale space, identify important spots using Hessian determinants and multiscale derivatives.
- 3)** Calculate the orientation and description vectors for each significant location.

The KAZE feature extraction algorithm is utilized to extract feature $F3$ from the upper eye fold region. Denoting ∇ as the operator for gradient and div as the operator for divergence (Ramachandra & Ramachandran, 2022), the equation for the non-linearity diffusion is expressed as ∂I .

$$\partial \delta = \text{div} \sigma \tau \tau \delta \cdot \nabla I \quad (6)$$

Adjusting the scale parameter δ alters the image representation. A higher δ value leads to blurred edges and a simpler representation of the image.

4.3.2.7 Feature matching

Consider Vt as the extracted features from the test image, given by

$$Vt = [V1 \ V2 \ V3 \ V4 \ V5] \quad (11)$$

V denotes the features extracted from K number of training images.

$$V_k = [V_{1,1} \ V_{2,1} \ V_{1,2} \ V_{2,2} \ V_{3,1} \ V_{4,1} \ V_{5,1} \ V_{3,2} \ V_{4,2} \ V_{5,2} \ \vdots \ V_{1,K} \ V_{2,K} \ \vdots \ \vdots \ V_{1,K} \ V_{1,K} \ V_{1,K}] \quad (12)$$

For $k = 1, 2, \dots, K$, where K represents the number of trained photos, the five distinct features extracted from the k th training image(Ramachandra & Ramachandran, 2022) are denoted as $V1k$, $V2k$, $V3k$, $V4k$, and $V5k$. Feature matching entails computing the cumulative similarity score between the features $V1, V2, V3, V4, V5$ and $V1k, V2k, V3k, V4k, V5k$. The similarity score between the test image and the K number of trained images is expressed as $T = [T_1 \ T_2 \ T_3 \dots \ T]^T$. The matched periocular recognition can be estimated by identifying the minimum similarity score.

$$R = T = \text{argmin}_k [T_1 \ T_2 \ T_3 \dots \ T]^T \quad (13)$$

4.3.3 RESULT AND ANALYSIS

4.3.3.1 Experimental images

The suggested periocular recognition method's performance was evaluated using datasets including UBIPr [36], CASIA-Iris Distance, and AR datasets. Representative images are illustrated in Figure. 4.31. Evaluation metrics such as rank-5 and rank-1 recognition accuracy, equal error rate (EER), and area under curve. (Ramachandra & Ramachandran, 2022)

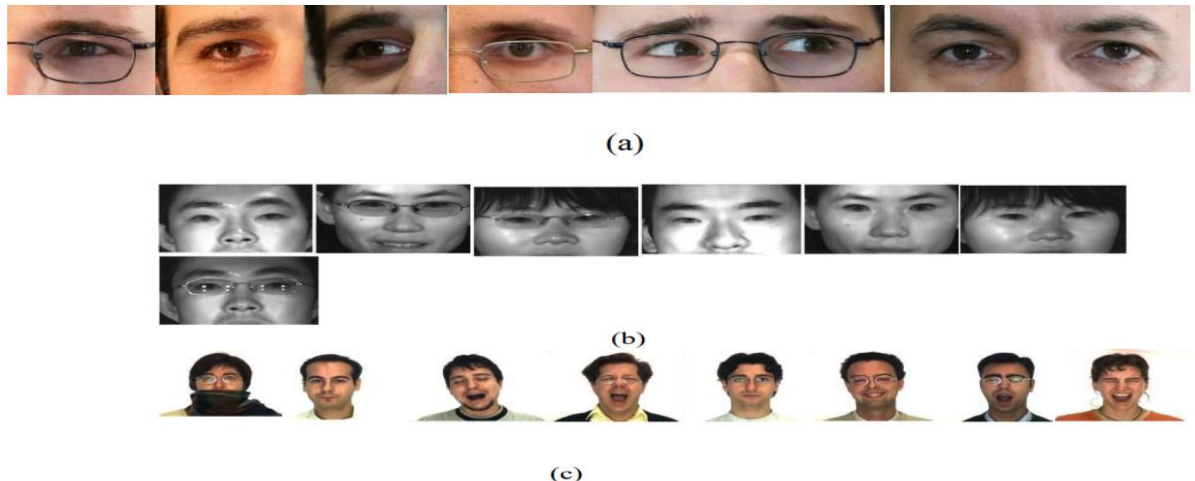


Fig 4.31 Illustrative test images from various datasets are presented as follows: (a) Samples from the UBIPr dataset (b) Samples from the CASIA-Iris Distance dataset (c) Samples from the AR dataset.

4.3.3.2 Experimental results

Performance evaluation was conducted using double and single images of periocular from UBIPr data set. Figure 4.32 illustrates the feature extraction process from the one region of periocular obtained from the UBIPr dataset(Ramachandra & Ramachandran, 2022).

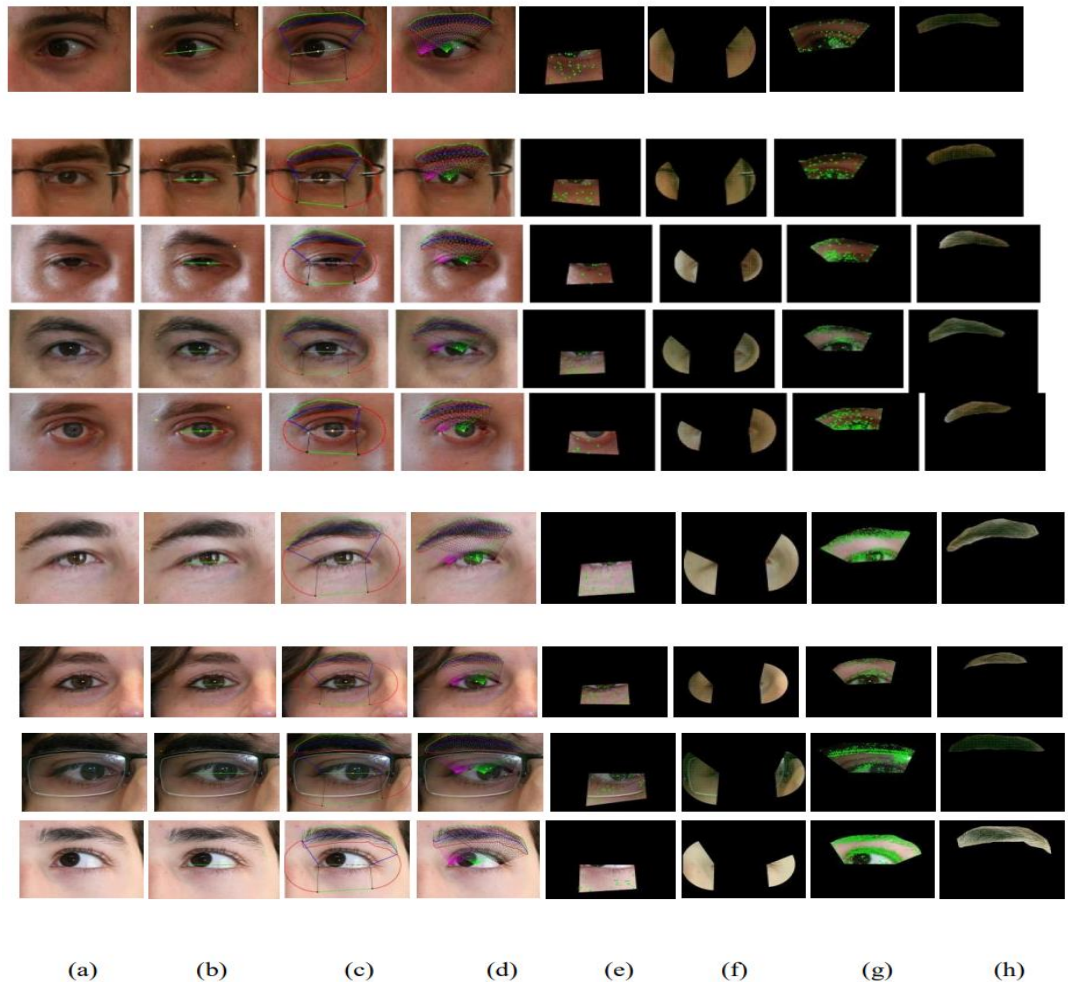


Figure. 4.32: Extraction of single eye periocular features from images in the UBIPr dataset is depicted as follows:(a) Detection of eye and eyebrow corners in the input periocular image.(b) Segmentation of the region of interest.(c) Extraction of eyebrow shape features.(d) Extraction of features in the lower eye region.(e) Extraction of features in the eye corner regions.(f) Feature retrieval in the top eye area.(g) Feature retrieval in the region of eyebrow.

Containing 4000 color face photos, the AR database comprises frontal views of faces belonging to 70 men and 56 women. These images showcase various lighting conditions, occlusions, and facial expressions. The CASIA Iris Distance dataset focuses on images featuring dual eye and face patterns as the region of interest. Meanwhile, the UBIPr dataset contains segmented versions of both single eye and both eye face images.

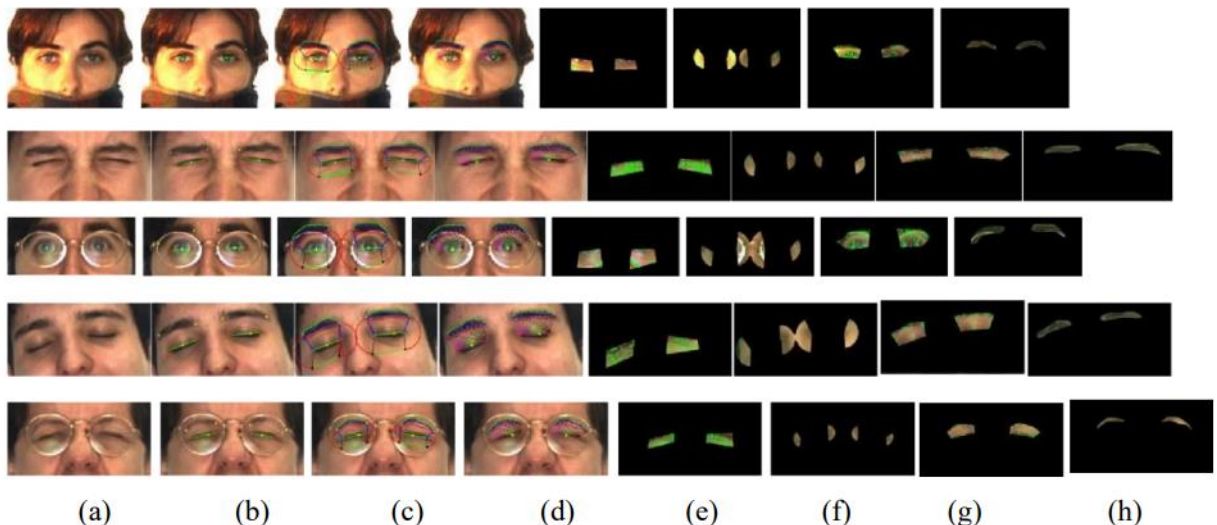


Figure. 4.33 Extracting periocular features from the AR dataset involves the following steps: (a) Initial periocular image input. (b) Detection of eye and eyebrow corners. (c) Segmentation of the region of interest. (d) Extraction of eyebrow shape features. (e) Feature extraction in the lower eye region. (f) Feature extraction in the eye corner regions. (g) Feature extraction in the upper eye regions. (h) Feature extraction in the eyebrow region.

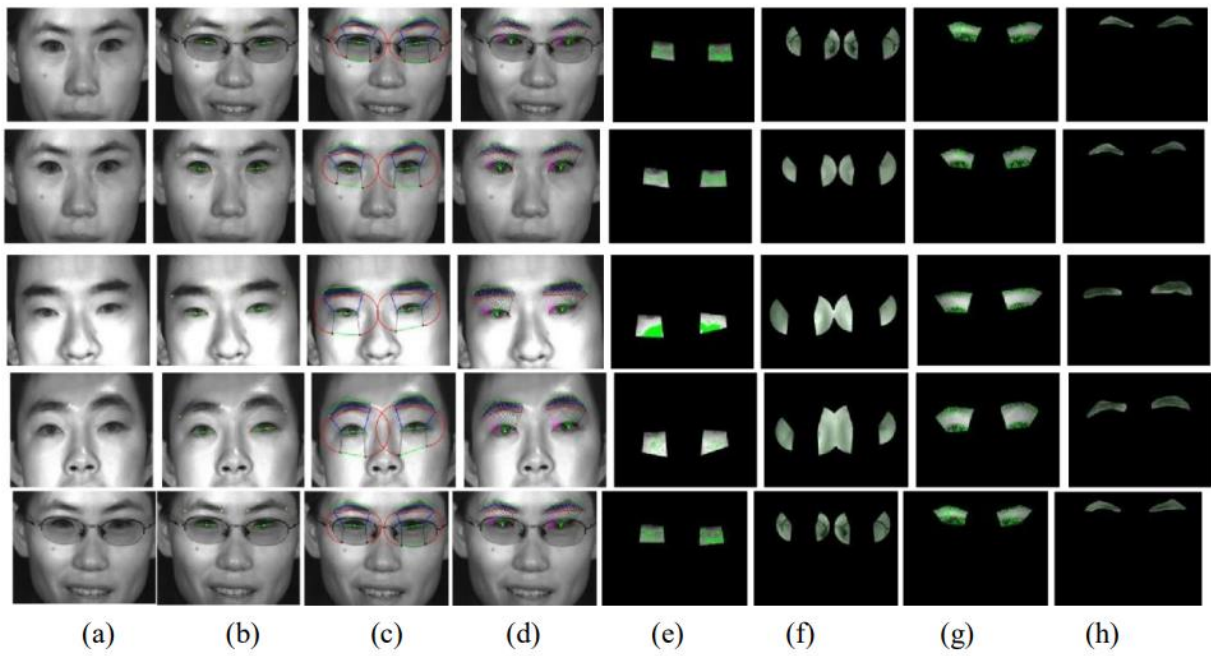


Figure. 4.34 The process of extracting periocular features from the CASIA-Iris dataset involves the following steps:(a) Importing the periocular image as input.(b) Detecting the corners of the eyes and eyebrows.(c) Segmenting the region of interest.(d) Extracting features related to eyebrow shape.(e) Identifying features in the lower eye region.(f) Extracting features from the eye corner regions.(g) Capturing features from the upper eye regions.(h) Extracting features from the eyebrow region.

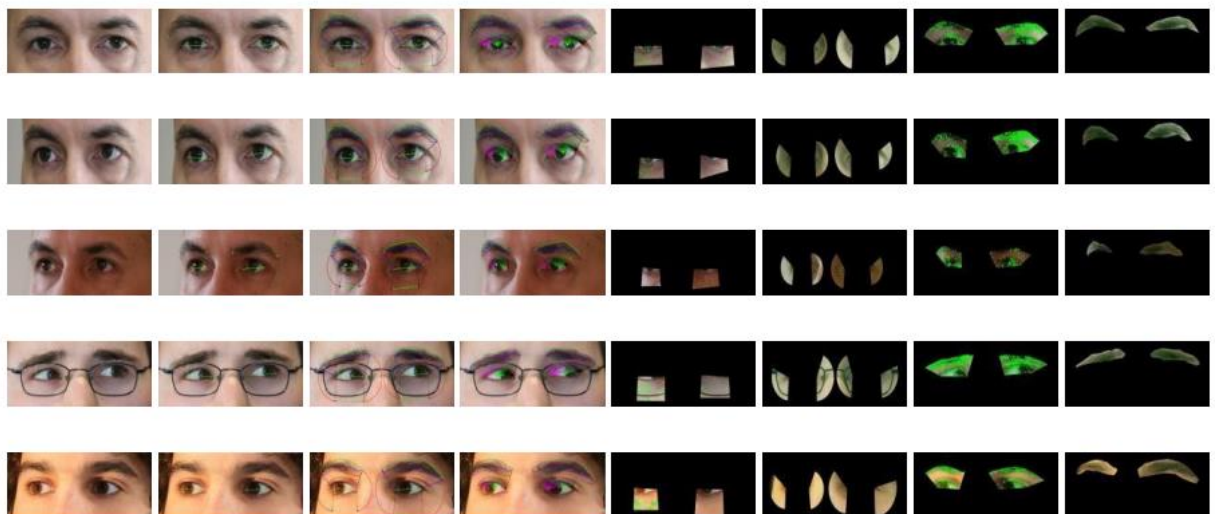


Figure. 4.35 Extracting periocular features from the dual eye images in the UBIPr dataset involves the following steps:(a) Initial input of the periocular image.(b) Detection of corners for eyes and eyebrows.(c) Segmentation of the region of interest.(d) Extraction of features related to eyebrow shape.(e) Identification of features in the lower eye region.(f) Extraction of features from the eye corner regions.(g) Capture of features from the upper eye regions.

eye regions.(h) Extraction of features from the eyebrow region.

4.3.3.3 Experimental results

Using the performance measures indicated above, the classifier system's performance is analyzed and contrasted with that of other techniques. The tables and graphs below demonstrate this.

Experiment No #1: Performance Analysis of Classifiers

Table 4.7 Comparison of Equal Error Rate (EER) with conventional methods.

	EER (%)
ImageNet	7.11 ± 2.9
Iris recognition	5.07 ± 2.2
Clustering	5.46 ± 1.5
LCNN	6.34 ± 2.1
Multilevel	4.09 ± 2.1
VGG16	4.38 ± 1.3
OC-LBCP	3.41 ± 1.8
Proposed	3.08 ± 1.6

Table 4.8 Comparison of Equal Error Rate (EER) with conventional

	EER (%)
ImageNet	8.06 ± 5.3
Iris recognition	7.51 ± 1.1
Clustering	6.10 ± 2.2
LCNN	6.34 ± 1.6
Multilevel	8.69 ± 1.1
VGG16	7.42 ± 1.7
OC-LBCP	4.35 ± 0.5
Proposed	4.12 ± 0.4

Table 4.9 Comparison of Equal Error Rate (EER) with conventional methods.

	EER (%)
ImageNet	14.53
Iris recognition	7.69
Clustering	9.4
LCNN	9.39

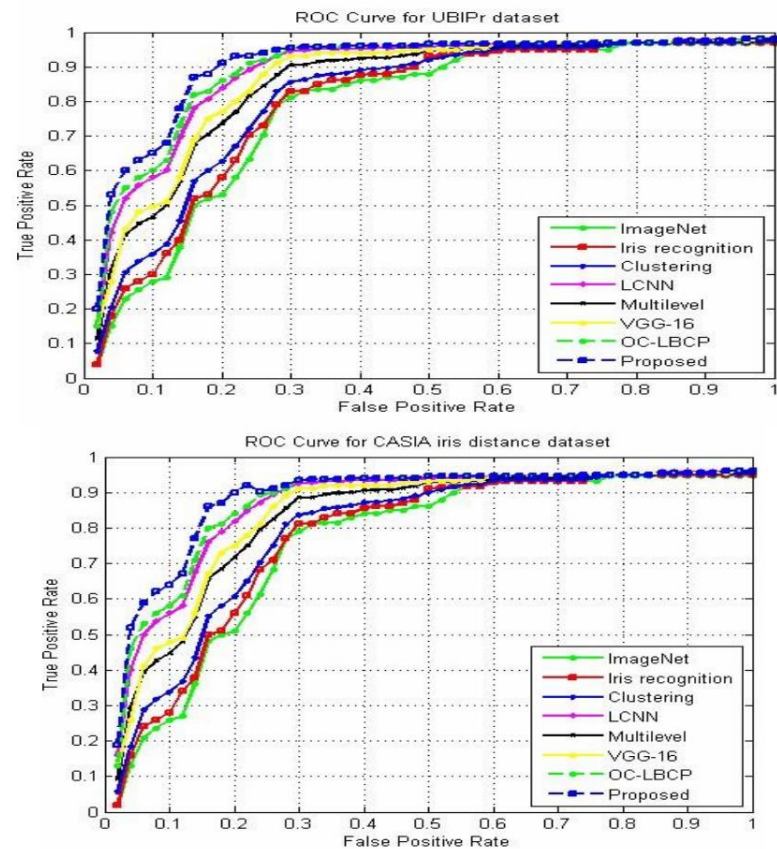
Multilevel	7.69
VGG16	7.69
OC-LBCP	5.13
Proposed	4.92

Table 4.10 Comparison of AUC with the old method

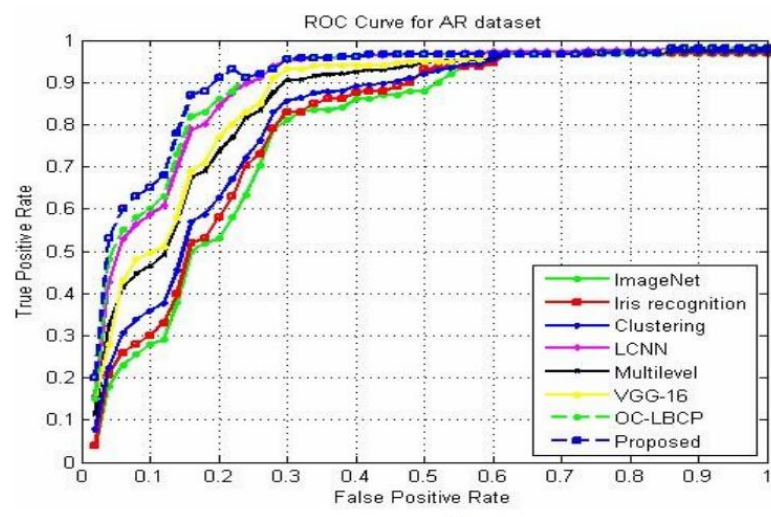
Scheme	UBIPr AUC	CASIA-Iris AUC	AR AUC
ImageNet	0.9805	0.9533	0.9363
Iris recognition	0.9877	0.9674	0.9751
Clustering	0.987	0.9738	0.9692
LCNN	0.9849	0.9719	0.9737
Multilevel	0.9913	0.9594	0.9756
VGG16	0.9892	0.9681	0.9747
OC-LBCP	0.9938	0.986	0.9882
Proposed	0.9948	0.9908	0.9901

Methodology proposed was benchmarked against several established techniques including ImageNet, iris recognition, Clustering, LCNN, Multilevel, VGG16, and OC-LBCP. Table 4.10 presents a comparison of the Equal Error Rate (EER) and Area Under the Curve (AUC) between the proposed method and traditional approaches. Across all datasets, the EER of the proposed method outperforms that of conventional methods. Specifically, for the UBIPr, CASIA Iris, and AR datasets, the EER of the proposed technique is 3.08%, 1.6%, and 4.12% respectively. Notably, the UBIPr dataset exhibits a higher AUC compared to the CASIA Iris and AR datasets. Moreover, the suggested method consistently achieves an AUC greater than 0.99 for all datasets. The Receiver Operating Characteristic (ROC) curve comparison between the proposed method and traditional approaches for the three datasets is illustrated below(Ramachandra & Ramachandran, 2022).

(a)



(b)



(c)

Figure. 4.36 Comparison of the Receiver Operating Characteristic (ROC) curves for the following datasets: (a) UBIPr dataset, (b) CASIA-Iris dataset, and (c) AR dataset.--C comparison for the datasets (a) UBIPr dataset (b) CASIA-Iris dataset (c) AR dataset

Table 4.11 Comparison of recognition accuracy metrics

Scheme	UBIPr		CASIA-Iris		AR	
	Rank-1	Rank-5	Rank-1	Rank-5	Rank-1	Rank-
ImageNet 5	84.88 ± 2.5	96.01 ± 1.8	95.00 ± 1.8	96.98 ± 2.5	93.59	
Iris recognition	90.30 ± 1.2	97.41 ± 1.1	95.95 ± 2.1	98.15 ± 0.6	95.24	98.38
Clustering	90.24 ± 1.4	97.36 ± 0.4	96.09 ± 2.1	98.10 ± 0.4	94.19	97.75
LCNN	90.28 ± 1.7	97.18 ± 0.7	96.01 ± 2.0	97.85 ± 0.9	94.27	97.52
Multilevel	90.75 ± 1.0	97.44 ± 0.3	95.81 ± 1.9	97.67 ± 1.0	96.07	98.71
VGG16	90.24 ± 1.4	97.09 ± 1.1	95.88 ± 0.1	97.99 ± 0.5	94.2	97.61
OC-LBCP	91.28 ± 1.2	98.59 ± 0.4	96.62 ± 1.3	98.45 ± 0.4	96.32	98.8
Proposed	92.32±1.5	98.73±0.6	97.41±1.1	98.95±0.8	97.87	99.12

Table 4.11 presents a comparison of the rank-1 and rank-5 recognition accuracy between the proposed method and conventional approach. Notably, for the UBIPr, CASIA-Iris Distance, and AR datasets, the rank-5 recognition accuracy exceeds the rank-1 recognition accuracy by 6.41%, 1.54%, and 1.25%, respectively. Specifically, for the UBIPr dataset, the rank 1 87.86% and a rank-5 recognition accuracy of 98.23% for single-eyed periocular images. For dual-eyed periocular images, the rank-1 and rank-5 recognition accuracy are computed to be 96.78% and 99.23%, respectively. These results suggest that the proposed technique demonstrates higher identification rates for dual-eye periocular images compared to one eye images of periocular (Ramachandra & Ramachandran, 2022).

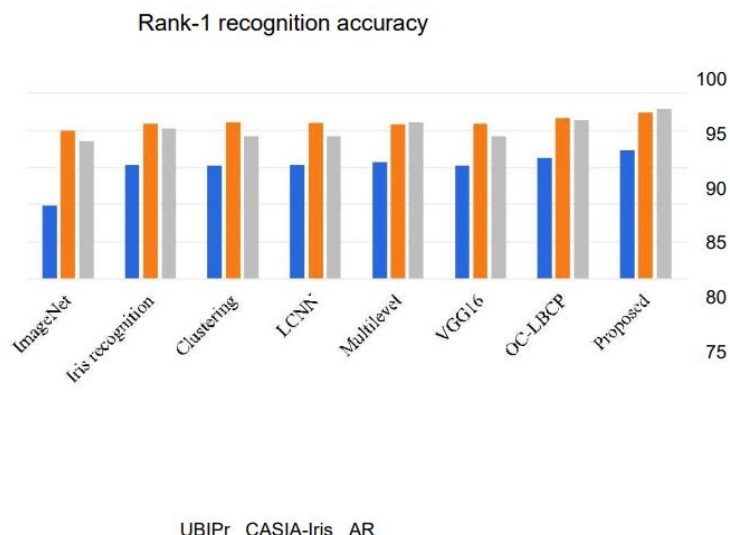


Figure. 4.37 Comparison of the Rank-1 recognition accuracy performance

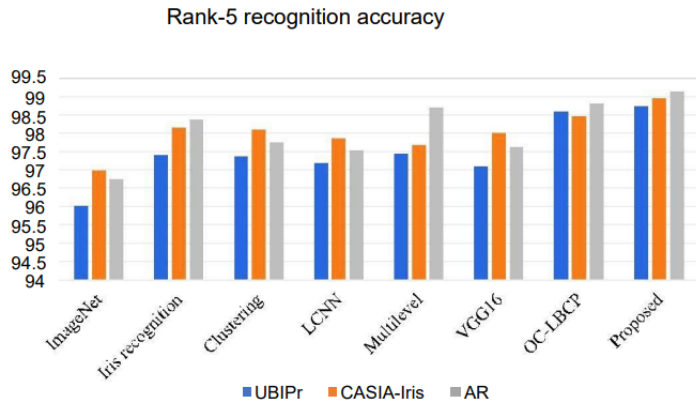


Figure. 4.38 Comparison of the Rank-5 recognition accuracy performance

Graphical comparison of rank-1 and rank-5 recognition accuracy between the proposed method and conventional methods is depicted in Figures 4.37 and 4.38. For the UBIPr, CASIA-Iris distance dataset, and AR dataset, the rank-1 recognition accuracy values are projected to be 92.32%, 97.41%, and 97.87%, respectively. Conclusion is presented in the subsequent section(Ramachandra & Ramachandran, 2022).

4.3.4 CONCLUSION

This chapter introduces a periocular recognition technique designed to extract features from four distinct regions: the brow, upper and lower eye folds, and eye corner regions. Utilizing conventional HOG and KAZE feature extraction methods, features are extracted from the eyebrow, upper eye fold, and eye corner areas. The eyebrow shape features are derived by estimating height and width features along the upper and lower boundaries of the eyebrow. Additionally, a sub-image-based neighbor gradient feature extraction method is proposed for extracting features from the lower eye fold region(Ramachandra & Ramachandran, 2022). The performance of the proposed technique is evaluated on datasets such as UBIPr, CASIA-Iris, and AR using metrics like rank-1 and rank-5 recognition accuracy, Equal Error Rate (EER), and Area under the Curve (AUC). The calculated AUC values for the UBIPr, CASIA-Iris, and AR datasets are 0.9948, 0.9908, and 0.9901, respectively. Moreover, the rank-1 recognition accuracy for these datasets is found to be 92.32%, 97.41%, and 97.87%, respectively. Experimental results demonstrate that the proposed periocular recognition algorithm outperforms conventional methods and is particularly effective for identifying individuals with incomplete facial information, relying solely on periocular regions(Ramachandra & Ramachandran, 2022).

4.4 Robust Periocular Recognition Using Modified Histogram of Gradient and Improved Accelerated KAZE

4.4.1 Introduction

The evolving landscape of biometric authentication systems has seen a significant shift towards the adoption of biometric data, with fingerprint scanners emerging as a reliable technology. However, the COVID-19 pandemic has necessitated the exploration of touchless biometric systems to minimize infection spread, leading to an increased interest in iris recognition technologies. Despite their accuracy, iris scanners are hindered by high costs and potential risks associated with the use of IR sensors. As an alternative, focusing on the periocular region—encompassing the area around the eyes and eyebrows—offers a cost-effective solution that leverages software-based recognition, avoiding the pitfalls associated with hardware dependency. This approach, termed telescopic authentication recognition, promises a balance between accuracy, usability, and cost-effectiveness. The periocular region, or the area between the nose and the eyes, includes critical facial features that can be utilized for biometric identification, sometimes referred to as "extended Iris detection." This paper proposes exploring the periocular region's potential to overcome challenges faced by traditional biometric systems, including facial occlusion and poor iris data. It aims to introduce a novel method for extracting periocular features without necessitating specific physical characteristics, thereby enhancing the discriminative capabilities of biometric systems.

4.4.2 Proposed Work

The proposed periocular recognition technique, illustrated in Figure. 4.39 and Algorithm 1, operates in two phases: training and testing. It involves extracting five different types of features, denoted as $F1, F2, F3, F4$ and $F5$, during both phases. Initially, the periocular region is segmented into four sub-regions: the brow, upper lid of eye, lower lid, and corner of eye. Features are then retrieved from each of these regions, including eyebrow shape features and others obtained from the four identified areas. This segmentation and feature extraction process constitutes the basis of the proposed periocular recognition technique.

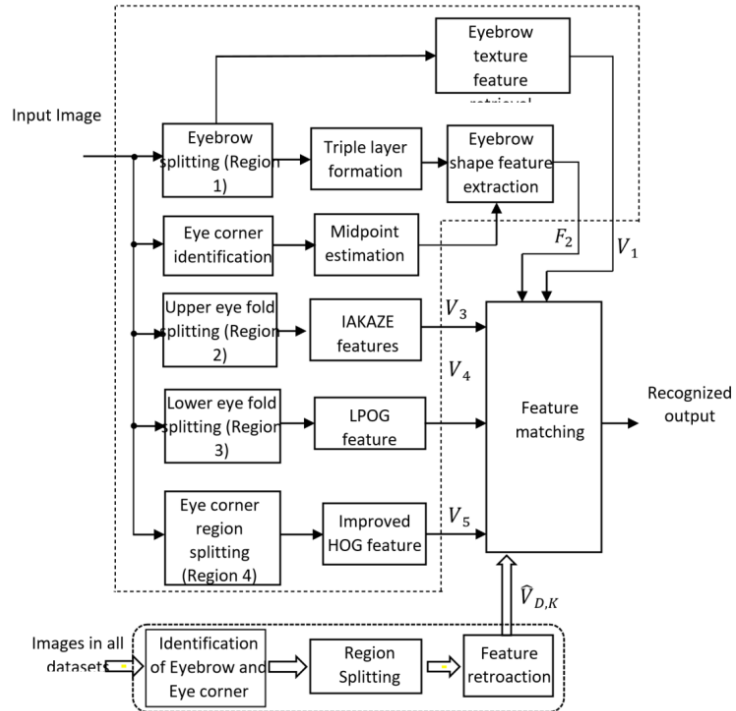


Figure. 4.39 Proposed block diagram for periocular recognition

The count of features within V_1, V_2, V_3, V_4 and V_5 is denoted N_1, N_2, N_3, N_4 and N_5 respectively. Consequently, the cumulative number of characteristics extracted from a single periocular region amounts to:

$$NT = N_1 + N_2 + N_3 + N_4 + N_5 \quad (1)$$

The number of characteristics extracted for a two-eyed periocular area is $2NT$

Algorithm 1: Robust Periocular Recognition using Modified Histogram of Gradient and Improved Accelerated KAZE

Input: Input Person Image I

Output: Recognized Person R

Step 1: Detect the eyebrow from I using Local Eyebrow Active Shape Model

Step 1: Extract the eyebrow shape features using Eq. 2 to Eq. 5

Step 2: Segment the eye corner region from I using semi-circle formation and distance calculation

Step 3: Extract the features from the eye corner region using the improved HOG method

Step 4: Segment the upper eye fold region from I using semi-circle

formation and distance calculation

Step 5: Extract the features from the upper eye fold region using IAKAZE approach

Step 6: Segment the upper eye fold region from I using semi-circle formation and distance calculation

Step 7: Extract the features from the lower eye fold region using LPOG approach
Step 8: Form the test feature set TER using Eq.11

Step 9: The output R is produced by calculating the cumulative similarity score between trained feature set TR and test feature set TER using Eq.13

The proposed work is divided into five steps.

1. Pre-processing
2. Segmentation
3. Feature Extraction
4. Matching

4.4.2.1 Pre-Processing

To counter the blur introduced by the camera, the first action is to refine the facial or periocular image using the technique known as unsharp masking. This effect is optically achieved by first producing a less sharp image on negative film and then employing this film as a mask in a later development phase. Mathematically, unsharp masking is represented as:

$$f^{\wedge} = \alpha f - \beta f_{lp} \quad (1)$$

Here, α and β represent positive constants, with $\alpha \geq \beta$. When processing digital images, it's crucial to maintain the image's local average. The specific equation for unsharp masking guarantees that the image's local mean remains unchanged, assuming the sum of the coefficients in the low-pass filter f_{lp} is normalized, meaning their aggregate is 1.

An illustration further down outlines the sequence involved in unsharp mask filtering.

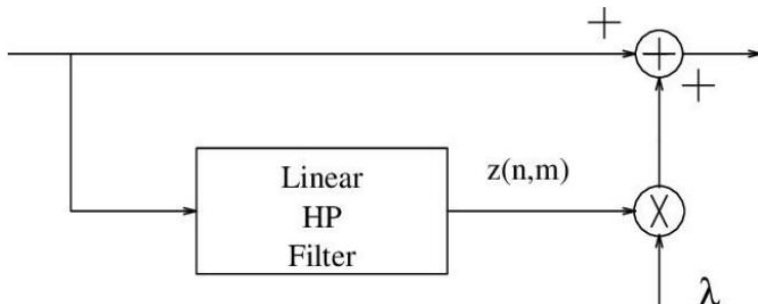


Figure. 4.40 Flow Diagram of Pre-processing

4.4.2.2 Improved HOG feature extraction

The modified HOG features in which are constructed as depicted in Figure 4.41, serve as the starting point. 7

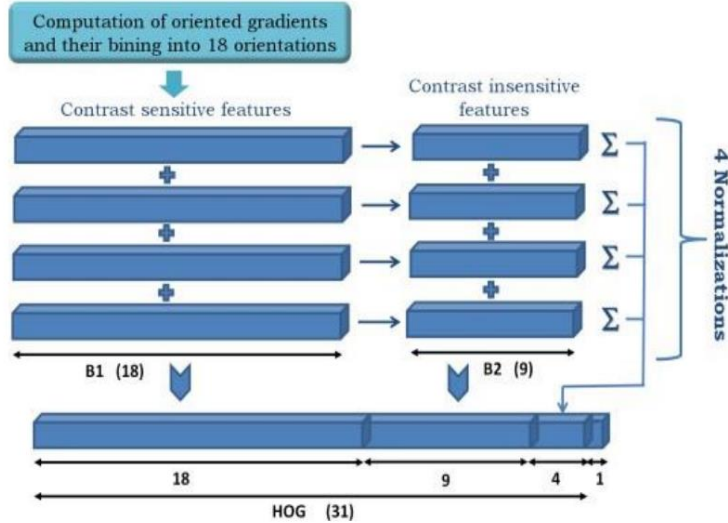


Figure 4.41 Structural Diagram of Improved HOG

A $M \times N$ input picture patch is split into squared HOG cells with an 88 percent pixel density and one cell of padding on each border. On each cell, an orientation histogram with $d = 32$ elements is then produced. As a consequence, the input picture patch is defined by a cube of dimensions $(hc \times wc \times d)$, wherein hc , as well as wc , are the height and width in cell count, respectively. Figure 4.41 depicts the feature formation procedure as a combination of contrast-sensitive (B1) and -insensitive (B2) gradients, as well as four dissimilar histograms characterized by an initial. "Contrast-sensitiveness" corresponds to the quantity of orientations used to discretize the gradients. B1 has 18 bins with the limit of $[0, 2\pi]$, but B2 has 9 bins with the limit of $[0, \pi]$, which is derived through dividing B1 in half as well as the addition of its values.

As a consequence, more measurement data is available for scoring bounding box assumptions, and richer models may be trained from the visual and depth characteristics of the elements. Gradients of color and disparity from 2.5D observations are added to these features. 8

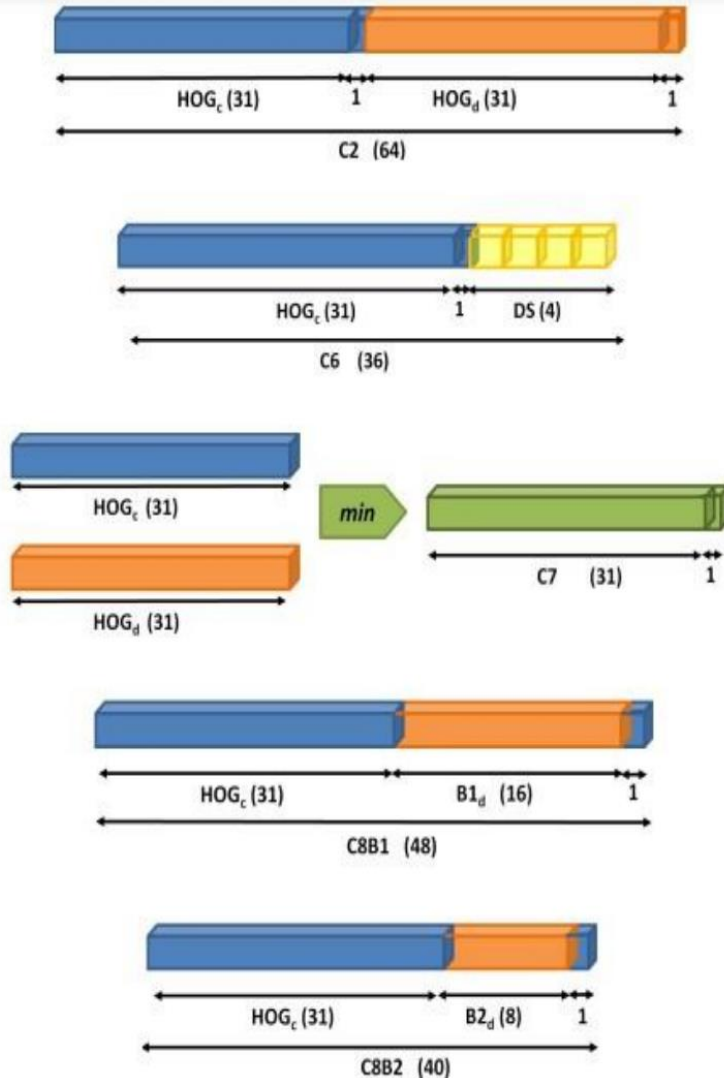


Figure 4.42 Improved HOG Method's 3D Feature Extraction Process Diagram

Despite the fact that does not include disparity maps, we generate them using the SGM approach from each pair of left-right images. In fact, we've seen in our research that disparity maps' gradient information can yield prediction 9 ratios that are nearly as good as those made employing gradients on color pictures. As a result, the disparity images retain the semantic information present in the sceneries, allowing discriminative models to be educated on the 2.5D information to enhance discovery process. The suggested 3D-aware features are shown in Figure 4.42 and are discussed above. Block Normalization in Improved HOG about four strategies for block normalizing are described by Dalal-Triggs in their discussion of the HOG feature. With respect to a given block of histograms, let v be the non-normalized vector containing all of them, $\|v\|_k$ be its k -norm for $k=12$, and e be a tiny constant. Following are the normalizing factors. L1- norm: Normalization Factor, L1-Sqrt: Normalization Factor, L2-Norm: Normalization Factor, L2-Hys Norm L2 -norm, then limiting and clipping the primary value, $v = 0.2$. In this instance, we normalize blocks using the L2 norm.

L1- norm: Normalization Factor,

$$f = \frac{v}{\|v\| + e}$$

L1-Sqrt: Normalization Factor,

$$f = \sqrt{\frac{v}{\|v\| + e}}$$

L2-Norm: Normalization Factor,

$$f = \frac{v}{\sqrt{\|v\|^2 + e^2}}$$

L2-Hys Norm

The Dalal-Triggs variant [1] copies each histogram hd four times, normalizes it using four different normalization factors, stacks the four vectors, saturates them at 0.2, and then stores the result as the cell's descriptor. A number of Orientations * 4-dimensional cell descriptions are the consequence of this. When constructing the final description, blocks are visited in the order left to right and top to bottom. They employ 13-dimensional features, capturing four more features without affecting detection accuracy and nine orientations under a single normalization. 10 We consider both the directed and undirected gradient orientations of the histogram in our descriptor (IHOG). The key distinction from the HOG description is this. It is more accurate as we investigate both directed and undirected orientation. By using a heuristic technique, we select a window size for feature creation that, in our case, is $35*40$ and where the gradient orientation is quite strong for identifying the region of interest.

4.4.2.3 Improved Accelerated KAZE feature extraction

To produce the feature $F3$, the enhanced accelerated KAZE feature extraction technique is applied to upper lid of eye region. The AKAZE algorithm discovers features using a four step framework as a quick multiscale feature finding and description technique:

- (i) Employing a non-linear filtering function to create a non-linear scale space that can be rectified through the FED method;
- (ii) Identification of features by a normalized Hessian matrix among various sizes;
- (iii) Determining the prevailing orientation as well as creating M-LDB descriptors
- (iv) Feature classification utilizing the Hamming distance as a correspondence metric. The SRP-AKAZE method uses a similar nonlinear size space building along with a feature discovery scheme as the AKAZE method, but in the last two steps, new operations are done to improve the algorithm's robustness and distinctness.

a) SRP-SIFT descriptor

i) Searching for the dominant direction: To achieve rotation invariance, the dominant orientation of the feature values is chosen based on their nearby picture model. If the size limit is set to I the dominant direction look for region will be a circle with a radius of $6\sigma_i$, centered at the target point. The Gaussian function weights the first-order differential ideals of B_x and B_y of each and every adjacent point inside the search region, so that the earlier they are to the feature values, the larger their involvement. The circular neighborhood is scanned using a sliding window with a 60° fan, and the total of the vectors in the fan is detected, with the greatest vector is chosen as the dominating direction.

ii) Building the feature descriptor: An $n \times n$ piece located in the middle of the target spot is retrieved on a known size as well as rotated to match the foremost direction of a 11 specification for a picture. We'll use $n = 41$ in this case. The patch's horizontal and vertical gradient maps can then be connected to form an input vector Z . The contribution vector thus has N elements, where $N = 2 \times n - 2 \times n - 2$ arbitrary dimension matrix R describes the very sparse arbitrary projection process. When dealing with huge photos, the sparse arbitrary matrix $R \times M \times N$ is developed to decrease computing difficulty.

b) Feature matching

By comparing the feature description vectors of two photos, it is possible to find the matching feature vectors. The closest neighbor is located using the most effective bin first [23] search technique. After obtaining two nearest neighbour feature vectors

$V_j = (v_{j1}, \dots, v_{jm})$ and $V_p = (v_{p1}, \dots, v_{pm})$ for each feature point vector $U_i = (u_{i1}, \dots, u_{im})$, the nearest neighbour distance ratio algorithm is used to find the optimal matching point

$$d(U_i, V_j) = \sum_{m=1}^M |u_{im} - v_{jm}|$$

$$d(U_j, V_p) = \sum_{m=1}^M |u_{jm} - v_{pm}|.$$

The matching findings are then verified again using the random sample consensus technique.

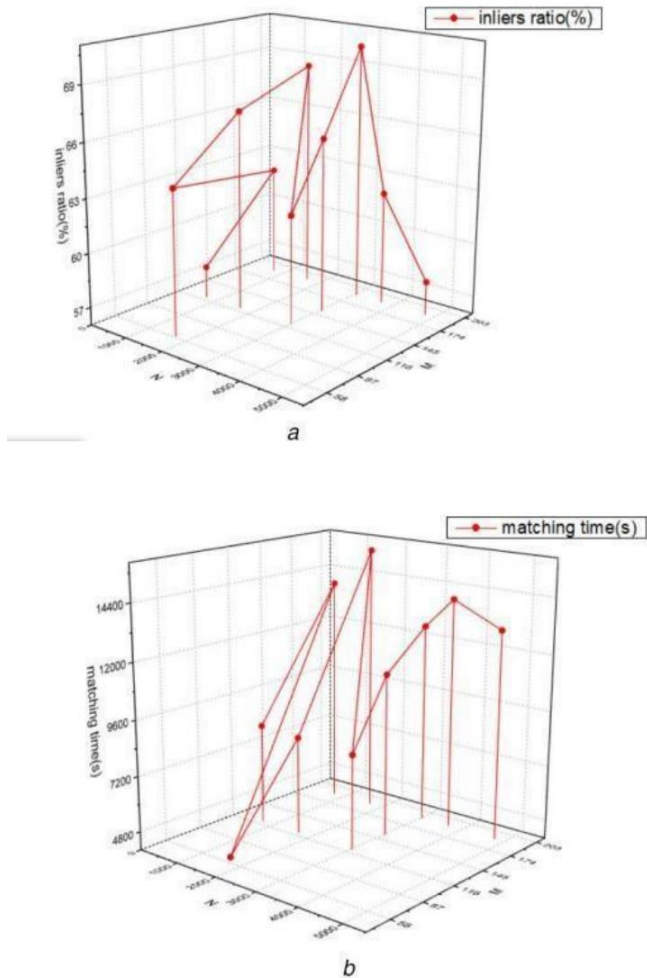


Figure. 4.43 Resultant Image (a) Representation of Inliers ratio, (b) Representation Matching time

4.4.2.4 Feature Retrieval by Local Patterns of Gradient (LPOG)

The LPOG feature extraction algorithm can extract the lower eye fold characteristics. The LPOG is explored in this section. This method encodes neighboring patterns in the appearance of histogram order using the BELBP and LPQ methods which are explained below on gradient imagery. Finally, by concatenating BELBP and LPQ descriptions, a novel feature extraction approach (LPOG) is created. So go over the BELBP and LPQ explanations in detail first. block-wised Elliptical local binary patterns (BELBP) An image S's block-wised ELBP (BELBP) operator is created by first producing two accumulating images (AI) that correspond to two block patterns (BP) as follows:

$$AI_{\nu^{BP}} h i j = \frac{1}{\sum_{i,j \in P} BP S i j} \quad (6)$$

For horizontal AI, the block patterns BPs are directed rectangular and horizontal, whereas, for vertical AI, they are vertical. This method employs a symmetric pair of BELBPs with 3 x 5 and

5 x 3 block layouts. When retrieving the nearby small texture of all pixels of the input picture S (i,j), the dependence between each pixel and its neighbors is taken into account.

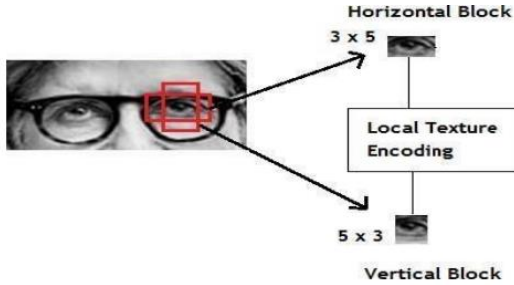


Figure. 4.44 Local Patterns of Gradient (LPOG)

Furthermore, utilizing a symmetric couple of BELBPs instead of a single horizontal BELBP provides an additional discriminative illustration of the face picture. As a result, every input image generates two BELBP images. Figure.8 depicts this. The BELBP code of each AI picture pixel is then calculated by matching its value to that of neighboring pixels on an ellipse whose center is at the present pixel. The BELBP label of one pixel is calculated using the following formula: The formula for determining the BELBP label of a single pixel with M adjacent pixels, horizontal radius R1 as well as vertical radius R2 is: P=AI is:

$$\text{BELBP}(i_c, j_c) = \sum_{i=1}^K S g_i - g \ 2^{i-1}$$

where S is the color of P as well as the color of its surrounding pixel value.

Local Phase Quantization (LPQ)

In LPQ, each NxN neighborhood of the center pixel in the original picture I is first subjected to the discrete Fourier transform. The DFT helps in the separation of the picture into segments of changing significance. The DFT translates a picture from the spatial sphere to the frequency sphere, comparable to the discrete Fourier transform. The following is a popular definition of a 2D DFT of an input picture I (x, y) of size M × N

$$F_v = \frac{1}{\sqrt{M}} \sum_{x=0}^{M-1} \sum_{y=0}^{N-1} I_{x,y} e^{-j2\pi x + vy} / = \quad (8)$$

F_v is the DFT transformed image. $I_{x,y}$ is the input picture, as well as M, is the full amount of rows, as well as N, is the total no of columns. And then LBP is applied to DFT coefficients to encode them.

Feature Extraction using Local Patterns of Gradient (LPOG)

Using the formulas (9)-(10), two-directional gradient pictures beside the x-direction and ydirection (G_x, G_y) are created from the input image S. (5). The local patterns are then extracted from each gradient image using an even couple of BELBP with LPQ operators in the form of

BELBP and LPQ images.

$$G_x = \frac{1}{2} \cdot S - 1 + 0 \cdot S + 1 \cdot S + 1 \quad 9$$

$$G_y = \frac{-1}{2} \cdot S - 1 + 0 \cdot S + \frac{1}{2} \cdot S + 1 \quad 10$$

The histogram sequences of each local pattern picture are then calculated and concatenated to generate an image description.

Algorithm of LPOG

Input: Image S, Current Pixel value, Current X Index, Current Y Index

Output: LPOG Bin

Algorithm:

Apply the below steps for all pixels in an input image

1. Apply gradient response of the x-axis and y-axis on the input image S to get the gradient image Gx and Gy.
2. Get the horizontal neighboring blocks with the size 3 x 5 and the vertical neighboring blocks with the size 5 x 3 of current pixel Sc on the Gx.
3. Get the neighborhood blocks of the current horizontal and vertical blocks.
4. Then compare the neighborhood block with the current blocks
5. If the neighborhood block value is greater than the current block value put 1
6. Otherwise, put 0. Then discover the description cost which is called BELBP description
7. Then store the description into the array which is called BELBP bin
8. And then get the surrounding pixels Sp of current pixel Sc depending on the pixel space P on gradient image Gy.
9. Apply DFT on Sp along with Sc to convert pixel into DFT Coefficient.
10. Then compare the current DFT Coefficient DFTCc with that of the neighboring DFT Coefficient DFT Cp.
11. If the center pixel DFTCc is greater than the neighboring pixel DFTCp put the value 1
12. Else put the value 0
13. Then convert these binary numbers into the decimal value
14. This is called LPQ description
15. Then store the description into the array. This array is called LPQ bin
16. Then combine the BELBP bin and LPQ bin to form the LPOG bin

4.4.3 Feature Retrieval by Local Patterns of Gradient (LPOG)

Let V_t denote the retrieved features from the test image represented by

$$V_t = [V_1 \ V_2 \ V_3 \ V_4 \ V_5] \quad (11)$$

V represents the features taken from the K number of train photos.

$$V_k = [V_{1,1} \ V_{2,1} \ V_{1,2} \ V_{2,2} \ V_{3,1} \ V_{4,1} \ V_{5,1} \ V_{3,2} \ V_{4,2} \ V_{5,2} \ \vdots \ V_{1,K} \ V_{1,K} \ \vdots \ \vdots \ V_{1,K} \ V_{1,K} \ V_{1,K}] \quad (12)$$

Where $k = 1, 2, \dots, K$ and K represent the number of photos that have been taught. The five distinct features derived from the k th training image are $V_1 k, V_2 k, V_3 k, V_4 k, V_5 k$.

The feature matching is done by estimating the cumulative similarity score between the features V_1, V_2, V_3, V_4, V_5 and $V_1 k, V_2 k, V_3 k, V_4 k, V_5 k$. The similarity score estimated between the test image and the K number of train images is given by, $T = [T_1 \ T_2 \ T_3 \ \dots \ T] \ T$. The matched periocular R can be estimated by the minimum similarity score

$$R = T = \arg \min_k [T_1 \ T_2 \ T_3 \ \dots \ T]^T \quad (13)$$

4.4.4 RESULT AND ANALYSIS

4.4.4.1 Experimental Images

The effectiveness of the proposed periocular recognition algorithm underwent assessment using datasets including UBIPr [36], CASIA-Iris distance, and AR datasets, with representative sample images illustrated in the figure below. The evaluation employed metrics such as rank-1 and rank-5 recognition accuracy, equal error rate (EER), and area under the ROC curve (AUC)(Ramachandra & Ramachandran, 2022).

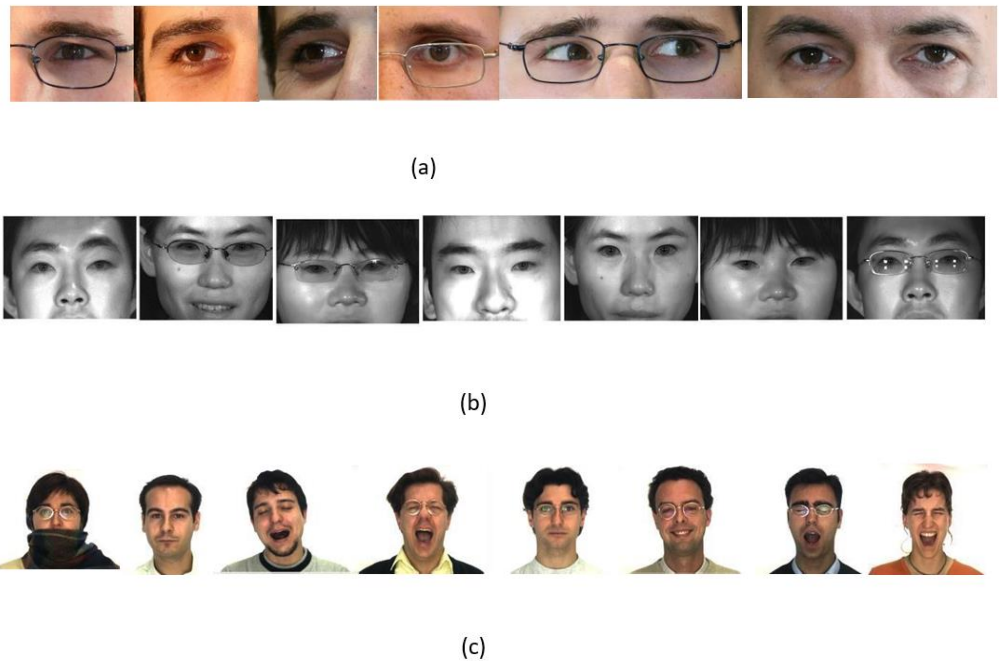


Figure. 4.45 Examples of test images from various datasets are provided: (a) from the UBIPr dataset, (b) from the CASIA-Iris distance dataset, and (c) from the AR dataset.

4.4.4.2 Experimental results

Performance evaluation utilized both single and dual periocular images from the UBIPr dataset. Figure 4.46 illustrates the feature retrieval process from one periocular region in the UBIPr dataset images(Ramachandra & Ramachandran, 2022).

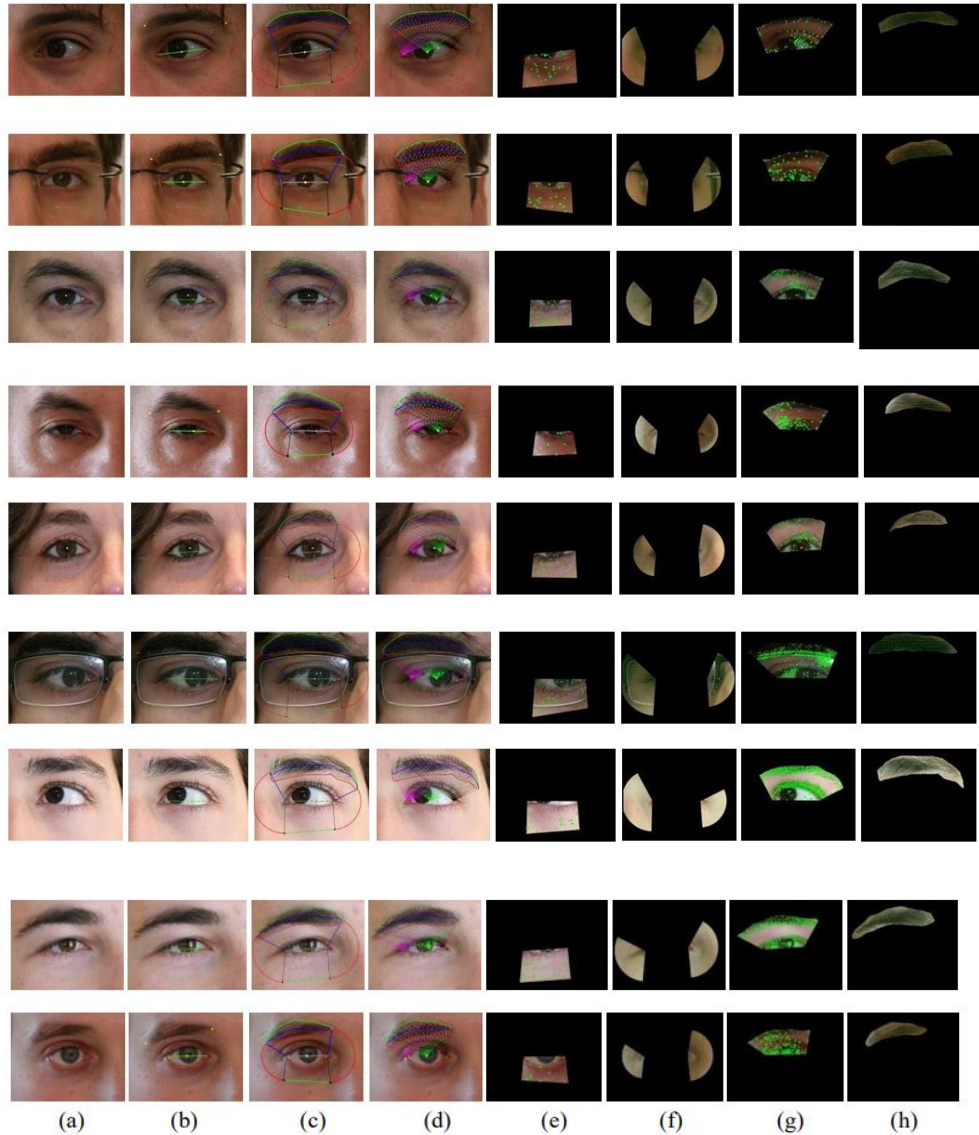


Figure. 4.46 Extraction of periocular features from single-eye UBIPr dataset images involves the following steps:(a) Detection of eye and eyebrow corners in the input periocular image,(b) Segmentation of the region of interest,(c) Extraction of eyebrow shape features,(d) Identification of features in the lower eye region,(e) Extraction of features from the corner eye regions,(f) Feature retrieval from the top of eye regions,(g) Feature retrieval from the eyebrow region.

The AR database comprises 4000 color face photos capturing frontal views of 70 men and 56 women, exhibiting various lighting conditions, occlusions, and facial expressions. The CASIA

iris distance dataset focuses on images featuring dual eye and face patterns. Additionally, the UBIPr dataset contains segmented single-eye and dual-eye versions of face images(Ramachandra & Ramachandran, 2022).

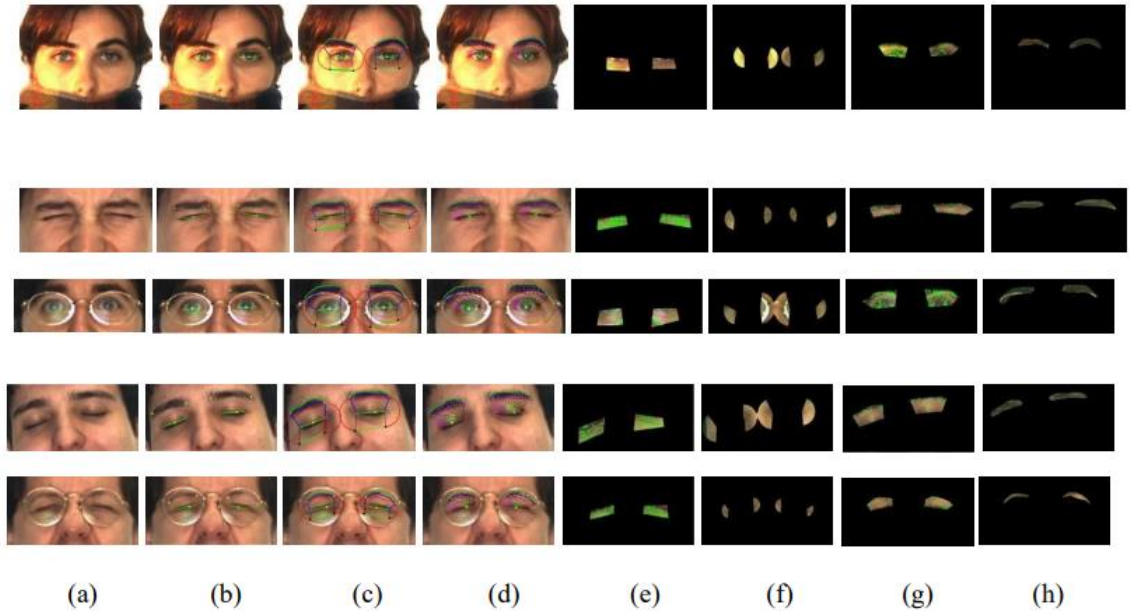


Figure. 4.47 Extraction of periocular features from the AR dataset involves the following steps:(a) Capturing the input periocular image.(b) Detection of eye and eyebrow corners.(c) Segmentation of the region of interest.(d) Extraction of eyebrow shape features.(e) Retrieval of features from the lower eye region.(f) Extraction of features from the eye corner regions.(g) Feature extraction from the upper eye regions.(h) Feature extraction from the eyebrow region.

The feature extraction from the AR dataset, CASIA-Iris dataset, and UBIPr dataset.

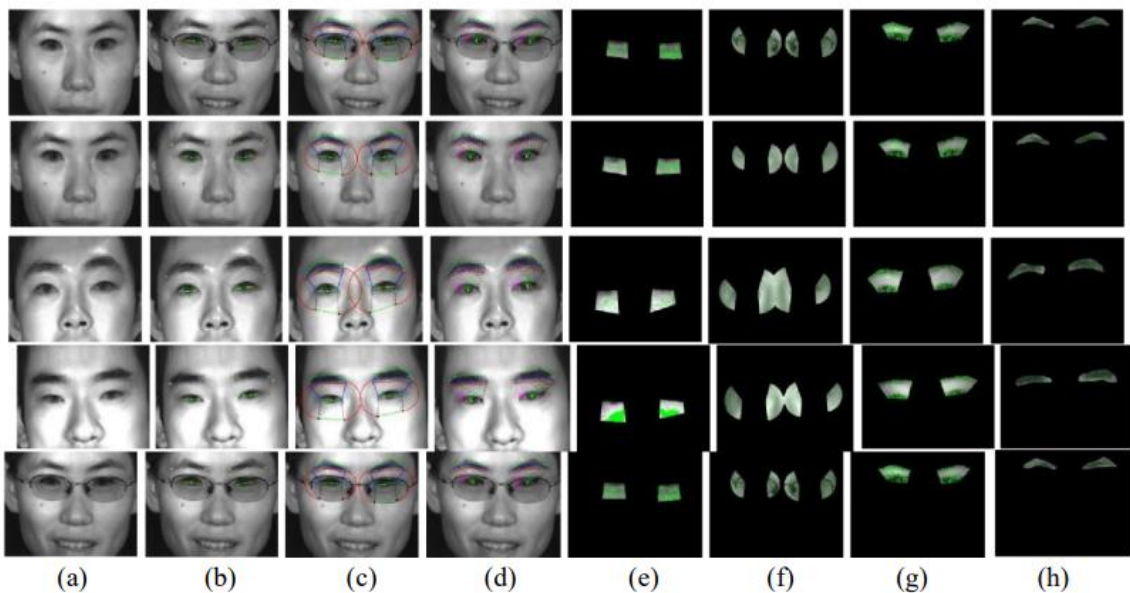


Figure. 4.48 Feature extraction from the CASIA-Iris dataset involves the following steps:(a) Input periocular image acquisition.(b) Detection of eye and eyebrow corners.(c) Segmentation of the region of interest.(d) Extraction of eyebrow shape features.(e) Retrieval of features from the lower eye region.(f) Extraction of features from the eye corner regions.(g) Feature extraction from the upper eye regions.(h) Feature extraction from the eyebrow region.

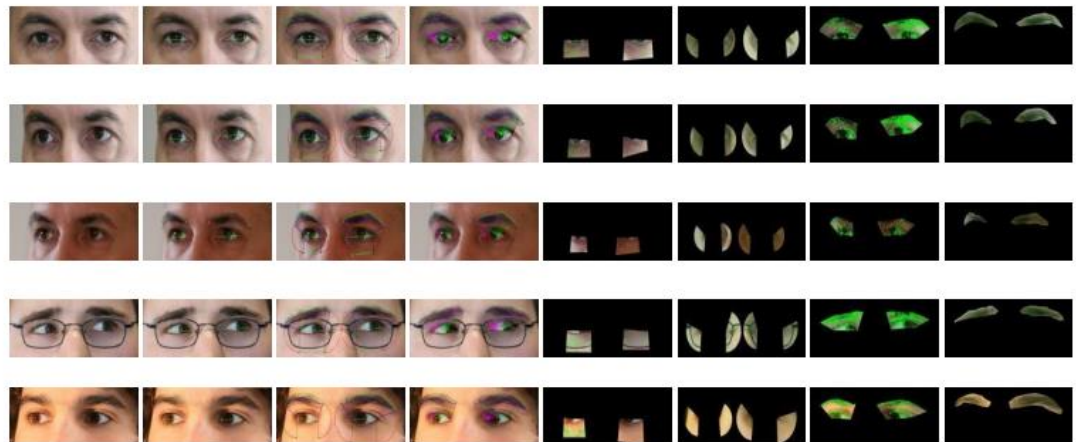


Figure. 4.49 Extracting features from the dual-eye periocular region in the UBIPr dataset involves the following steps:(a) Capturing the input periocular image.(b) Detecting the corners of the eyes and eyebrows.(c) Segmenting the region of interest.(d) Extracting features related to eyebrow shape.(e) Retrieving features from the lower eye region.(f) Extracting features from the eye corner regions.(g) Performing feature extraction on the upper eye regions.(h) Extracting features from the eyebrow region.

4.4.4.3 Experiment No #1: Performance Analysis of Classifiers

Using the performance measures indicated above, the classifier system's performance is analyzed and contrasted with that of other techniques. The tables and graphs below demonstrate this.

Table 4.12 Performance Evaluation of EER and AUC with the existing approaches

Scheme	UBIPr		CASIA-Iris		AR	
	EER (%)	AUC	EER (%)	AUC	EER (%)	AUC
ImageNet	7.11 ± 2.9	0.9805	8.06 ± 5.3	0.9533	14.53	0.9363
Iris recognition	5.07 ± 2.2	0.9877	7.51 ± 1.1	0.9674	7.69	0.9751
Clustering	5.46 ± 1.5	0.987	6.10 ± 2.2	0.9738	9.4	0.9692
LCNN	6.34 ± 2.1	0.9849	6.34 ± 1.6	0.9719	9.39	0.9737
Multilevel	4.09 ± 2.1	0.9913	8.69 ± 1.1	0.9594	7.69	0.9756
VGG16	4.38 ± 1.3	0.9892	7.42 ± 1.7	0.9681	7.69	0.9747
OC-LBCP	3.41 ± 1.8	0.9938	4.35 ± 0.5	0.986	5.13	0.9882
Proposed	2.88 ± 1.6	0.9969	3.11 ± 0.4	0.9978	3.85	0.9961

The proposed approach's performance was compared against conventional methods including ImageNet, iris recognition, clustering, LCNN, multilevel, VGG16, and OC-LBCP. Table 4.12 contrasts the EER and AUC of the proposed method with those of conventional methods. The EER of the proposed method is lower than that of conventional methods for all three datasets. Specifically, for the UBIPr, CASIA Iris, and AR datasets, the proposed method achieves an EER of 2.88, 3.11, and 3.85, respectively. Furthermore, the AUC of the proposed method surpasses 0.99 for each of the three datasets, indicating its superior performance compared to conventional methods(Ramachandra & Ramachandran, 2022).

Table 4.13 Comparison of recognition accuracy at Rank-1 and Rank-5 levels.

Scheme	UBIPr		CASIA-Iris		AR	
	Rank-1	Rank-5	Rank-1	Rank-5	Rank-1	Rank-5
ImageNet	84.88 ± 2.5	96.01 ± 1.8	95.00 ± 1.8	96.98 ± 2.5	93.59	96.75
Iris recognition	90.30 ± 1.2	97.41 ± 1.1	95.95 ± 2.1	98.15 ± 0.6	95.24	98.38
Clustering	90.24 ± 1.4	97.36 ± 0.4	96.09 ± 2.1	98.10 ± 0.4	94.19	97.75
LCNN	90.28 ± 1.7	97.18 ± 0.7	96.01 ± 2.0	97.85 ± 0.9	94.27	97.52
Multilevel	90.75 ± 1.0	97.44 ± 0.3	95.81 ± 1.9	97.67 ± 1.0	96.07	98.71
VGG16	90.24 ± 1.4	97.09 ± 1.1	95.88 ± 0.1	97.99 ± 0.5	94.2	97.61
OC-LBCP	91.28 ± 1.2	98.59 ± 0.4	96.62 ± 1.3	98.45 ± 0.4	96.32	98.8
Proposed	94.85 ± 1.2	99.13 ± 0.3	98.31 ± 1.5	99.15 ± 0.9	98.99	99.34

Table 4.13 presents a comparison of the rank-1 and rank-5 recognition accuracy between the proposed method and conventional approaches across the three datasets. The suggested method demonstrates superior performance compared to conventional methods in both rank-1 and rank-5 recognition accuracy for all three datasets. Notably, the rank-5 recognition rate surpasses the rank-1 recognition accuracy by 6.41%, 1.54%, and 1.25% for the UBIPr, CASIA Iris Distance,

and AR datasets, respectively. Specifically, the rank-1 and rank-5 recognition accuracies for single-eyed periocular images in the UBIPr dataset are calculated as 87.86% and 98.23%, while for dual-eyed periocular images, they are 96.78% and 99.23%, respectively. These results indicate that the proposed technique exhibits higher identification rates for dual-eye periocular images compared to single-eyed periocular images(Ramachandra & Ramachandran, 2022).

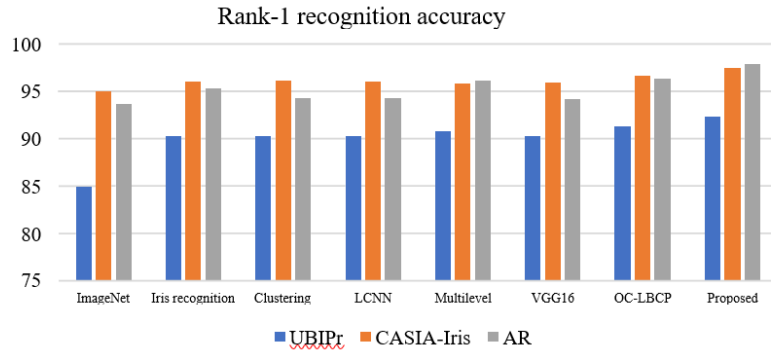


Figure. 4.50 Comparison of rank-1 and rank-5 recognition accuracy performance

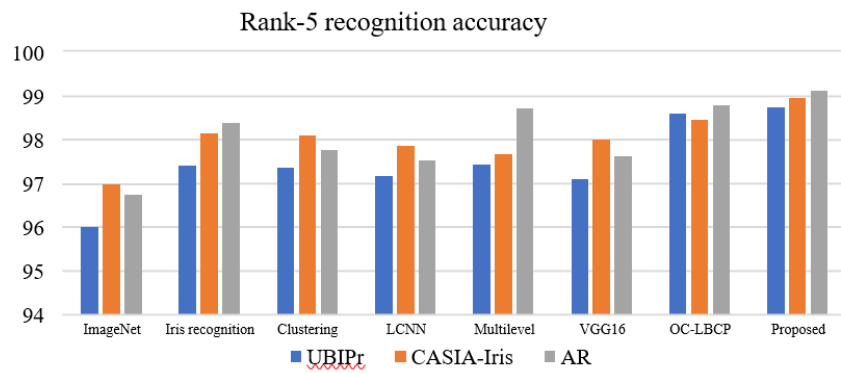


Figure. 4.51 Comparison of rank-5 recognition accuracy performance

The rank-1 and rank-5 recognition accuracy of both the suggested method and the conventional method are depicted graphically in Figures 4.50 and 4.51. The rank-1 recognition accuracy for the UBIPr dataset, the CASIA-Iris distance dataset, and the AR dataset is estimated at 94.85%, 99.15%, and 99.34%, respectively. The subsequent section presents the culmination of the newly developed approach(Ramachandra & Ramachandran, 2022).

Table 4.14 Evaluation of area under curve and EER in Comparison to Existing Approaches

Scheme	UBIPr		CASIA-Iris		AR	
	EER (%)	AUC	EER (%)	AUC	EER (%)	AUC
Histogram	0.0417	0.9583	0.0497	0.9503	0.0637	0.9363
HOG	0.0229	0.9771	0.0309	0.9691	0.0449	0.9551
IHOG	0.0088	0.9912	0.0168	0.9832	0.0308	0.9692
SIFT	0.0043	0.9957	0.0123	0.9877	0.0263	0.9737
AKAZE	0.0024	0.9976	0.0104	0.9896	0.0244	0.9756
IAKAZE	0.0014	0.9986	0.0094	0.9906	0.0136	0.9864
DLBP	0.0127	0.9873	0.0207	0.9793	0.0347	0.9653
LTP	0.0038	0.9962	0.0118	0.9882	0.0258	0.9742
LPOG	0.0016	0.9984	0.0036	0.9964	0.0088	0.9912

	EER			EER			
	IAKAZE	0.0014	0.9986	0.0094	0.9906	0.0136	0.9864
DLBP	0.0127	0.9873	0.0207	0.9796	0.0347	0.9653	
LTP	0.0038	0.9962	0.0118	0.9883	0.0258	0.9742	
LPOG	0.0016	0.9984	0.0036	0.9962	0.0088	0.9912	

Table 4.15 Performance Evaluation of EER and AUC

Table 4.15 presents a comparative analysis between the proposed method and conventional approaches in terms of error rates and recognition accuracy. For the UBIPr, CASIA-Iris distance, and AR datasets, recognition accuracy is estimated to be 99.84%, 99.64%, and 99.12%, respectively, showcasing superior performance over conventional methods. Hence, the proposed method stands out as the optimal choice for periocular area recognition(Ramachandra & Ramachandran, 2022).

4.4.5 CONCLUSION

This study presents a periocular recognition approach that aggregates data from four distinct regions: the eyebrow, upper and lower eye folds, and eye corner. Enhanced accelerated KAZE and updated HOG feature extraction methods are employed to extract features from the brow,

upper eye fold, and eye corner regions. Features related to eyebrow shape are derived from height and width measurements along the eyebrow's top and bottom edges. Additionally, a sub-image-based neighbor gradient feature extraction technique is utilized for the lower eye fold region(Ramachandra & Ramachandran, 2022). Performance evaluation, conducted on UBIPr, CASIA-iris, and AR datasets, includes metrics such as rank-1, rank-5 recognition accuracy, EER, and AUC. The AUC values for UBIPr, Casia-iris, and AR datasets are 0.9978, 0.9969, and 0.9961, respectively. Furthermore, the rank-1 recognition accuracies for these datasets are 94.85%, 99.15%, and 99.34%, respectively. The proposed periocular recognition method surpasses standard algorithms and demonstrates efficacy in identifying individuals using only the periocular region of the face(Ramachandra & Ramachandran, 2022).

4.5 Training Strategy Using empirical multivariate mode and CNN for eye area Identification: An Ensemble Approach

4.5.1 Introduction

The development and refinement of periocular recognition technology have become increasingly crucial in the realm of biometric security, particularly for identifying individuals when the full face is obscured or partially visible. The introduction of an ensemble training approach that leverages a FA-MVEMD alongside Convolutional Neural Networks (CNN) marks a significant advancement in this field. This methodology begins with the preprocessing of periocular images, followed by their decomposition using single-level discrete wavelet transform into four distinct coefficients. Breaking down the Low-Low (LL) coefficients with FA-MVEMD results in K+2 ensemble images derived from intrinsic mode functions (IMFs), residuals, and High-High (HH) coefficients. With rank-1 recognition accuracies surpassing 93% across various datasets, such as UBPIr, AR, and CASIA Iris. This level of precision is particularly notable in environments where traditional facial recognition systems falter, such as when subjects wear masks or other face-obscuring items. By focusing on the periocular region, which encompasses features around the eye including the eyebrow, cheekbone, and eye folds, the system provides a robust solution for recognizing individuals in less-than-ideal conditions. This has profound implications for security and surveillance, especially in scenarios where individuals may attempt to conceal their identity using facial coverings.

The ensemble training approach distinguishes itself by generating multiple ensemble images for each periocular image, employing a combination of DWT for initial decomposition and FA-MVEMD for further processing of the LL band images. This technique not only enriches the

training dataset but also enhances the model's ability to recognize periocular features under various conditions. The inclusion of CNN in this methodology underscores the role of deep learning in advancing biometric recognition technologies, providing a powerful tool for feature extraction and classification based on the complex patterns found in periocular regions.



Figure. 4.52 Few examples for periocular images

Furthermore, the versatility and effectiveness of this approach are evident through its comparative analysis with existing methods, including local and global feature extraction techniques like Local Binary Pattern (LBP), Scale-Invariant Feature Transform (SIFT), and block histogram of gradients (HOG). The ensemble training method, with its focus on generating a diverse set of ensemble images for training, offers a significant improvement over traditional methods, particularly in dealing with the challenges posed by partial facial recognition and the degradation of performance due to facial coverings or expressions.

In conclusion, the proposed ensemble training approach utilizing FA-MVEMD and CNN for periocular recognition represents a significant leap forward in biometric technology. Its ability to accurately recognize individuals based on the periocular region, even in challenging conditions, not only enhances security measures but also opens up new avenues for application in various fields. As this technology continues to evolve, it holds the promise of becoming an indispensable tool in the ongoing effort to improve identification and verification processes in a world where the ability to quickly and accurately recognize individuals is of paramount importance.

4.5.2 Proposed periocular recognition algorithm

The suggested algorithm for periocular recognition comprises five key phases, including (i) Pre-processing, (ii) Application of Single Level Discrete Wavelet Transforms, (iii) Creation of Ensemble Images, (iv) Model Training, and (v) Model Evaluation. A diagrammatic representation of this system is illustrated in the provided figure.

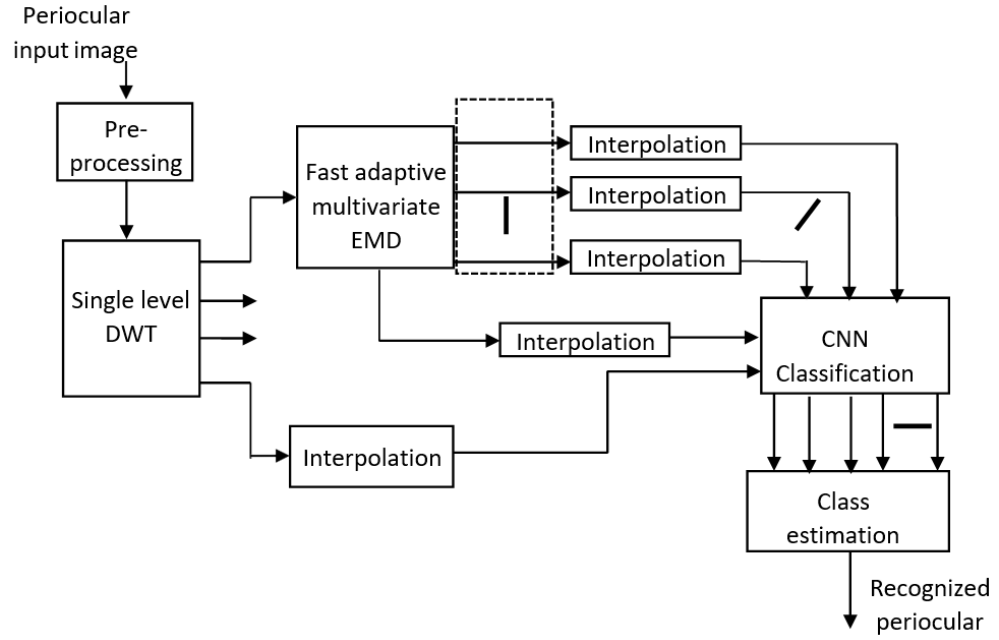


Figure. 4.53 Schematic illustration of the suggested approach for periocular identification

(a). Pre-processing

Assume the original periocular image to be denoted as I_1 . This stage involves several adjustments: cropping to isolate the periocular area, resizing to a standard dimension of $M \times N$, and applying a high-pass filter to mitigate any blurring introduced by the camera lens. The outcome of this process is referred to as I_2 (Ramachandra & Ramachandran, 2022).

(b) Discrete Wavelet Transformation

At this phase, the polished image is prepared for creating a collection of training images. This is achieved through decomposition algorithms, specifically single-level Discrete Wavelet Transform (DWT) and Fast Adaptive Multivariate Empirical Mode Decomposition, which break down the image into various frequency bands. Assume the pre-processed image is denoted as I_2 . This image I_2 undergoes decomposition via a single-level DWT, resulting in the extraction of frequency bands LL , LH , HL , and HH . The coefficients of the LL and HH bands are then represented accordingly(Ramachandra & Ramachandran, 2022).

I_3 and w as denoted in Figure. 3 whose dimension is $(M_2 \times N_2)$. The HH band coefficient

w Then it is interpolated by 2 to obtain the interpolated HH band W . The coefficient

W has the dimension of $M \times N$.

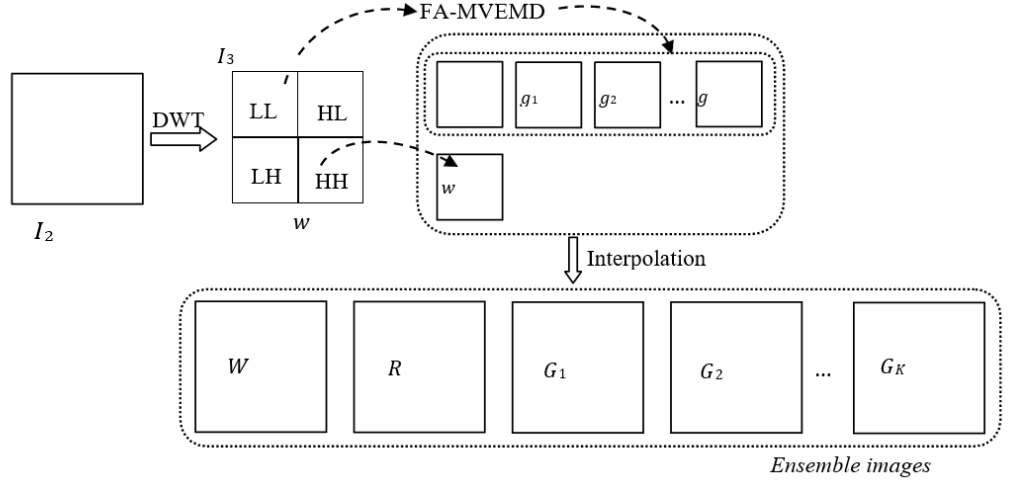


Figure. 4.54 Illustration of DWT decomposition and compilation of ensemble images for training image assembly

The *LL* band coefficients, denoted as I_3 , are subjected to further decomposition through FA-MVEMD to yield set of K Intrinsic Mode Functions (IMF) along with a residual component. Consider I_3 as the image processed via empirical mode decomposition. The steps of the FA-MVEMD process are outlined as follows:

Algorithm: Fast Adaptive MVEMD Procedure

Input: Coefficients of LL band I_3 , Desired IMF count K

Output: Sequence of IMFs $g_1, g_2, g_3 \dots, g$ plus residual component

Initialize: $h_1 = I_3$.

Step 1: Determine the amplitude and location of local minima in the image h_1 . Likewise, assess the amplitudes and locations of local maxima in the signal h_1 .

Step 2: By leveraging the amplitude and position of local minima, calculate the lower envelope via spline interpolation, denoting this as F_k . In a similar manner, utilize the position and amplitude of local maxima to compute the upper envelope with spline interpolation, marking this as F_{k+} . In this context, l represents the iteration step, and k ranges from 1 to K .

Step 3: Calculate the mean μ_k of both the lower and upper envelopes across all positions as given by

$$\mu_k = F_{kl} - 2x \cdot y + F_{k+1} - 2x \cdot y \quad (1)$$

Step 4: The mean envelope μ_k is deducted from the preceding signal as illustrated by

$$h_k = h_{k-1} - \mu_k \quad (2)$$

Step 5: Determine if the signal h_k qualifies as an IMF by evaluating the specified condition.

$$|\mu_{kl}| < \Delta \quad \forall \quad (3)$$

In this context, Δ represents the threshold level determining the termination point of the

iterative process.

Step 6: If equation (3) meets the specified criteria, the iteration process may conclude. Should the condition within the equation remain unmet, the procedure from steps 1 to 5 should be reiterated until fulfillment is achieved.

Step 7: Once the stopping criterion is met, the IMF is derived from the latest outcome of h_k

$$g_k = h_k \quad (4)$$

Step 8: The residual is determined through the specified relationship.

$$\eta_k = h_k - g \quad (5)$$

Step 9: The subsequent IMF is derived by iterating the aforementioned procedures, using the residual η as the input signal.

$$h_{k+1} = \eta_k \quad (6)$$

The ultimate residual, denoted by η , after extracting K IMFs, relates to the original image I_3 along with the IMFs in the following manner.

$$I_3 = \eta_k + \sum_{j=1}^k g_j \quad (7)$$

Consider the IMFs generated through FA-MVEMD as indicated by g_1, g_2, g_3, \dots, g and the residual image is denoted, with its dimensions specified as $(M \times N)$. The IMFs and the residual undergo interpolation by a factor of 2 to ensure their dimensions match $M \times N$. The interpolated IMFs and residual are then denoted accordingly G_1, G_2, G_3, \dots, G as depicted in Figure.3.

(d). Convolutional neural network

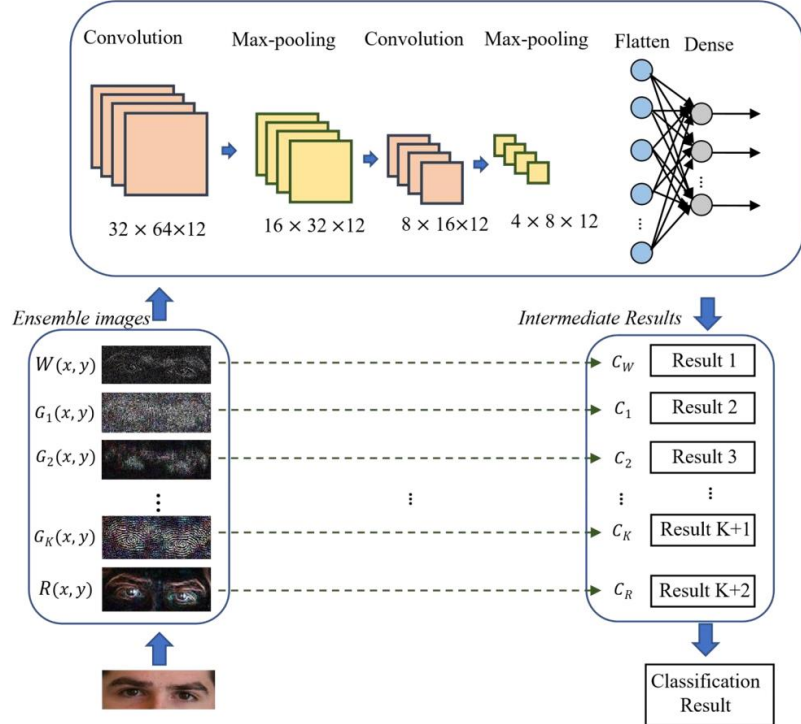


Figure. 4.55 Training Ensemble Images in a Convolutional Neural Network

Before being utilized in training or testing within the CNN framework, the ensemble images generated through DWT and FA-MVEMD are transformed into grayscale. The ensemble images fed into the CNN have dimensions of $M \times N = 32 \times 64$. Convolution operations are applied using the input pixel values and filter weights. With 12 convolutional filters employed, the convolution layer's output holds a dimensionality of $32 \times 64 \times 12$. To normalize the output values within a range of 0 to 1, a sigmoid activation function is employed post-convolution, maintaining the output dimensions at $32 \times 64 \times 12$. The sigmoid function is defined as

$$\sigma n = \frac{e^n}{1+e^{-n}} \quad (8)$$

Utilizing a 2×2 pooling window, the outcomes of the max-pooling process are reduced to dimensions of $16 \times 32 \times 12$. Following the second max-pooling layer, the feature dimensions decrease to $4 \times 8 \times 12$. The configuration of the CNN model is illustrated in Figure 4. Consider the intermediary outcomes derived for

Let the ensemble images, totaling $K+2$ in number, be denoted as -

$$P_i = \{P_{i1}, P_{i2}, \dots, P_{iK+2}\} \text{ where } P_i \in \{1, 2, \dots, N_{ss}\}$$

(9)

Where N_{ss} represents the total number of classes trained by the model. The ultimate outcome is derived from the intermediary result of the $K+2$ ensemble image as

$$\hat{P} = \{P_i \text{ if the length } P_i == P_i=1 \text{ otherwise not matching} \quad (10)$$

4.5.3 Experimental Analysis

The evaluation of the proposed scheme for periocular recognition utilizes datasets including UBIPr, AR, and CASIA-Iris, as illustrated in Figure 4.56 with select sample images. To assess the algorithm's performance, metrics such as the Equal Error Rate (EER), Area under the ROC Curve (AUC), rank-1 recognition accuracy, and rank-5 recognition accuracy were employed. The UBIPr dataset contains 10,950 images from 261 individuals, comprising 45.6% female and 54.4% male periocular images. It offers segmented periocular region images for both single and dual eyes. The AR dataset encompasses facial images under varied expressions, obstructions, and lighting, featuring 56 females and 70 males, totaling 4,000 images. The CASIA-Iris dataset includes dual-eye face images from 200 subjects, amassing 6,000 images at a resolution of 1968x1024. Experimental tests were conducted across different values of K ranging from 3 to 12. The model's validation involved using approximately 30% of the images per subject for testing, while the remaining approximately 70% were utilized for training purposes(Ramachandra & Ramachandran, 2022).

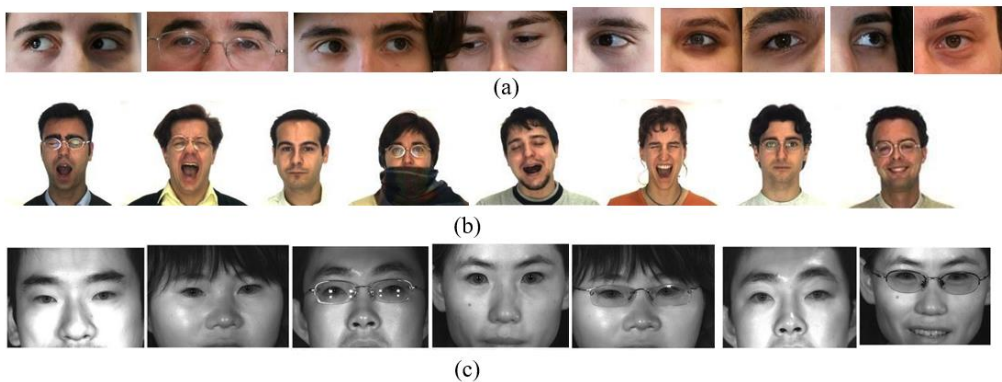


Figure 4.56 Example images for testing from various collections: (a) the UBIPr collection, (b) the AR collection, and (c) the CASIA-Iris distance collection.

Some experimental findings from the proposed system for recognizing periocular features within the UBIPr dataset are illustrated in Figure 4.57. Assessments were conducted on both single-eye and dual-eye periocular images. These findings were achieved with an IMF count of K=3. Ensemble images were derived from the HH band through DWT, alongside three IMF images, culminating with the residual, as shown in the subsequent figure.

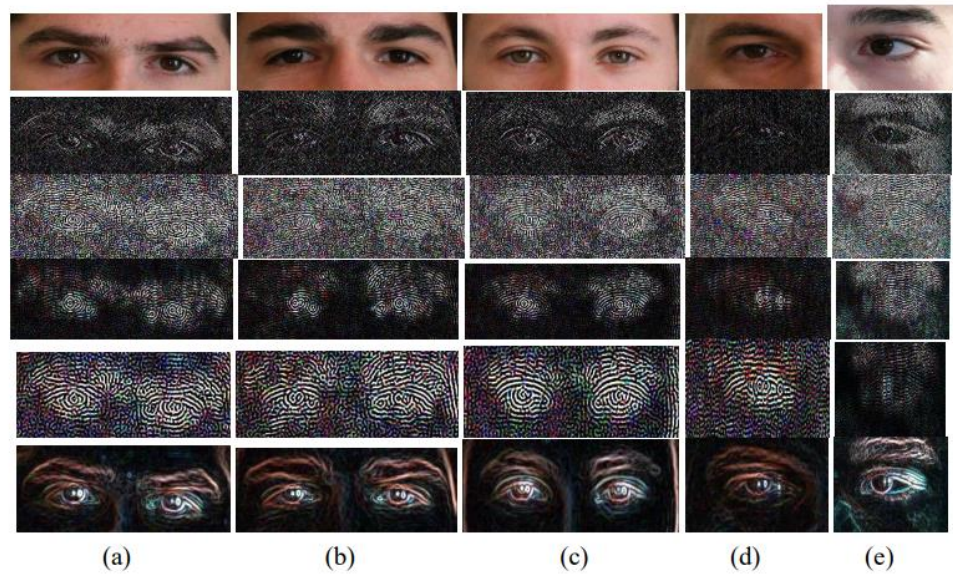


Figure. 4.57 Experimental outcomes from the periocular recognition approach using the UBIPr dataset include: (row 1) the original periocular image, (row 2) HH coefficients from single-level DWT, (row 3) the first IMF (IMF1) result, (row 4) the second IMF (IMF2) result, (row 5) the third IMF (IMF3) result, and (row 6) the residual result

Selected outcomes from the experimental application of the proposed periocular recognition method on the AR and CASIA-Iris datasets are illustrated in Figures 4.58 and 4.59, respectively. These outcomes were generated with a total of three Intrinsic Mode Functions (IMFs, K=3). The compiled images consist of the HH band derived from DWT, followed by three distinct IMF images, and ultimately, the residual image.

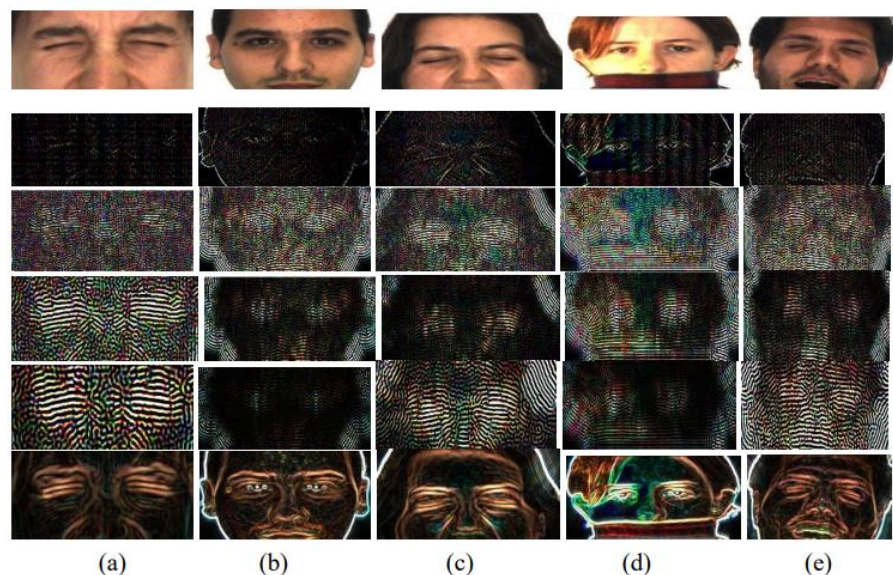


Figure. 4.58 Experimental findings from the periocular recognition system designed for the AR dataset are as follows: (row 1) showcases the initial periocular image, (row 2) displays HH coefficients obtained from single-level DWT, (row 3) presents the output of the first IMF (IMF1), (row 4) reveals the second IMF (IMF2) output, (row 5) illustrates the third IMF (IMF3) output, and (row 6) depicts the output of the residual.

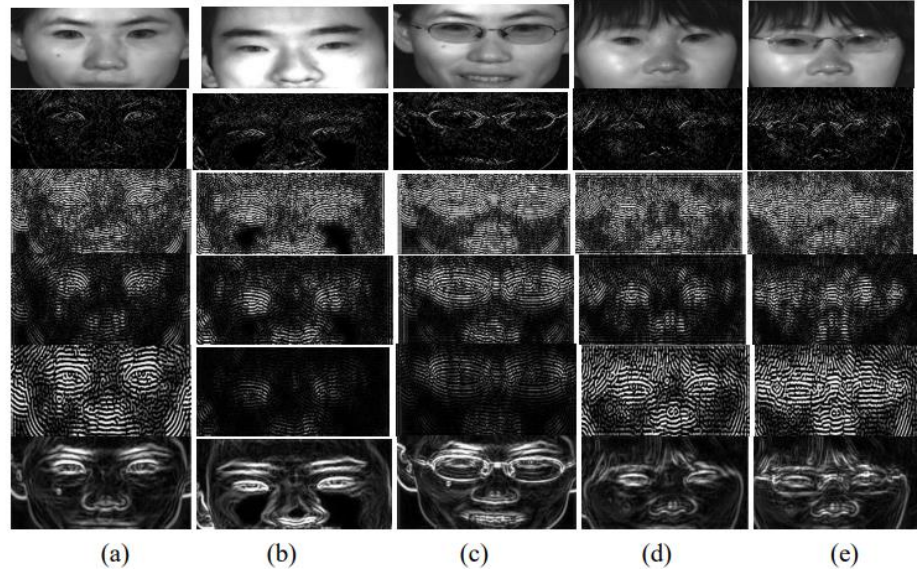


Figure. 4.59 Experimental outcomes for the CASIA-Iris distance dataset using the proposed periocular recognition framework include: (row 1) the provided periocular image, (row 2) HH coefficients from a single-level DWT, (row 3) output for the first IMF (IMF1), (row 4) output for the second IMF (IMF2), (row 5) output for the third IMF (IMF3), and (row 6) the resulting residual

Figure 4.59 illustrates that the high-frequency band (HH) of the Discrete Wavelet Transform (DWT) preserves the general contour of the periocular region, whereas the three Intrinsic Mode Functions (IMFs) capture periocular details across various frequency ranges. The residual component retains broader facial features.

Table 4.16 Contrasting the Equal Error Rate (EER) and Area under the Curve (AUC) of the proposed approach with conventional methods across various datasets

Scheme	UBIPr		AR		CASIA-Iris	
	EER (%)	AUC	EER (%)	AUC	EER (%)	AUC
ImageNet [57]	7.11 ± 2.9	0.9805	14.53	0.9363	8.06 ± 5.3	0.9533
VGG16 [39]	4.38 ± 1.3	0.9892	7.69	0.9747	7.42 ± 1.7	0.9681
Clustering [35]	5.46 ± 1.5	0.987	9.4	0.9692	6.10 ± 2.2	0.9738
Iris recognition [34]	5.07 ± 2.2	0.9877	7.69	0.9751	7.51 ± 1.1	0.9674
Multilevel [37]	4.09 ± 2.1	0.9913	7.69	0.9756	8.69 ± 1.1	0.9594
LCNN [36]	6.34 ± 2.1	0.9849	9.39	0.9737	6.34 ± 1.6	0.9719
OC-LBCP [38]	4.21 ± 1.8	0.9898	6.83	0.9782	6.35 ± 0.5	0.976
Attention [24]	3.91 ± 1.3	0.9909	5.93	0.9834	5.86 ± 0.7	0.9813
I-LBP [23]	4.03 ± 1.3	0.9901	6.27	0.9792	6.08 ± 1.3	0.9798
EN-IR [25]	3.75 ± 1.4	0.9913	5.49	0.9869	5.06 ± 0.5	0.9878
Proposed	2.87 ± 1.5	0.9961	4.71	0.9932	3.92 ± 0.5	0.9925

The effectiveness of the introduced technique was evaluated against a range of contemporary methods in periocular identification, such as EN-IR, I-LBP, attention mechanisms, OC-LBCP, LCNN, Multilevel analysis, Iris detection, Clustering algorithms, VGG16, and ImageNet. Table 1 outlines a comparative analysis against these technologies, with $K = 9$ as a reference point. For the datasets UBIPr, AR, and CASIA-Iris, the introduced method recorded EERs of 2.87%, 4.71%, and 3.92% respectively. Remarkably, the EER for this new method is reduced by 0.88%, 0.78%, and 1.14% in comparison to the EN-IR approach.

Furthermore, for the UBIPr, AR, and CASIA-Iris datasets, the new method showcased AUC scores of 0.9961, 0.9932, and 0.9925 respectively, outshining other recent technologies.

The analysis also included recognition precision using rank-1 and rank-5 measures. The newly proposed method registered rank-1 identification precision of 93.47%, 98.23%, and 98.03% for the UBIPr, AR, and CASIA-Iris datasets, respectively. When contrasted, this new ensemble training technique excels over the EN-IR method by 2.21%, 1.87%, and 1.32% in rank-1 identification precision across these databases.

Rank-5 identification precision reflects the accuracy of the top-5 predictions by the system. Here, the new approach marked rank-5 accuracies of 98.01%, 99.31%, and 99.14% respectively. Although the rank-5 accuracy for UBIPr dataset is slightly less by 0.02% compared to the EN-IR method, it outperforms the multilevel and EN-IR methods by 0.6% and 0.68% for the AR and CASIA-Iris datasets, respectively. These outcomes are detailed in the subsequent table.

Table 4.17 Contrast in recognition accuracy across the UBIPr, AR, and CASIA-Iris datasets

Scheme	UBIPr		AR		CASIA-Iris	
	Rank-1	Rank-5	Rank-1	Rank-5	Rank-1	Rank-5
ImageNet [33]	84.88 ± 2.5	96.01 ± 1.8	93.59	96.75	95.00 ± 1.8	96.98 ± 2.5
VGG16 [39]	90.24 ± 1.4	97.09 ± 1.1	94.2	97.61	95.88 ± 0.1	97.99 ± 0.5
Clustering [35]	90.24 ± 1.4	97.36 ± 0.4	94.19	97.75	96.09 ± 2.1	98.10 ± 0.4
Iris recognition [34]	90.30 ± 1.2	97.41 ± 1.1	95.24	98.38	95.95 ± 2.1	98.15 ± 0.6
Multilevel [37]	90.75 ± 1.0	97.44 ± 0.3	96.07	98.71	95.81 ± 1.9	97.67 ± 1.0
LCNN [36]	90.28 ± 1.7	97.18 ± 0.7	94.27	97.52	96.01 ± 2.0	97.85 ± 0.9
OC-LBCP [38]	90.28 ± 1.2	97.39 ± 0.4	95.32	97.8	95.92 ± 1.3	98.12 ± 0.4
Attention [24]	91.02 ± 1.1	97.89 ± 0.8	96.17	98.01	96.32 ± 1.2	98.32 ± 0.6
I-LBP [23]	90.81 ± 1.3	97.53 ± 0.7	95.86	97.93	96.12 ± 1.5	98.01 ± 0.5

EN-IR [25]	91.26 ± 1.2	98.03 ± 0.7	96.36	98.17	96.71 ± 1.3	98.46 ± 0.7
<u>Proposed</u>	<u>93.47 ± 1.4</u>	<u>98.01 ± 0.6</u>	<u>98.23</u>	<u>99.31</u>	<u>98.03 ± 1.2</u>	<u>99.14 ± 0.5</u>

Figure 4.60 illustrates a graphical representation of the rank-1 and rank-5 recognition accuracy for the UBIPr, AR, and CASIA-Iris datasets. It is evident from the plot that the proposed method outperforms other recent schemes, demonstrating superior performance in both rank-1 and rank-5 recognition accuracy.

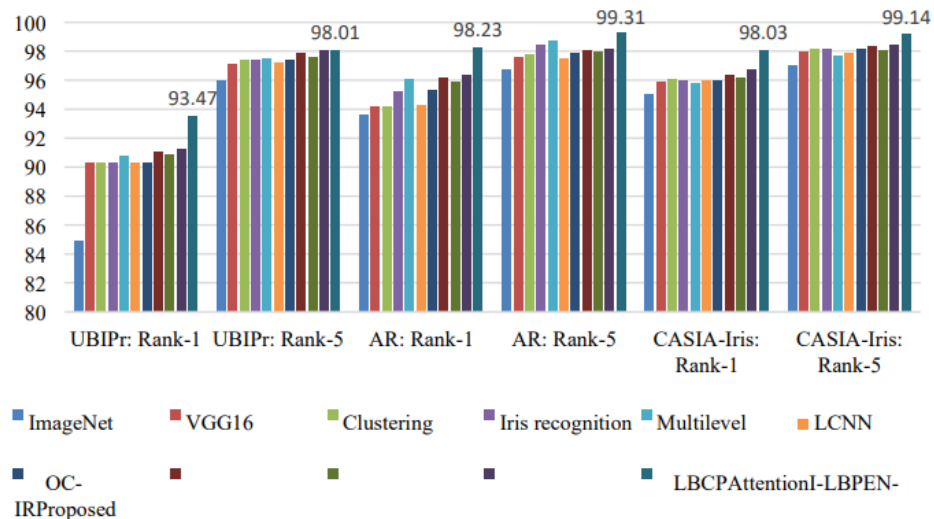


Figure. 4.60 Comparative graphical analysis of rank-1 and rank-5 recognition accuracy across various datasets

The evaluation of rank-1 and rank-5 recognition accuracy was conducted for different numbers of Intrinsic Mode Functions (IMFs) K . The assessment covered K values ranging from 3 to 12, resulting in ensemble images ranging from 5 to 14. It was observed that as K increased from 3, both rank-1 and rank-5 recognition accuracy improved, peaking at $K = 9$. However, with further increments in K , the recognition accuracy gradually declined(Ramachandra & Ramachandran, 2022). For instance, in the UBIPr dataset, the rank-1 recognition accuracy was 89.12% for $K = 3$, reaching a maximum of 93.47% at $K = 9$. However, with $K = 12$, the rank-1 recognition accuracy decreased to 93.04%, as shown in table 3.

Table 4.18 Rank-1 and Rank-5 recognition accuracy across varying numbers of Intrinsic Mode Functions (IMFs) K .

No. of IMFs K	Rank-1			Rank-5		
	UBIPr	AR	CASIA-Iris	UBIPr	AR	CASIA-Iris
3	89.12	93.79	92.87	93.66	94.87	93.98
4	90.24	94.17	93.76	94.78	95.25	94.87
5	90.76	94.92	94.19	95.3	96	95.3
6	91.37	95.88	95.76	95.91	96.96	96.87
7	92.42	96.72	96.91	96.96	97.8	98.02

8	93.36	98.01	97.83	97.9	99.09	98.94
9	93.47	98.23	98.03	98.01	99.31	99.14
10	93.21	98.08	97.91	97.75	99.16	99.02
11	93.17	97.92	97.68	97.71	99	98.79
12	93.04	97.79	97.52	97.58	98.87	98.63

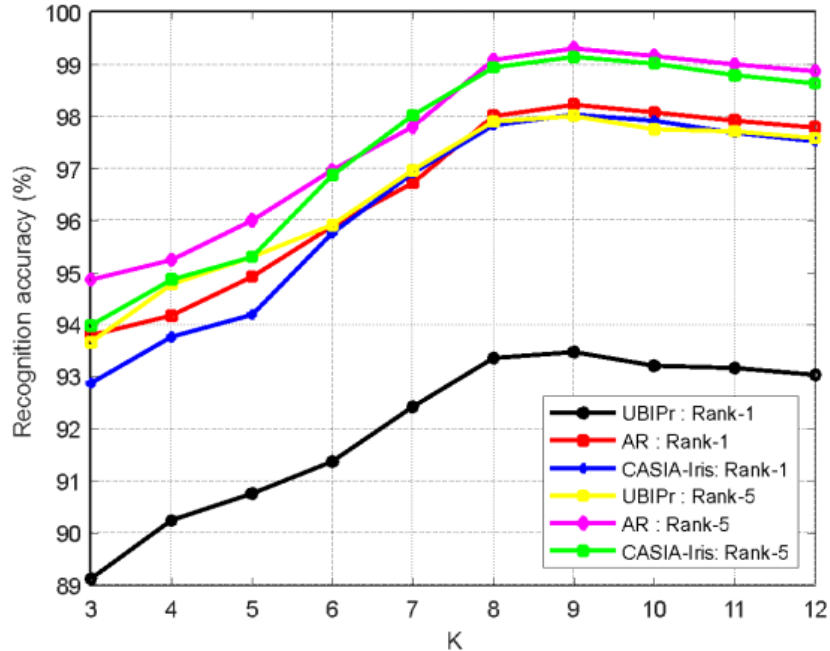


Figure. 4.61 Graphical comparison of rank-1 and rank-5 recognition accuracy for various values of K .

Figure 4.61 illustrates a graphical comparison of rank-1 and rank-5 recognition accuracy across different values of K for the UBIPr, AR, and CASIA-Iris datasets. Optimal performance is observed at $K = 9$. Additionally, Figure 11 presents the ROC comparison for various schemes across the UBIPr, AR, and CASIA-Iris datasets.

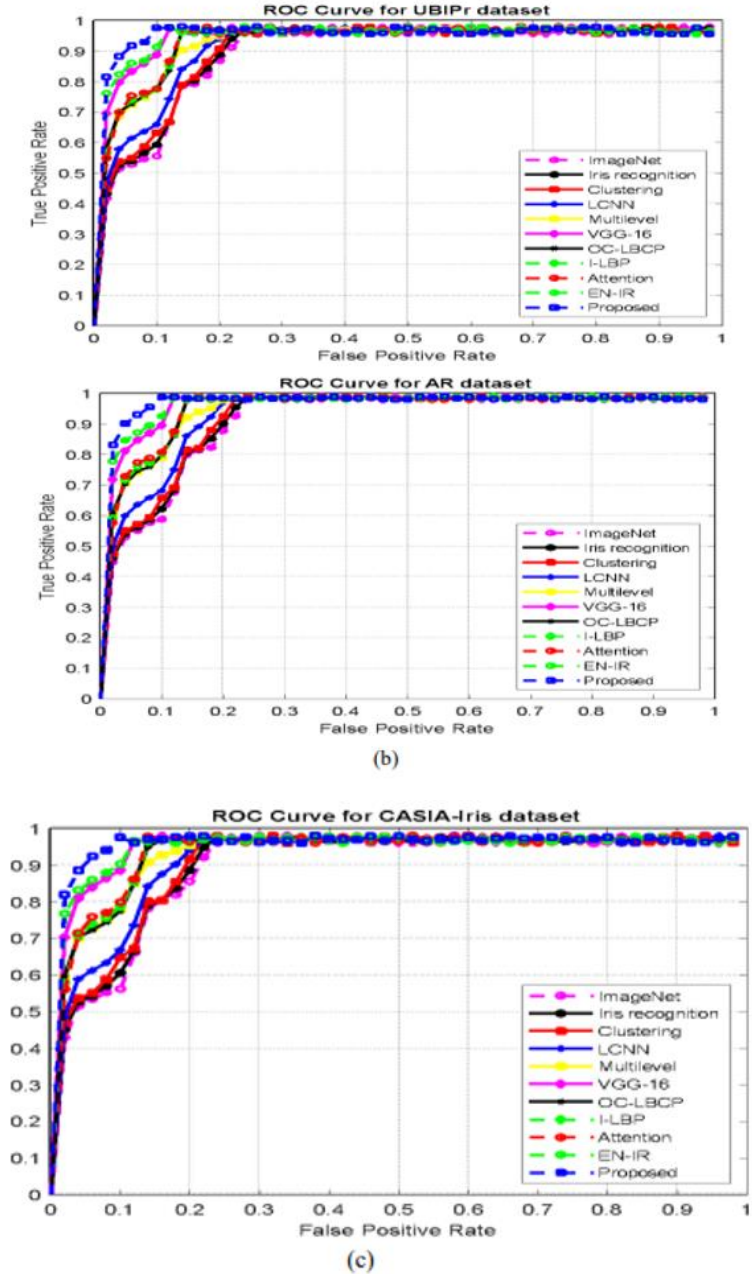


Figure 4.63 Comparing the ROC curves for different datasets: (a) UBIPr dataset, (b) AR dataset, and (c) CASIA Iris dataset.

The time complexity of the proposed periocular recognition algorithm was assessed using Matlab2018a on an Intel Core i5 processor with a clock speed of 3.00 GHz, 8GB RAM, running Windows 10, a 64-bit operating system. Denoting T_p , T_W , T_E , T_I , T_C and T_{C_tr} as the times for pre-processing, DWT estimation, EMD decomposition, interpolation(Ramachandra & Ramachandran, 2022), CNN classification, and CNN training respectively, the time for testing can be expressed as follows:

$$T_{test} = T_p + T_W + T_E + T_I + T_C \quad (11)$$

Table 4.19 Comparing time complexity for varying numbers of Intrinsic Mode

Functions (IMFs) K .

Dataset	K	T_p (s)	T_w (s)	T_E (s)	T_I (s)	$Tc\ tr$ (s)	Tc (s)	T_{test} (s)
UBIPr	3	0.561	0.478	0.21	0.213	2877	0.23	1.692
	5			0.86	0.326	4795	0.32	2.545
	7			1.21	0.458	6713	0.46	3.167
	9			1.51	0.567	8631	0.57	3.686
AR	3	0.568	0.482	0.28	0.213	1233	0.15	1.693
	5			0.92	0.326	2055	0.24	2.536
	7			1.41	0.458	2877	0.35	3.268
	9			1.54	0.567	3699	0.44	3.597
CASIA Iris	3	0.581	0.489	0.46	0.213	1644	0.18	1.923
	5			0.98	0.326	2740	0.27	2.646
	7			1.68	0.458	3836	0.38	3.588
	9			1.73	0.567	4932	0.49	3.857

The table presented above illustrates the time consumption of various processes in the proposed periocular recognition algorithm across different values of K . With an increase in the value of K , the time required for IMF estimation, interpolation, CNN training, and CNN classification also increases. Consequently, the time required for testing also escalates as K increases.

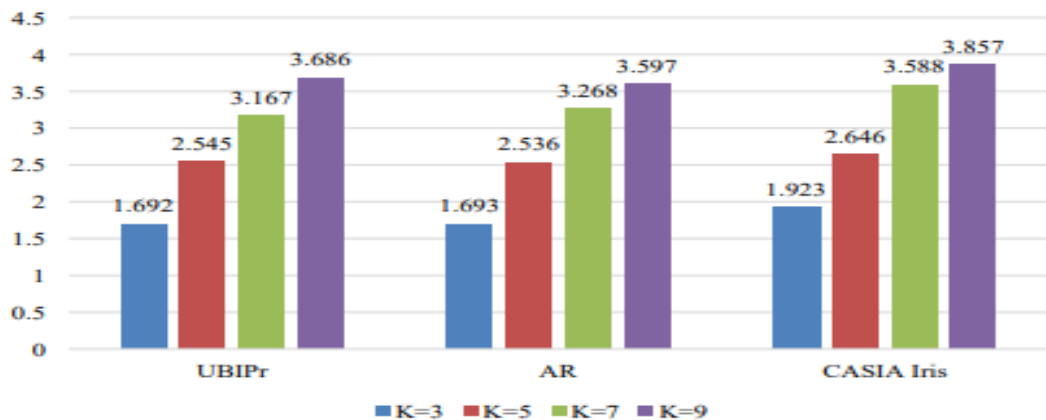


Figure 4.64 Graphical representation of testing time across varying values of K .

For $K = 9$, the UBIPr dataset, AR dataset, and CASIA Iris dataset exhibit testing times of 3.686s, 3.597s, and 3.857s respectively. Figure 4.64 illustrates the graphical comparison of testing time across various values of K . The subsequent section presents the conclusion of the study(Ramachandra & Ramachandran, 2022).

4.5.4 Conclusion

In this section, a novel ensemble training strategy was presented for enhancing periocular recognition with the CNN classifier. For each periocular image, $K+2$ ensemble images were produced. The process began with the image being split into four components using a single-level Discrete Wavelet Transform (DWT): LL , LH , HL , and HH . The LL component was further divided into K levels through the FA-MVEMD algorithm. This division produced a set of K -level Mode of Intrinsic Functions, which, together with remaining and the HH component from the DWT, formed the ensemble set of images. These images were subsequently employed in training the CNN model. In the evaluation stage, $K+2$ intermediate outcomes were derived from the test ensemble images, culminating in a final decision. The effectiveness of this method was assessed on the UBIPr, AR, and CASIA-Iris datasets using metrics like Equal Error Rate (EER), Area Under the Curve (AUC), and rank-1 and rank-5 recognition precision. This innovative approach reached rank-1 accuracy levels of 93.47%, 98.23%, and 98.03% across the UBIPr, AR, and CASIA-Iris datasets, respectively. It was also noted that an increase in the number of IMFs led to a higher time complexity. However, for $K = 9$, this methodology exhibited the highest accuracy in recognition. (Ramachandra & Ramachandran, 2022).

CHAPTER 5

RESULTS AND DISCUSSIONS

This chapter analyses all proposed methods with the recent state-of-the-art methods.

5.1 Introduction

The objective is to analyze all three proposed methods. To meet the objective, a comparative analysis is done of all the existing and proposed methods. The proposed periocular recognition methods include pre-processing, ROI segmentation, feature extraction, and classification. The pre-processing is done for improving the input quality. For feature extraction, many methods are analyzed and finally, it is concluded to use texture, shape, and shape models for classification, different classifiers are analyzed. Then cumulative similarity score is chosen from this analysis, then after this analysis, new feature extraction models are proposed. Then an overall framework is designed for periocular recognition models. This chapter compares the above-mentioned methods with recent methods in terms of some performance metrics. The remaining work is structured as follows. A summary of the proposed methodologies is given in Section 5.2. Section 5.3 demonstrates the experimental analysis. Finally, the work is concluded in Section 5.4.

5.2 SUMMARY OF PROPOSED METHODOLOGIES

The standard steps in an identification system for a periocular region includes image acquisition, applying pre-processing on the acquired image, localization of the ROI, extracting the feature, post-processing of extracted features, and then matching of two feature sets.. The periocular picture is recorded using a sensor or camera during the acquisition phase. Otherwise, the periocular recognition system also uses benchmark datasets. In the initial study, the UBIPr, CASIA-Iris distance, and AR datasets were used to assess the performance of the proposed periocular recognition algorithm. The next phase in the preprocessing process seeks to improve an image's visual appeal. Frequently, pre-processing methods are used to normalize fluctuations in illumination. Unsharp mask filtering algorithm is employed in our work for this purpose. Applying the localization procedure comes next when the pre-processing stage has been completed. The acquired or previously processed picture is used in the localization step to extract the periocular region. In our research, we first identify the left and right eye corner points before breaking the periocular region into four sub-regions, including the eyebrow, eye corner regions, and upper, and lower eye fold regions. The next step is to retire the characteristics after extracting all the points necessary to recognize the periocular region. In the feature extraction

stage, the localized periocular region is used to extract robust and discriminative features. Global and local strategies are used in the feature extraction procedures. Local features are those that are only taken from a group of discrete locations, such as key points, as opposed to global features, which are extracted from the entire image or area of interest (ROI). In our job, we must just extract the feature from the key derived points, not the entire image. We, therefore, employed local feature extraction techniques. We choose two methods among a variety of local extraction techniques already in use, such as Histogram of Oriented Gradients (HOG) and KAZE. HOG is used to extract the color features from the key points using one of these two methods. The form characteristics are extracted from the key points using KAZE. In this work, a brand-new texture feature extraction method called Sub-image-based Neighbour gradient is proposed (SING). There are several methods for extracting texture features, including Local Binary Pattern (LBP), Wavelet, and Local Ternary Pattern (LTP). These methods, however, are less resistant to "in the wild" variables such as resolutions, degrees of lighting, postures, and occlusions since handcrafted texture descriptors are inadequate and rigid for accurately expressing periocular characteristics. Therefore, it is still difficult to identify periocular in the field. This paper introduced a novel texture feature extraction method to address this problem. This is known as a neighbor gradient based on sub-images (SING). The matching algorithm is then used to identify the person using the traits that were extracted. This is accomplished in our study using the cumulative similarity score approach. Three feature extraction techniques are established in the second proposed study to extract the color, shape, and texture aspects. HOG is employed in the initial phase to extract the color feature. However, because HOG uses a sliding window technique to extract characteristics from each pixel of an image, its computation time is slow when trying to find objects in largescale images. Because of this, when the input image is obscured, the accuracy is not very trustworthy. As a result, it generates low accuracy values and takes a long time to compute. The second piece of work develops an updated HOG algorithm to address this flaw. Additionally, the original KAZE algorithm is replaced with an improved KAZE approach. With the aid of the SIFT descriptor, which is based on sparse random projection, the second paper proposes an updated and enhanced version of the AKAZE algorithm (SRP). The suggested approach keeps the AKAZE algorithm's strong feature detection efficiency advantage while also having SIFT descriptor stability. Additionally, the SRP technique significantly lowers the computational cost brought on by the high dimension of the SIFT descriptor, which limits the speed of feature matching. In the second work, the Local Patterns of Gradient (LPOG) approach likewise takes the place of the SING approach. Three drawbacks exist for the SING operators: (1) They create fairly lengthy histograms, which reduce

identification speed, particularly for large-scale face databases; (2) In some situations, they fail to recognize local structure because they ignore the impact of the center pixel; (3) They produce binary data that is noise-sensitive. To address these issues, we suggested the LPOG operator. LPOG operator offers the following benefits: (1) By comparing pairs of neighbors in the operator, it significantly reduces the dimensionality of the histograms; (2) It takes into account the effect of the center pixel point and gives it the most weight; (3) By changing the sign function of the existing SING operator, it lessens the influence of occlusion on face images. In the third work, an ensemble training approach is proposed instead of using a cumulative similarity score. This work used a deep learning classifier is used to improve the detection accuracy.

5.3 EXPERIMENTAL ANALYSIS

The performance analysis of the suggested methods is covered in this section. UBIPr, CASIAIris distance, and AR datasets were used to assess the performance of the proposed periocular recognition algorithm. Metrics including rank-1, rank-5 recognition accuracy, and equal mistake rate were used in the evaluation (EER).

5.3.1 Analysis of Proposed Works

Table 5.1: Comparison of EER and AUC with the traditional methods

Scheme	UBIPr		CASIA-Iris		AR	
	EER	AUC (%)	EER	AU	EER	AUC
First Work	3.08 ±1.6	0.9948	4.12 ±0.4	0.99 08	4.92	0.990 1
Second Work	2.88 ±1.6	0.9969	3.11 ±0.4	0.99 78	3.85	0.996 1
Third Work	2.87 ±1.5	0.9961	4.71	0.99 32	3.92 ±0.5	0.992 5

The comparison of EER and AUC for the two suggested techniques is shown in Table 5.1. For all three datasets, the EER of the second proposed approach is lower than the EER of the first and third proposed methods.

Table 5.2: Comparison of Rank -1 and Rank-5 recognition accuracy

Scheme	UBIPr		CASIA-Iris		AR	
	Rank-1	Rank-5	Rank-1	Rank-5	Rank-1	Rank-5
First work	92.32±1.5	98.73±0.6	97.41±1.1	98.95±0.8	97.87	99.12
Second work	94.85±1.2	99.13±0.3 98.03±1.	98.31±1.5 99.14±0.	99.15±0.9	98.99	99.34
Third Work	93.47±1.4	98.01±0.6	98.23	99.31	2	5

Table 5.2 above compares the two suggested approaches' rank-1 and rank-5 recognition accuracy for the three datasets. For the three datasets, the second proposed method outperforms the first and third proposed methods in terms of rank-1 and rank-5 recognition accuracy(Ramachandra & Ramachandran, 2022).

CHAPTER 6

CONCLUSIONS AND RECOMMENDATIONS

6.1 Introduction

The objective of this chapter is to present the concluding remarks of the research work. In this thesis, four new feature extraction techniques are proposed. After identifying the left and right eye corner points, this method divides the periocular area into four sub-area. The upper eye fold region's features are extracted using the Shape feature extraction technique, while the brow and eye corner regions' features are extracted using the Color feature extraction algorithm. By calculating the distance between N spots on the eyebrow region and the middle of the eye corner, this method also determines the form of the brow. The eyebrow form characteristic also includes the height and width measurements taken at each of the N points that make up the eyebrow. The texture feature extraction method takes a 3×3 sub-image and extracts the neighbor gradient features. Several experiments are conducted with real-time satellite images to assess the performance of the newly proposed approaches(Ramachandra & Ramachandran, 2022).

The work carried out in each chapter is summarized in section 6.2. The contribution and significance of the report in 6.3. The strength and limitations of the research are presented in section 6.4. The future scope of the research is given in section 6.5.

6.2 Summary of the report

Chapter 1 introduces biometric recognition methods, detailing the roles, types, and various techniques of biometric recognition. It focuses on ocular and periocular detection applications, highlighting issues and challenges in periocular biometric recognition using image processing. The chapter also discusses the motivation and justification for the research, outlines the research, and presents its contributions. A background survey reviews available biometric recognition techniques, assessing their limitations and advantages for periocular biometric recognition in Chapter 2.

Chapter 3 discusses about the research methodology used for the research and details about the dataset and it's preparation. The requirement of software and hardware needed for the research.

Chapter 4 evaluates and compares periocular recognition techniques, including ReLU non-linearity, DeepIrisNet, FaceNet, Light CNN, Multimodal CNN, Deep CNN, and RGB-OCLBCP. It applies a dataset of images from UBIPr, CASIA-Iris, and AR datasets.

Experimental results assess the performance of these techniques using Equal Error Rate (EER) and recognition rate values. It proposes a periocular identification method utilizing area and subimage-based neighbor gradient extracting features for improved recognition outcomes. It describes the retrieval of the upper eye fold area using the KAZE feature extraction method and the extraction of brow and eye corner regions using the HOG feature selection algorithm, detailing both algorithms' architecture. Also, it introduces a periocular recognition method that employs region-specific, sub-image-based neighbor gradient feature estimation. It improves upon the HOG feature extraction algorithm for eyebrow and eye corner regions and uses an accelerated KAZE feature extraction algorithm for the upper eye fold region. The chapter provides a detailed explanation and architecture of both algorithms, showing that the proposed approach surpasses conventional periocular recognition methods in performance. Last, the discussion related to results and analysis of the newly proposed approaches, determining the best method for the periocular biometric recognition system and explaining its superiority over traditional approaches(Ramachandra & Ramachandran, 2022).

6.3 Discussion and conclusion

The following are the chief contributions of the research.

The proposed techniques are used for manmade object detection and change detection from the given input satellite imagery.

- A new texture feature descriptor is proposed to find the detailed texture information of the periocular region from the input face image.
- The three spectral filters DCT, DWT, and DFT are given into the CNN for generating the deep features to improve the efficiency of the traditional LBP approach.
- A new segmentation approach is introduced for eyebrow and eye corner regions from a given high-resolution input face image(Ramachandra & Ramachandran, 2022).
- The SIFT descriptor based on sparse random projection (SRP) is fused with the traditional KAZE shape feature extraction approach to improve its efficiency.
- A new improved HOG algorithm is proposed to differentiate the detailed information of each object in a periocular region which is segmented by the newly proposed segmentation approach.
- The Local Patterns of Gradient (LPOG) is used to develop a novel texture feature extraction approach based on local key point information.
- The proposed technique is tested on high-resolution face images which are taken from UBIPr, CASIA-Iris distance, and AR datasets.
- The proposed technique has substantiated its ability to produce a good result for periocular

region segmentation, feature extraction, and classification.

The significance of the proposed research is as follows;

- The proposed feature descriptor considers intensity variations in eight directions and can, therefore, detect the significant shapes clearly.
- In face images given that the periocular region is visually different from the non- periocular region, the proposed segmentation approach is most suitable to identify the difference between those regions.
- Ambiguous pixels in periocular region points are cleverly handled by the proposed feature extraction method.
- The proposed texture feature extraction technique possesses rotational and illumination invariance properties (Ramachandra & Ramachandran, 2022).

6.4 Strengths and Limitations

The following are the strengths of the following research

- In the proposed segmentation work, the periocular region and non-periocular region are separated from the given input face image. So this proposed segmentation approach acts as the Region of Interest (ROI) operator. This ROI operation greatly reduces the execution time because it eliminates the nonperiocular region from the given input image. So this novel segmentation approach adds strength to the proposed work in locating regions where the periocular region occurs.
- The proposed texture feature descriptor considers feature information in vertical, horizontal, and diagonal directions, thereby helping find significant features.
- The kernel information integration with SING helps to improve the performance of the SING to recognize the person. Since periocular region recognition using image processing is an emerging area, the proposed SING method helps in developing an automatic periocular region recognition system. The following are the limitation of the research
- Since the proposed method can only be used for benchmark images, real-time images cannot be processed unless they are converted to proper images.
- The proposed method lacks a very close distance between the two regions. It could detect the periocular region in the high-resolution image only.

6.5 Future recommendations

This dissertation creates lots of scope in the area of cyber forensics. This work can extend its scope by including gender, and age as the other parameter which enhances the identification

process. Faces that are altered due to surgeries/ accidents and eye inflammations can also be considered as an extension of this work. The system will also be experimented with in future use of 3D and color image datasets(Ramachandra & Ramachandran, 2022).

References

- Agrawal, E., & Christopher, J. (2020). Emotion Recognition from Periocular Features. *Communications in Computer and Information Science, 1240 CCIS*. https://doi.org/10.1007/978-981-15-6315-7_16
- Agrawal, E., Christopher, J., & Arunachalam, V. (2021). Emotion recognition through voting on expressions in multiple facial regions. *ICAART 2021 - Proceedings of the 13th International Conference on Agents and Artificial Intelligence*, 2. <https://doi.org/10.5220/0010306810381045>
- Ahonen, T., Hadid, A., & Pietikäinen, M. (2006). Face description with local binary patterns: Application to face recognition. *IEEE Transactions on Pattern Analysis and Machine Intelligence*, 28(12). <https://doi.org/10.1109/TPAMI.2006.244>
- Alahmadi, A., Hussain, M., Aboalsamh, H., & Azmi, A. (2020). ConvSRC: SmartPhone-based periocular recognition using deep convolutional neural network and sparsity augmented collaborative representation. *Journal of Intelligent and Fuzzy Systems*, 38(3). <https://doi.org/10.3233/JIFS-190834>
- Almadan, A., & Rattani, A. (2021). Compact CNN Models for On-device Ocular-based User Recognition in Mobile Devices. *2021 IEEE Symposium Series on Computational Intelligence, SSCI 2021 - Proceedings*. <https://doi.org/10.1109/SSCI50451.2021.9660033>
- Alonso-Fernandez, F., Diaz, K. H., Ramis, S., Perales, F. J., & Bigun, J. (2020). Soft-Biometrics Estimation In the Era of Facial Masks. *Lecture Notes in Informatics (LNI), Proceedings - Series of the Gesellschaft Fur Informatik (GI)*, P-306.
- Alonso-Fernandez, F., Mikaelyan, A., & Bigun, J. (2015). Comparison and fusion of multiple iris and periocular matchers using near-infrared and visible images. *3rd International Workshop on Biometrics and Forensics, IWBF 2015*. <https://doi.org/10.1109/TWBF.2015.7110234>
- Alonso-Fernandez, F., Raja, K. B., Raghavendra, R., Busch, C., Bigun, J., Vera-Rodriguez, R., & Fierrez, J. (2022). Cross-sensor periocular biometrics in a global pandemic: Comparative benchmark and novel multialgorithmic approach. *Information Fusion*, 83–84. <https://doi.org/10.1016/j.inffus.2022.03.008>
- Ambika, D. R., Radhika, K. R., & Seshachalam, D. (2020). Identity verification using biometrics in smart-cities. In *EAI/Springer Innovations in Communication and Computing*. https://doi.org/10.1007/978-3-030-14718-1_9
- Bakshi, S., Sa, P. K., & Majhi, B. (2015a). A novel phase-intensive local pattern for periocular recognition under visible spectrum. *Biocybernetics and Biomedical Engineering*, 35(1). <https://doi.org/10.1016/j.bbe.2014.05.003>
- Bakshi, S., Sa, P. K., & Majhi, B. (2015b). Phase Intensive Global Pattern for periocular recognition. *11th IEEE India Conference: Emerging Trends and Innovation in Technology, INDICON 2014*. <https://doi.org/10.1109/INDICON.2014.7030362>
- Bakshi, S., Sa, P. K., Wang, H., Barpanda, S. S., & Majhi, B. (2018). Fast periocular authentication in handheld devices with reduced phase intensive local pattern. *Multimedia Tools and Applications*, 77(14). <https://doi.org/10.1007/s11042-017-4965-6>
- Barcellos, W., & Gonzaga, A. (2022). *Periocular authentication in smartphones applying uLBP descriptor on CNN Feature Maps*. <https://doi.org/10.5753/wvc.2021.18890>
- Behera, S. S., & Puhan, N. B. (2023). Dual-spectrum network: exploring deep visual feature to attribute mapping for cross-spectral periocular recognition. *Journal of Electronic Imaging*, 32(03). <https://doi.org/10.1117/1.jei.32.3.033031>
- Bharadwaj, S., Bhatt, H. S., Vatsa, M., & Singh, R. (2010). Periocular biometrics: When Iris recognition fails. *IEEE 4th International Conference on Biometrics: Theory, Applications and Systems, BTAS 2010*. <https://doi.org/10.1109/BTAS.2010.5634498>
- Boutros, F., Damer, N., Fang, M., Raja, K., Kirchbuchner, F., & Kuijper, A. (2020). Compact Models for Periocular Verification Through Knowledge Distillation. *Lecture Notes in Informatics (LNI), Proceedings - Series of the Gesellschaft Fur Informatik (GI)*, P-306.
- Boutros, F., Damer, N., Raja, K., Kirchbuchner, F., & Kuijper, A. (2022). Template-Driven Knowledge Distillation for Compact and Accurate Periocular Biometrics Deep-Learning Models. *Sensors*, 22(5). <https://doi.org/10.3390/s22051921>
- Boutros, F., Damer, N., Raja, K., Ramachandra, R., Kirchbuchner, F., & Kuijper, A. (2020a). Fusing iris and periocular region for user verification in head mounted displays. *Proceedings of 2020 23rd International Conference on Information Fusion, FUSION 2020*.

- https://doi.org/10.23919/FUSION45008.2020.9190282
- Boutros, F., Damer, N., Raja, K., Ramachandra, R., Kirchbuchner, F., & Kuijper, A. (2020b). Iris and periocular biometrics for head mounted displays: Segmentation, recognition, and synthetic data generation. *Image and Vision Computing*, 104. https://doi.org/10.1016/j.imavis.2020.104007
- Boutros, F., Damer, N., Raja, K., Ramachandra, R., Kirchbuchner, F., & Kuijper, A. (2020c). Periocular Biometrics in Head-Mounted Displays: A Sample Selection Approach for Better Recognition. *2020 8th International Workshop on Biometrics and Forensics, IWBF 2020 - Proceedings*. https://doi.org/10.1109/IWBF49977.2020.9107939
- Cascone, L. (2021). Periocular features as a window on cognitive processing: From memory to understanding the semantic complexity of an image. *BioSMART 2021 - Proceedings: 4th International Conference on Bio-Engineering for Smart Technologies*. https://doi.org/10.1109/BioSMART54244.2021.9677876
- Chen, H., Gao, M., Ricanek, K., Xu, W., & Fang, B. (2017). A Novel Race Classification Method Based on Periocular Features Fusion. *International Journal of Pattern Recognition and Artificial Intelligence*, 31(8). https://doi.org/10.1142/S0218001417500264
- Chen, Y., Wu, W., Xu, L., & Guo, S. (2023). Iris-periocular features-fused non-collaborative authentication. *Journal of Image and Graphics*, 28(5). https://doi.org/10.11834/jig.220649
- Cho, S. R., Nam, G. P., Shin, K. Y., Nguyen, D. T., Pham, T. D., Lee, E. C., & Park, K. R. (2017). Periocular-based biometrics robust to eye rotation based on polar coordinates. *Multimedia Tools and Applications*, 76(9). https://doi.org/10.1007/s11042-015-3052-0
- Dadi, H. S., & Mohan Pillutla, G. K. (2016). Improved Face Recognition Rate Using HOG Features and SVM Classifier. *IOSR Journal of Electronics and Communication Engineering*, 11(04). https://doi.org/10.9790/2834-1104013444
- da Silva, E. P., Fambrini, F., & Saito, J. H. (2020). Convolutional Neural Networks and Periocular Region Image Recognition. *Communications in Computer and Information Science*, 1332. https://doi.org/10.1007/978-3-030-63820-7_36
- Das, S., Kharbanda, K., M, S., Raman, R., & D, E. D. (2021). Deep learning architecture based on segmented fundus image features for classification of diabetic retinopathy. *Biomedical Signal Processing and Control*, 68. https://doi.org/10.1016/j.bspc.2021.102600
- Gangwar, A., & Joshi, A. (2016). DeepIrisNet: Deep iris representation with applications in iris recognition and cross-sensor iris recognition. *Proceedings - International Conference on Image Processing, ICIP, 2016-August*. https://doi.org/10.1109/ICIP.2016.7532769
- Han, N. Y., Seong, S. W., Ryu, J., Hwang, H., Joung, J., Lee, J., & Lee, E. C. (2021). Authentication of Facial Images with Masks Using Periocular Biometrics. *Lecture Notes in Computer Science (Including Subseries Lecture Notes in Artificial Intelligence and Lecture Notes in Bioinformatics)*, 12616 LNCS. https://doi.org/10.1007/978-3-030-68452-5_34
- Hernandez-Diaz, K., Alonso-Fernandez, F., & Bigun, J. (2020). Cross-spectral periocular recognition with conditional adversarial networks. *IJCB 2020 - IEEE/IAPR International Joint Conference on Biometrics*. https://doi.org/10.1109/IJCB48548.2020.9304899
- Hernandez V, J. J., Dejournett, R., Nannuri, U., Gwyn, T., Yuan, X., & Roy, K. (2022). Face Authentication from Masked Face Images Using Deep Learning on Periocular Biometrics. *Lecture Notes in Computer Science (Including Subseries Lecture Notes in Artificial Intelligence and Lecture Notes in Bioinformatics)*, 13343 LNAI. https://doi.org/10.1007/978-3-031-08530-7_38
- Hollingsworth, K., Clark, S., Thompson, J., Flynn, P. J., & Bowyer, K. W. (2013). Eyebrow segmentation using active shape models. *Biometric and Surveillance Technology for Human and Activity Identification X*, 8712. https://doi.org/10.1117/12.2017646
- Ipe, V. M., & Thomas, T. (2021). Periocular Recognition Under Unconstrained Image Capture Distances. *Communications in Computer and Information Science*, 1365. https://doi.org/10.1007/978-981-16-0425-6_14
- Joshi, A., Gangwar, A., Sharma, R., Singh, A., & Saquib, Z. (2014). Periocular recognition based on Gabor and Parzen PNN. *2014 IEEE International Conference on Image Processing, ICIP 2014*. https://doi.org/10.1109/ICIP.2014.7026008
- Kaur, B. (2023). Iris and Periocular Recognition using Shape Descriptors and Local Invariant Features. *2nd Edition of IEEE Delhi Section Owned Conference, DELCON 2023 - Proceedings*. https://doi.org/10.1109/DELCON57910.2023.10127462

- Kaur, P., & Kumar, N. (2023). Enhanced Biometric Cryptosystem Using Ear & Iris Modality Based On Binary Robust Independent Elementary Feature. *2023 6th International Conference on Information Systems and Computer Networks, ISCON 2023*.
<https://doi.org/10.1109/ISCON57294.2023.10112197>
- Khellat-Kihel, S., Muhammad, J., Sun, Z., & Tistarelli, M. (2022). Gender and ethnicity recognition based on visual attention-driven deep architectures. *Journal of Visual Communication and Image Representation*, 88. <https://doi.org/10.1016/j.jvcir.2022.103627>
- Kirchgasser, S., Debiasi, L., Schraml, R., Hofbauer, H., Uhl, A., Boyle, J., & Ferryman, J. (2020). Template Protection on Multiple Facial Biometrics in the Signal Domain under Visible and Near-Infrared Light. *2020 8th International Workshop on Biometrics and Forensics, IWBF 2020 - Proceedings*. <https://doi.org/10.1109/IWBF49977.2020.9107964>
- K. M, S. K. (2021). Recognition of Masked Face Using Convolutional Neural Network Algorithm. *International Journal for Research in Applied Science and Engineering Technology*, 9(VII).
<https://doi.org/10.22214/ijraset.2021.37051>
- Kumar, G., Bakshi, S., Sa, P. K., & Majhi, B. (2021). Non-overlapped blockwise interpolated local binary pattern as periocular feature. *Multimedia Tools and Applications*, 80(11).
<https://doi.org/10.1007/s11042-020-08708-w>
- Kumari, P., & R, S. K. (2020). Periocular Biometrics for Non-ideal Images Using Deep Convolutional Neural Networks. *Advances in Intelligent Systems and Computing*, 1034.
https://doi.org/10.1007/978-981-15-1084-7_15
- Kumari, P., & Seeja, K. R. (2020). Periocular Biometrics for non-ideal images: With off-the-shelf Deep CNN & Transfer Learning approach. *Procedia Computer Science*, 167.
<https://doi.org/10.1016/j.procs.2020.03.234>
- Kumari, P., & Seeja, K. R. (2021). A novel periocular biometrics solution for authentication during Covid-19 pandemic situation. *Journal of Ambient Intelligence and Humanized Computing*, 12(11).
<https://doi.org/10.1007/s12652-020-02814-1>
- Kumari, P., & Seeja, K. R. (2022). Periocular biometrics: A survey. In *Journal of King Saud University - Computer and Information Sciences* (Vol. 34, Issue 4). <https://doi.org/10.1016/j.jksuci.2019.06.003>
- Lee, M. B., Kang, J. K., Yoon, H. S., & Park, K. R. (2021). Enhanced Iris Recognition Method by Generative Adversarial Network-Based Image Reconstruction. *IEEE Access*, 9.
<https://doi.org/10.1109/ACCESS.2021.3050788>
- Lee, Y. W., Kim, J. S., & Park, K. R. (2022). Ocular Biometrics with Low-Resolution Images Based on Ocular Super-Resolution CycleGAN. *Mathematics*, 10(20). <https://doi.org/10.3390/math10203818>
- Le, T. H. N., Prabhu, U., & Savvides, M. (2014). A novel eyebrow segmentation and eyebrow shape-based identification. *IJCB 2014 - 2014 IEEE/IAPR International Joint Conference on Biometrics*.
<https://doi.org/10.1109/BTAS.2014.6996262>
- Lionnie, R., Apriono, C., & Gunawan, D. (2022). Eyes versus Eyebrows: A Comprehensive Evaluation Using the Multiscale Analysis and Curvature-Based Combination Methods in Partial Face Recognition. *Algorithms*, 15(6). <https://doi.org/10.3390/a15060208>
- Liu, J., Hu, D., Ni, M., Zou, Y., Gu, Y., Han, Z., Li, J., He, Y., Zhang, Z., & Xu, X. (2022). Monolithic RGB-NIR Perovskite Photodetector for Fused Multispectral Sensing and Imaging. *Journal of Physical Chemistry Letters*, 13(16). <https://doi.org/10.1021/acs.jpclett.2c00701>
- Lohith, M. S., Manjunath, Y. S. K., & Eshwarappa, M. N. (2023). Multimodal Biometric Person Authentication Using Face, Ear and Periocular Region Based on Convolution Neural Networks. *International Journal of Image and Graphics*, 23(2). <https://doi.org/10.1142/S0219467823500195>
- Luo, Z., Li, J., & Zhu, Y. (2021). A Deep Feature Fusion Network Based on Multiple Attention Mechanisms for Joint Iris-Periocular Biometric Recognition. *IEEE Signal Processing Letters*, 28.
<https://doi.org/10.1109/LSP.2021.3079850>
- Ma, J., Zhao, J., Tian, J., Tu, Z., & Yuille, A. L. (2013). Robust estimation of nonrigid transformation for point set registration. *Proceedings of the IEEE Computer Society Conference on Computer Vision and Pattern Recognition*. <https://doi.org/10.1109/CVPR.2013.279>
- Mon, C. S., Hussin, A. A. A., Sin, T. K., & Mon, C. S. (2020). Analyzing the periocular biometric-based access control systems. *Journal of Physics: Conference Series*, 1529(3).
<https://doi.org/10.1088/1742-6596/1529/3/032024>
- Morris, C., Abegaz, T. T., & Payne, B. R. (2022). Effectiveness of Periocular Biometric Recognition

- Under Face Mask Restrictions. In *Breakthroughs in Digital Biometrics and Forensics*. https://doi.org/10.1007/978-3-031-10706-1_11
- Nascimeno, L. F., & Souza, J. M. de. (2023). *Deep Learning Utilized for Person Recognition Based on the Biometric Features of the Periocular Region*. <https://doi.org/10.5753/sibgrapi.est.2022.23270>
- Ogawa, K., & Kameyama, K. (2021). Adaptive Selection of Classifiers for Person Recognition by Iris Pattern and Periocular Image. *Lecture Notes in Computer Science (Including Subseries Lecture Notes in Artificial Intelligence and Lecture Notes in Bioinformatics)*, 13111 LNCS. https://doi.org/10.1007/978-3-030-92273-3_54
- Park, S., Moon, B., Ko, S., Yu, S., & Paik, J. (2017). Low-light image restoration using bright channel prior-based variational Retinex model. *Eurasip Journal on Image and Video Processing*, 2017(1). <https://doi.org/10.1186/s13640-017-0192-3>
- Phillips, S., & Karakaya, M. (2022). Effects of Distance and Gaze Angle on CNN-based Standoff Iris Recognition. *Conference Proceedings - IEEE SOUTHEASTCON, 2022-March*. <https://doi.org/10.1109/SoutheastCon48659.2022.9764014>
- Prasanth, N., Kiran, C. U. S., Nethi, S., Ketineni, T., Srinivasu, N., & Pradeepini, G. (2023). Fusion of Iris and Periocular Biometrics Authentication using CNN. *Proceedings - 7th International Conference on Computing Methodologies and Communication, ICCMC 2023*. <https://doi.org/10.1109/ICCMC56507.2023.10083982>
- Rahmad, C., Asmara, R. A., Putra, D. R. H., Dharmia, I., Darmono, H., & Muhiqquin, I. (2020). Comparison of Viola-Jones Haar Cascade Classifier and Histogram of Oriented Gradients (HOG) for face detection. *IOP Conference Series: Materials Science and Engineering*, 732(1). <https://doi.org/10.1088/1757-899X/732/1/012038>
- Ramachandra, S., & Ramachandran, S. (2022). Region specific and subimage based neighbour gradient feature extraction for robust periocular recognition. *Journal of King Saud University - Computer and Information Sciences*, 34(10). <https://doi.org/10.1016/j.jksuci.2022.07.013>
- Ramaraj, P. (2021). A Neural Network in Convolution with Constant Error Carousel Based Long Short Term Memory for Better Face Recognition. *Turkish Journal of Computer and Mathematics Education (TURCOMAT)*, 12(2). <https://doi.org/10.17762/turcomat.v12i2.1808>
- Rao, M. G., Priyanka, H., Pawar, S., Reddy, K. H. K., & Divakarla, U. (2022). Novel approach of Using Periocular and Iris Biometric Recognition in the Authentication of ITS. *2022 4th International Conference on Cognitive Computing and Information Processing, CCIP 2022*. <https://doi.org/10.1109/CCIP57447.2022.10058656>
- Reddy, N., & Derakhshani, R. (2020). Emotion Detection using Periocular Region: A Cross-Dataset Study. *Proceedings of the International Joint Conference on Neural Networks*. <https://doi.org/10.1109/IJCNN48605.2020.9207542>
- Rot, P., Vitek, M., Grm, K., Emeršič, Ž., Peer, P., & Štruc, V. (2020). Deep Sclera Segmentation and Recognition. In *Advances in Computer Vision and Pattern Recognition*. https://doi.org/10.1007/978-3-030-27731-4_13
- Saad Shakeel, M., & Lam, K. M. (2022). Deep low-rank feature learning and encoding for cross-age face recognition. *Journal of Visual Communication and Image Representation*, 82. <https://doi.org/10.1016/j.jvcir.2021.103423>
- Seha, S. N. A., Hatzinakos, D., Zandi, A. S., & Comeau, F. J. E. (2021). Improving eye movement biometrics in low frame rate eye-tracking devices using periocular and eye blinking features. *Image and Vision Computing*, 108. <https://doi.org/10.1016/j.imavis.2021.104124>
- Shao, H., Li, J., Zhang, J., Yu, H., & Sun, J. (2021). Eye-based Recognition for User Identification on Mobile Devices. *ACM Transactions on Multimedia Computing, Communications and Applications*, 16(4). <https://doi.org/10.1145/3399659>
- Srivika, S., Gayathri, L., Nivetha, B., Sri Devi, N., & Sujatha, R. (2023). Biometric Verification using Periocular Features based on Convolutional Neural Network. *2nd International Conference on Sustainable Computing and Data Communication Systems, ICSCDS 2023 - Proceedings*. <https://doi.org/10.1109/ICSCDS56580.2023.10104783>
- Sujanthy, S., Bowshika, A., Dharaneesh, S. K., & Jai Sivadharshini, A. (2023). Iris Liveness Detection using Deep Learning Networks. *7th International Conference on Trends in Electronics and Informatics, ICOEI 2023 - Proceedings*. <https://doi.org/10.1109/ICOEI56765.2023.10125665>
- Toledo Ferraz, C., Barcellos, W., Pereira Junior, O., Trevisan Negri Borges, T., Garcia Manzato, M.,

- Gonzaga, A., & Hiroki Saito, J. (2021). A comparison among keyframe extraction techniques for CNN classification based on video periocular images. *Multimedia Tools and Applications*, 80(8). <https://doi.org/10.1007/s11042-020-10384-9>
- Tripathi, R. K., & Jalal, A. S. (2021). Novel local feature extraction for age invariant face recognition. *Expert Systems with Applications*, 175. <https://doi.org/10.1016/j.eswa.2021.114786>
- Tripathi, R. K., & Jalal, A. S. (2022). A robust approach based on local feature extraction for age invariant face recognition. *Multimedia Tools and Applications*, 81(15). <https://doi.org/10.1007/s11042-022-12783-6>
- Umer, S., Sardar, A., Rout, R. K., Tanveer, M., & Razzak, I. (2023). IoT-Enabled Multimodal Biometric Recognition System in Secure Environment. *IEEE Internet of Things Journal*. <https://doi.org/10.1109/JIOT.2023.3299465>
- Vitek, M., Rot, P., Štruc, V., & Peer, P. (2020). A comprehensive investigation into sclera biometrics: a novel dataset and performance study. *Neural Computing and Applications*, 32(24). <https://doi.org/10.1007/s00521-020-04782-1>
- Vyas, R., Kanumuri, T., Sheoran, G., & Dubey, P. (2020). Towards ocular recognition through local image descriptors. *Communications in Computer and Information Science*, 1147 CCIS. https://doi.org/10.1007/978-981-15-4015-8_1
- Wang, Y., Lei, S., Li, Y., Liu, B., & Zuo, H. (2022). Score Level Fusion for Iris and Periocular Biometrics Recogniton Based on Deep Learning. *International Journal of Advanced Network, Monitoring and Controls*, 7(4). <https://doi.org/10.2478/ijanmc-2022-0033>
- Wazirali, R., & Ahmed, R. (2022). Hybrid feature extractions and CNN for enhanced periocular identification during Covid-19. *Computer Systems Science and Engineering*, 41(1). <https://doi.org/10.32604/csse.2022.020504>
- Zabin, A., & Bourlai, T. (2020). A Deep Learning Based Approach to Iris Sensor Identification. *Proceedings of the 2020 IEEE/ACM International Conference on Advances in Social Networks Analysis and Mining, ASONAM 2020*. <https://doi.org/10.1109/ASONAM49781.2020.9381354>
- Zanlorensi, L. A., Lucio, D. R., de Souza Britto Junior, A., Proen  a, H., & Menotti, D. (2020). Deep representations for cross-spectral ocular biometrics. *IET Biometrics*, 9(2). <https://doi.org/10.1049/iet-bmt.2019.0116>

APPENDIX A: RESEARCH PROPOSAL

Periocular Region-Based Face Recognition Model for
Identifying Masked Faces

Mohd Saif

Research Proposal for
Master of Science in Data Science

Liverpool John Moores University & upGrad

November 2023

Abstract

The most arising field of computer vision is facial recognition where the identification of existent has captured the interest of numerous scientists. For further than four decades the area of face recognition has surfaced as a wide metric for assessing human identification. Reliability of the being facial recognition systems still has a lot of challenges with respect to computer vision and pattern recognition irrespective of the colorful advancements made. The difficult part in recognizing faces occur mostly in scenarios like recognition of twins' face, different profile views of the face, having different accessories like beard, glasses, etc. The encircling environment conditions also plays a major part like light intensity, illumination condition, occlusion, etc. still, face recognition systems experience a decrease in accuracy when faces are partially obscured. Various scenarios involve partial coverage of the face, such as helmets, hair, glasses, or ski masks. In many instances, only the area around the eyes (periocular region) remains visible and can serve as a viable biometric identifier.

The main idea of this work is to develop a novel effective frame for relating humans using periocular biometric. Several periocular biometric discovery approaches were formerly developed earlier. But all the well-established approaches are not robust enough to handle variations in resolution, illuminated images, postures due to the inefficiency of hand-drafted texture descriptors, especially while working with periocular features. Therefore, periocular recognition still paves a way for a lot of exploration advancements in face recognition.

Table of Contents

Abstract.....	2
1. Background.....	4
2. Related Work.....	5
3. Research Questions.....	7
4. Aim and Objectives	8
5. Significance of the Study	8
6. Scope of the Study.....	9
7. Research Methodology	9
7.1 Dataset Description	11
7.2 Data Preparation	11
7.3 Algorithms & Techniques Description	12
7.3.1 An Analysis of Periocular Region Recognition	12
7.3.2 Extraction of neighbor gradient features based on region specificity and sub-image for resilient periocular recognition	12
7.3.3. Robust Periocular Recognition Using Modified Histogram of Gradient and Improved Accelerated KAZE	12
7.3.4 Training Strategy Using empirical multivariate mode and CNN for eye area Identification: An Ensemble Approach	13
7.4Implementation.....	13
7.5 Evaluation	14
8. Required Resources	15
8.1 Hardware Requirements	15
8.2 Software Requirements.....	15
8.3 Dataset Requirements.....	16
9. Research Plan	16
9.1 Gantt Chart	16
9.2 Risk Mitigation and Contingency Plan.....	17
References.....	18

1. Background

In face recognition biometrics with incomplete faces, automatically identifying persons is a difficult issue. Consequently, the goal of periocular recognition is to recognize a person based on characteristics that are taken from area encircling the eye. The area surrounded by top of the eyebrow, cheekbone, and nose midline is used for this periocular recognition. The periocular facial attribute comprises elements derived from the corners of the eyes, eyebrows, creases around the eyes, and the texture of the skin. When faced with incomplete faces, that has hair, spectacles, a helmet, and a face mask on it, the face recognition system performs poorly. One of the periocular region's real-time applications is the recognition of offenders wearing masks on face in surveillance footage. Due to COVID-19 epidemic, wearing a face mask is now required. In situations like these, face recognition-based biometrics work poorly, necessitating the use of effective periocular-based biometric recognition. Expression variation also lowers the performance of facial biometrics. In contrast to the lower part of the face, the upper portion exhibits greater resilience to transitions. Periocular recognition proves more dependable than facial identification during expressions, as it encompasses a larger facial area. Ocular identification, such as iris recognition, works well when faced with partial faces, but it necessitates intense eye focus. Unlike ocular biometrics, which require the camera to concentrate closely on the iris, retina, and sclera, periocular recognition does not require this.

The proposed research contribution is as follows: (i) Hybrid approach for feature extraction that takes distinct features from various areas of the periocular facial picture. The goal of hybrid feature retrieval is to retrieve more crucial personality-differentiating descriptors. (ii) Utilizing a compatible feature extraction method to derive diverse area-based features from the periocular region can enhance the precision of periocular recognition. As a result, this technique employs several (region-specific) feature extraction algorithms depending on the periocular regions. (iii) The shape of the eyebrows plays a vital role, and recognition results can be obtained by extracting features related to the form along the upper and lower limits of the eyebrows, encompassing both width and height. As a result, the three-layer structure predicted from the eyebrow regions is segmented into N points through the employed technique for extracting eyebrow shape features. The form variations throughout the N points are provided by this characteristic of the eyebrow. (iv) Study also suggests a SING feature extraction approach that can enhance recognition performance by being more resilient to rotation.

2. Related Work

A number of studies proposed several methods for effective periocular recognition. There are two possible approaches: local and global. The entire periocular region's features are extracted via the feature extraction of global technique. The histogram color (Ahonen et al., 2006), gradient's histogram (Kumar et al., 2021), and HOG block (Joshi et al., 2014) are a few examples of these global feature extraction techniques. The objective of feature extraction of local technique is to retrieve the features after segmenting periocular regions into multiple sections. Scale-invariant robust feature (SIFT) (Gangwar & Joshi, 2016), accelerated robust feature (SURF) (Ahonen et al., 2006), symmetrical assessing by feature's expansion, phase-intensive local pattern, and the local's binary pattern (Das et al., 2021) are the most often used local feature extraction algorithms. Distance-based methods like Euclidean, mean square error, Chi-square, hamming distance, Bhattacharya distance, and K-nearest neighbor (KNN) are used for the classification of test images. Deep learning algorithms provide superior performance in several classification applications (Ma et al., 2013).

It is difficult to train model because deep CNN algorithms need's huge dataset. To extract shape information, a region's boundary is typically used. Le et al. (2014) employed eyebrow form, while Proen  a (2015) used shape of eyelid. For MBGC and AR datasets, the accuracy of using eyebrow shape features is 76.0% and 85.0%. Following the extraction of components of HSV from image RGB, (H. Chen et al., 2017) calculated the color characteristics. Necessary texture information can be retrieved from periocular regions utilizing methods such as Leung Malik filters (Alonso-Fernandez et al., 2022), Binary statistic image feature (Gangwar & Joshi, 2016), and LBP (Ahonen et al., 2006). Utilizing LBP characteristics yields a 76.83% rank-1 accuracy. However, using Leung Malik filters increases accuracy for UBIRIS v2, CASIA V4 distance and FRGC databases by 9.5%, 4.3%, and 25.7%, respectively.

Part-based representation is used to enhance the face recognition algorithm's performance with partial faces (Alonso-Fernandez et al., 2022). This method divides the face regions into many blocks and estimates the similarity between the blocks during face matching. The unstructured regions of real-world partial faces are a drawback of this approach. A deterministic annealing procedure is suggested to align two point set according to the geometric distributions (Kumari & Seeja, 2022). However, as this method makes use of geometric or textural data, it is unsuitable for most partial face recognition applications.

A window is used in the local binary pattern approach (Cho et al., 2017), and features are retrieved in either a clockwise or counterclockwise path from the center pixel to its vicinity. This feature depends on the window's rotation, meaning that rotating the window will alter the feature value. Independent component analysis is used by Binary Statistical Image information (BSIF) to extract texture information (Bakshi et al., 2015). Principal component analysis and linear discriminant analysis (Ahonen et al., 2006) are two optimization techniques that can be used to reduce dimension of the features extracted using features extraction algorithm. (Alonso-Fernandez et al., 2022) presented a periocular method based on the curvature of the eyebrow, in which the iris region is hidden (Alahmadi et al., 2020). However, this masking lowers the accuracy of recognition. As a result, (Luo et al., 2021) combined local binary patterns with shape and texture data that were obtained using Zernike moments (Bakshi et al., 2015a).

To reduce the rotation effects of the eye, (Das et al., 2021) translated the facial image's Cartesian coordinates to polar coordinates. (Ahonen et al., 2006) suggested a convolutional neural network technique that trains the CNN model using additional information like gender and ethnicity. Reduce face intensity local pattern were used in smart-phone biometrics by Chen (H. Chen et al., 2017). An attentional module and ROI detection network were presented by Rahmad (Rahmad et al., 2020), giving priority to essential elements in matching. (Chen et al., 2017) used five distinct local feature, including iris color, textures feature from the duct tear region (Bharadwaj et al., 2010), intensity in top region of inside eye corner, and feature derived from the region spanning the eyebrow to the upper eyelid. (Bakshi et al., 2018). After identification, feature using a statistics active shape's model, they implemented the LBP feature retrieval technique. (Park et al., 2017) Park propose an enhanced theory of retinex that may be utilized to enhance photos with weak texture information. In (Kumar et al., 2021), hand-crafted features and deep features were rendered collaboratively. The method divides the periocular picture into various groups to estimate the local statistical features (Dadi and Mohan Pillutla, 2016).

To extract the deep features, the ResNet-101 model of convolutional neural networks (CNNs) is utilized. Using shared CNN layer whose output are fed two modality specific layer, attribute-based periocular recognition (Kumari & Seeja, 2022) integrate periocular feature with expected soft biometrics' feature (Hollingsworth et al., 2013). For iris periocular recognition, utilizing a technique involving multiple attention mechanisms and deep feature fusion. (Alonso-Fernandez et al., 2022). Joint attention and self-focus are two of the processes that make up the multiple

attentive mechanism (Kumari and Seeja, 2021). Non-overlap interpolate LBP feature from four equivalent non-overlap sub-region were utilized by (Alonso-Fernandez et al., 2015) to retrieve the periocular feature (Le et al., 2014). To enhance recognition, it additionally extracts binned histogram features and face-intensive global pattern features.

Remarkable recognition performances are also obtained using hand crafted feature of HOG and CNN Pre-existing, uncrafted feature with classifier of SVM (Kumari & Seeja, 2022). To improve performance in periocular recognition, most deep learning algorithms require many periocular images. If fewer photos are used for training, the deep learning model's performance declines. Furthermore, the publications do not extract more unique elements that distinguish the personality that is specific to a given place. Consequently, in comparison to other conventional techniques, the suggested strategy enhances recognition outcomes by extracting distinct features from various regions. The periocular region is divided into four sections by the region-specific segmentation proposed in this study, from which five distinct features are derived. Additionally, a feature extraction approach for extracting feature from bottom eye lid area and the contour of the eyebrow is proposed in this study. The suggested region-based periocular recognition algorithm is presented in the following section.

3. Research Questions

This thesis aims to address the subsequent inquiries:

1. How can the periocular region will be effectively utilized in design of a face recognition model to accurately identify individuals wearing masks?
2. What are the key opportunities associated with incorporating periocular features into a face recognition system for the purpose of identifying masked faces?
3. To what extent does the performance of a face recognition model using periocular features compare to traditional face recognition models when applied to masked faces?
4. How do different mask types and variations impact the accuracy and robustness of a face recognition model that incorporates periocular features?
5. How can deep learning techniques be optimized and tailored specifically for the periocular region to enhance the accuracy and efficiency of a face recognition model for masked faces?

4. Aim and Objectives

The initial aim of the thesis is to identify the most suitable machine learning technique for the recognition of periocular regions. The second aim of this thesis is to recognize a person with a periocular region using machine learning techniques.

Objectives:

- To implement a Sub image based neighbor gradient (SING) feature's extraction for recognizing a person.
- To improve the recognition accuracy using improved HOG and accelerated KAZE feature descriptor.
- To reduce the error rate by using a newly developed feature extraction technique.
- To develop a new method for Eyebrow Shape Feature Estimation that could make accurate recognition of the periocular region.
- To detect eyebrow and eye's corner point from input face images to extract the periocular region.
- To match the person based on features using a cumulative similarity score.
- To comparatively analyze the proposed models in terms of performance measures.

5. Significance of the Study

The significance of the proposed research is as follows:

- The proposed feature descriptor considers intensity variations in eight directions and can, therefore, detect the significant shapes clearly.
- In face images given that periocular region is visually different from non-periocular region, the proposed segmentation approach is most suitable to identify the difference between those regions.
- Ambiguous pixels in periocular region points are cleverly handled by the proposed feature extraction method.
- The proposed texture feature extraction technique possesses rotational and illumination invariance properties.

6. Scope of the Study

This thesis outlines its boundaries as follows:

- The completion of the thesis is expected within 17 weeks following the submission of

the research proposal.

- The experimentation will take place utilizing freely available software and models.
- Feature Extraction Methods: Evaluate and enhance the performance of feature extraction methods such as KAZE, HOG, and SING in capturing diverse characteristics of periocular regions. Specifically, focus on the unique challenges posed by eyebrows, eye corners, and top eye fold region.
- Scalability and Robustness: Investigate the scalability of the algorithm to handle a variety of periocular images and its robustness to factors like variations in expression, lighting conditions, and partial occlusions.

7. Research Methodology

A typical identification method for a periocular region consists of the following steps: obtaining an image, pre-processing it, matching two feature sets, localizing the ROI, extracting the feature, and post-processing the extracted feature. During the acquisition stage, a sensor or camera records the periocular image. Benchmark datasets are also utilized by the periocular recognition system in other cases.

In the initial investigation, the suggested algorithm for periocular recognition was assessed utilizing the UBIPr, AR, and CASIA-Iris distance datasets. Enhancing an image's aesthetic appeal is the goal of the following step in the preprocessing procedure. Pre-processing techniques are often employed to normalize lighting variations. In our work, we use the unsharp mask filtering algorithm for this. After the pre-processing phase is finished, the localization process is applied. The periocular region is extracted in the localization step using the acquired or previously processed picture. Within our research, the periocular area is subdivided into four segments: the eyebrow region, eye side areas, top and down eye fold sections, and points corresponding to the left and right corners of the eyes.

After extracting all the points required to identify the periocular region, the characteristics are derived. In the feature extraction stage, robust and distinctive attributes are derived from the delimited periocular area. The feature extraction procedures employ a combination of global and local approaches. Unlike global features, which are derived from the entire image or the region of interest (ROI), local features are specifically acquired from distinct areas known as key points. Our task is to extract the feature, not the complete image, from the key derived

points. Thus, we used methods for extracting local features. From a range of existing local extraction strategies, including Histogram of Oriented Gradients (HOG) and KAZE, we select two approaches. Either of these two approaches is employed by HOG to extract the color features from the key spots. KAZE is used to derive the form properties from the key points. This paper proposes a novel approach to texture feature extraction: Sub-image-based Neighbour gradient (SING). Texture features can be extracted using a variety of techniques, such as Wavelet, Local Binary Pattern (LBP), and Local Ternary Pattern (LTP).

However, because handcrafted texture descriptors are too rigid and insufficient to accurately capture periocular properties, the methods are less robust against "in wild" variables including resolution, illuminating degrees, postures, and occlusion. Consequently, it remains challenging to identify periocular in the field. To solve this issue, a unique texture feature extraction technique was presented in this paper. A neighbor gradient based on sub-images (SING) is what this is called. Then, using the extracted traits, the matching algorithm is utilized to determine the person's identity. In our study, the cumulative similarity score method is used to achieve this.

The second proposed study establishes three features extraction techniques to retrieve the feature of colour, design, and texture. In the first stage, HOG is used to extract the color feature. However, HOG's computation time is lengthy when attempting to locate objects in large-scale images since it uses a sliding window technique to extract attributes from each pixel of an image. This is why the accuracy is not particularly reliable when the input image is blurry. It computes slowly and produces low accuracy numbers as a result. To fix this issue, the second piece of work creates an updated HOG algorithm. Furthermore, an enhanced KAZE methodology takes the place of the first KAZE algorithm. The better version of the AKAZE-algorithm (SRP) is proposed in the second publication, using SIFT descriptors, and it is based on sparse random projection. Proposed approach maintains SIFT descriptor stability and the high feature detection efficiency advantage of the AKAZE algorithm. Furthermore, the speed of feature matching is constrained by the elevated dimensionality of the SIFT descriptor; nevertheless, the SRP approach considerably reduces the computational cost caused by this limitation.

The SING approach is also replaced in the second work with the Local Patterns of Gradient (LPOG) approach. The SING operator's exhibit three drawbacks: firstly, they generate

relatively lengthy histograms, causing delays in identification, particularly with extensive face databases; secondly, they may overlook local structures due to their disregard for the center pixel's impact; and thirdly, they yield noisy binary data. To address these issues, we suggest employing the LPOG operator. The LPOG operator offers the following benefits: firstly, it significantly reduces histogram dimensionality by comparing pairs of neighbors in the operator; secondly, it takes into account and assigns the highest weight to the central pixel point; (3) It reduces the impact of occlusion on facial images by altering the sign function of the current SING operator. Rather of employing a cumulative similarity score, an ensemble training strategy is proposed in the third paper. For periocular recognition in this work, a convolutional neural network. To increase the detection accuracy, a deep learning classifier was employed in this study.

7.1 Dataset Description

This work makes use of three datasets:

- **UBIPr:** A variation of the UBIRIS.v2 set, called UBIPr, has images trimmed to cover a larger area of the ocular region than the original UBIRIS.v2 data. It works very well for periocular recognition trials.
- **CASIA-Iris-Distance:** The dataset originates from the Institute of Automation at the Chinese Academy of Sciences. The image region of interest encompasses dual eye iris and face patterns due to the high-resolution camera used to capture iris images in CASIA-Iris-Distance. Additionally, the fusion of multi-modal biometric information enables the observation of detailed facial characteristics, such as skin patterns.
- **AR Dataset:** The AR Face Database contains over 3000 mug shots of 130 individuals exhibiting various facial expressions.

7.2 Data Preparation

Preprocessing steps involve grayscale and color correction, color space conversion, histogram normalization or equivalence, and automatic removal of low-quality photos using global or average intensity thresholding. Rotation correction is performed through horizontal alignment using the eyes' centers or corners, and photometric normalization corrects for illumination variance. Finally, gaussian blurring is employed to smooth out fluctuations among local pixel intensities, and morphological procedures or 1D rank filters can remove short line edges like eyelashes.

7.3 Algorithms & Techniques Description

7.3.1 An Analysis of Periocular Region Recognition

This study assesses the effectiveness of seven varied periocular recognition approaches, including ReLU non-linearity, Deep-Iris-Net, Face-Net, Light CNN, Multimodal CNN, Deep CNN, and RGB-OCLBCP. These methodologies are tested on three distinct image datasets, namely UBIPr, CASIA-Iris, and AR. The comparison of these approaches reveals that, depending on the real-world application for which a system is designed, each algorithm exhibits its benefits and drawbacks in different ways. From this deep evaluation of their performance, we found that the RGB-OCLBCP technique gives many promising outcomes when compared with other techniques. [3].

7.3.2 Extraction of neighbor gradient features based on region specificity and sub-image for resilient periocular recognition

A periocular recognition approach is implemented to capture periocular features from four distinct regions: the brow, upper and lower eye folds, and eye corners. Conventional HOG and KAZE featuring retrieving techniques are applied to the eyebrows, top eye folds, and eye sidelines areas to retrieve feature. The estimation of height and width features along the top and down boundaries of the eyebrows facilitates the retrieval of eyebrows size. For the down eye fold region, a sub-image-based neighbour gradient feature extraction method is recommended. Evaluation of performance on datasets like UBIPr, CASIA-iris, and AR will be conducted using metrics such as rank-1 and rank-5 identification correctness, EER, and AUC.

7.3.3 Robust Periocular Recognition Using Modified Histogram of Gradient and Improved Accelerated KAZE

An approach to periocular recognition gathers data from four distinct regions, encompassing the eyebrow, top and down eye folds, and the eye corner. Enhanced accelerated KAZE feature extraction techniques and updated HOG feature retrieval methods are employed to retrieve features from the brow, top eye fold, and eye sideline areas. Extraction of eyebrows form feature involves predicting height and width features along the top and down boundaries of the eyebrows. To capture features in the lower eye fold region, a method based on sub-image neighbor gradient feature retrieval is outlined. The evaluation of performance utilizes metrics

such as rank-1 and rank-5 identification accuracy, EER, and AUC on datasets including UBIPr, CASIA-iris, and AR.

7.3.4 Training Strategy Using empirical multivariate mode and CNN for eye area Identification: An Ensemble Approach

The ensemble training approach for the CNN classifier involves generating $K+2$ ensemble images from a single periocular image. Initially, the approach employs a single-level Discrete Wavelet Transform (DWT) to break down the periocular image into four bands: LL , LH , HL , and HH . Subsequently, the LL band undergoes further decomposition using the FA-MVEMD algorithm into K levels. The resulting K -level Intrinsic Mode Function (IMF), along with the residual and HH band of DWT, constitutes the ensemble image set. These ensemble images are then utilized for training the CNN model.

7.4 Implementation

The algorithm employs a novel approach of area specific and the sub image based neighbor gradient features retrieval to enhance identification accuracy. It begins by segmenting the periocular region into 4 sub-region: eyebrows, eye-corner regions, top and bottom eye fold region. Different feature extraction algorithms, such as KAZE for upper eye fold and HOG for eyebrow and eye corner regions, are utilized to capture diverse characteristics.

Additionally, the algorithm estimate size of eyebrows by analyzing distances from N point on eyebrows regions to eye-side mid-point. This eyebrow shape and size feature includes breadth and length measure, providing valuable information for effective recognition. A sub-image-based neighbor's gradient (SING) feature retrieval is proposed for increased robustness to rotation. The extracted feature are then trained using Naïve Bayes classifier.

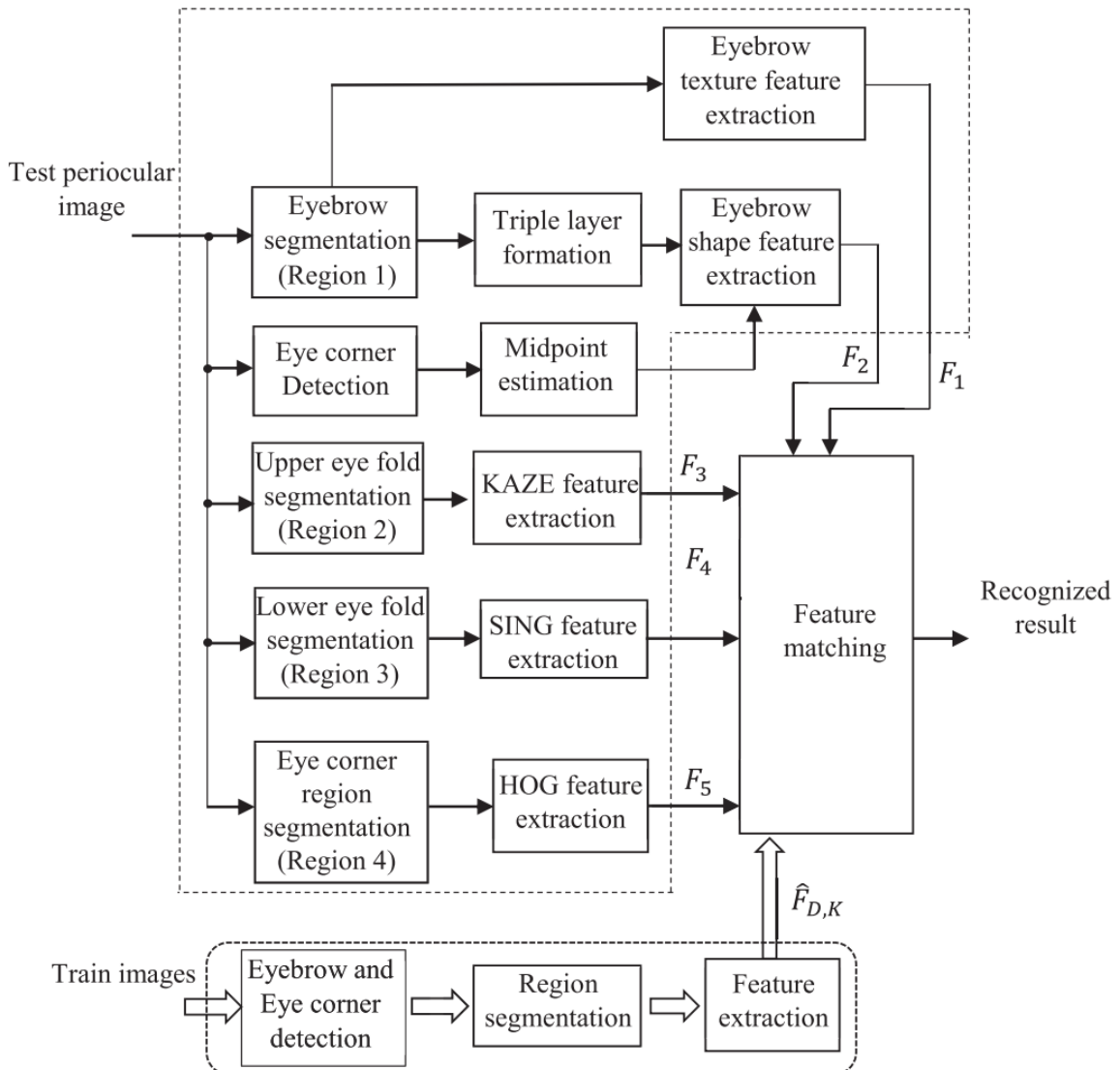


Figure 7.4.1 – Flow diagram

7.5 Evaluation

The evaluation will be achieved using metrics such as rank-2, rank-1, AUC, and EER for dataset UBPIr, AR, and CASIA-Iris datasets.

The proposed metrics for evaluation are:

- **Equal error rate (EER)** - The Error Equal Rate is a point on the Receiver Operating Characteristic (ROC) curve where the false acceptance rate (FAR) is equal's to the false rejection rate (FRR).

- **Area Under the Curve (AUC)** - The region below the ROC Curve quantifies the overall performances of a binary classification model across various decision thresholds.
- **Rank-1 Recognition Accuracy** – Rank-1 accuracy measures the percentage of cases where the correct match is ranked first among all possible matches.
- **Rank-5 Recognition Accuracy** – Rank-5 accuracy is similar to Rank-1, but it considers whether the correct match is present within the top 5 ranked choices.

8. Required Resources

8.1 Hardware Requirements

For the successful completion of this research, certain hardware prerequisites need to be satisfied:

- A laptop or desktop computer equipped with internet connectivity, capable of browsing, document creation, and code compilation/execution is essential for this research.
- RAM (Random Access Memory): A minimum of 16GB RAM is recommended.

8.2 Software Requirements

For the successful completion of this research, certain software prerequisites need to be satisfied:

- Web-browser
- Coding IDE Python 3.7+
- PIL (Pillow)
- Deep Learning libraries such as TensorFlow, PyTorch and Keras (which can be integrated with TensorFlow)
- Libraries required: Pandas, Numpy, OpenCV, etc.

8.3 Dataset Requirements

To conduct this research, specific criteria for the dataset must be fulfilled:

- **UBIPr (Ubiquitous and Robust Iris Recognition Dataset):** The dataset may include images of irises captured in different scenarios, such as indoor and outdoor environments, varying lighting conditions, and at different distances.
- **CASIA-Iris-Distance:** The dataset likely contains iris images captured at different distances, allowing researchers to assess the performance of iris recognition systems under such conditions.
- **AR Dataset:** The dataset may include images of faces with variations in pose, illumination, and facial expressions.

9. Research Plan

9.1 Gantt Chart

Generating Stories by Prompting Pre-trained Language Models

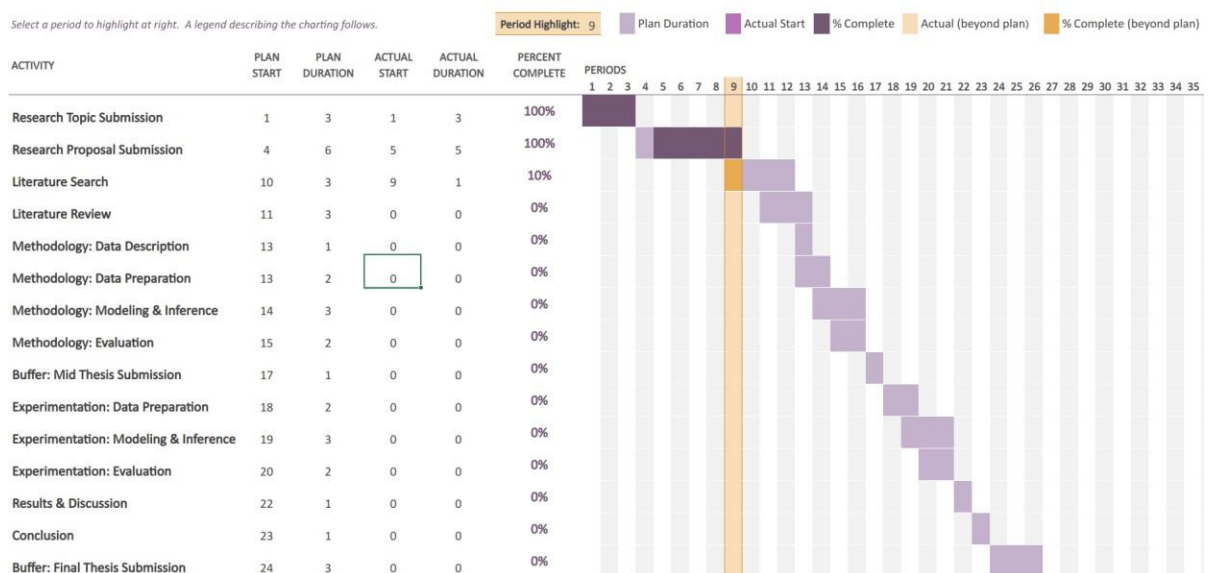


Figure 9.1.1 – Gantt Chart

Note: 1 Interval = 1 Calendar Week

9.2 Risk Mitigation and Contingency Plan

The possible challenges to the successful completion of the thesis and the corresponding backup plans are outlined as follows:

Table 9.2.1 – Risk and Contingency

Risk	Contingency
If the candidate faces health issues or personal challenges that impede research progress, it may impact the project timelines.	In project management, incorporate a contingency period into the plan. Notify the University/Upgrad administration and request an extension.
Unforeseen technical issues may arise during the development of the face recognition model.	Ensure rigorous data validation, anonymization, and compliance with ethical guidelines. Have alternative data sources ready.

References

- Agrawal, E., & Christopher, J. (2020). Emotion Recognition from Periocular Features. *Communications in Computer and Information Science, 1240 CCIS*. https://doi.org/10.1007/978-981-15-6315-7_16
- Agrawal, E., Christopher, J., & Arunachalam, V. (2021). Emotion recognition through voting on expressions in multiple facial regions. *ICAART 2021 - Proceedings of the 13th International Conference on Agents and Artificial Intelligence, 2*. <https://doi.org/10.5220/0010306810381045>
- Ahonen, T., Hadid, A., & Pietikäinen, M. (2006). Face description with local binary patterns: Application to face recognition. *IEEE Transactions on Pattern Analysis and Machine Intelligence, 28*(12). <https://doi.org/10.1109/TPAMI.2006.244>
- Alahmadi, A., Hussain, M., Aboalsamh, H., & Azmi, A. (2020). ConvSRC: SmartPhone-based periocular recognition using deep convolutional neural network and sparsity augmented collaborative representation. *Journal of Intelligent and Fuzzy Systems, 38*(3). <https://doi.org/10.3233/JIFS-190834>
- Almadan, A., & Rattani, A. (2021). Compact CNN Models for On-device Ocular-based User Recognition in Mobile Devices. *2021 IEEE Symposium Series on Computational Intelligence, SSCI 2021 - Proceedings*. <https://doi.org/10.1109/SSCI50451.2021.9660033>
- Alonso-Fernandez, F., Diaz, K. H., Ramis, S., Perales, F. J., & Bigun, J. (2020). Soft-Biometrics Estimation In the Era of Facial Masks. *Lecture Notes in Informatics (LNI), Proceedings - Series of the Gesellschaft Fur Informatik (GI), P-306*.
- Alonso-Fernandez, F., Mikaelyan, A., & Bigun, J. (2015). Comparison and fusion of multiple iris and periocular matchers using near-infrared and visible images. *3rd International Workshop on Biometrics and Forensics, IWBF 2015*. <https://doi.org/10.1109/TWBF.2015.7110234>
- Alonso-Fernandez, F., Raja, K. B., Raghavendra, R., Busch, C., Bigun, J., Vera-Rodriguez, R., & Fierrez, J. (2022). Cross-sensor periocular biometrics in a global pandemic: Comparative benchmark and novel multialgorithmic approach. *Information Fusion, 83–84*. <https://doi.org/10.1016/j.inffus.2022.03.008>
- Ambika, D. R., Radhika, K. R., & Seshachalam, D. (2020). Identity verification using biometrics in smart-cities. In *EAI/Springer Innovations in Communication and Computing*. https://doi.org/10.1007/978-3-030-14718-1_9
- Bakshi, S., Sa, P. K., & Majhi, B. (2015a). A novel phase-intensive local pattern for periocular recognition under visible spectrum. *Biocybernetics and Biomedical Engineering, 35*(1). <https://doi.org/10.1016/j.bbe.2014.05.003>
- Bakshi, S., Sa, P. K., & Majhi, B. (2015b). Phase Intensive Global Pattern for periocular recognition. *11th IEEE India Conference: Emerging Trends and Innovation in Technology, INDICON 2014*. <https://doi.org/10.1109/INDICON.2014.7030362>
- Bakshi, S., Sa, P. K., Wang, H., Barpanda, S. S., & Majhi, B. (2018). Fast periocular authentication in handheld devices with reduced phase intensive local pattern. *Multimedia Tools and Applications, 77*(14). <https://doi.org/10.1007/s11042-017-4965-6>
- Barcellos, W., & Gonzaga, A. (2022). *Periocular authentication in smartphones applying uLBP descriptor on CNN Feature Maps*. <https://doi.org/10.5753/wvc.2021.18890>
- Behera, S. S., & Puhan, N. B. (2023). Dual-spectrum network: exploring deep visual feature to attribute mapping for cross-spectral periocular recognition. *Journal of Electronic Imaging, 32*(03). <https://doi.org/10.1117/1.jei.32.3.033031>
- Bharadwaj, S., Bhatt, H. S., Vatsa, M., & Singh, R. (2010). Periocular biometrics: When Iris recognition fails. *IEEE 4th International Conference on Biometrics: Theory, Applications and Systems, BTAS 2010*. <https://doi.org/10.1109/BTAS.2010.5634498>
- Boutros, F., Damer, N., Fang, M., Raja, K., Kirchbuchner, F., & Kuijper, A. (2020). Compact Models for Periocular Verification Through Knowledge Distillation. *Lecture Notes in Informatics (LNI), Proceedings - Series of the Gesellschaft Fur Informatik (GI), P-306*.
- Boutros, F., Damer, N., Raja, K., Kirchbuchner, F., & Kuijper, A. (2022). Template-Driven Knowledge Distillation for Compact and Accurate Periocular Biometrics Deep-Learning Models. *Sensors, 22*(5). <https://doi.org/10.3390/s22051921>
- Boutros, F., Damer, N., Raja, K., Ramachandra, R., Kirchbuchner, F., & Kuijper, A. (2020a). Fusing iris

- and periocular region for user verification in head mounted displays. *Proceedings of 2020 23rd International Conference on Information Fusion, FUSION 2020*.
<https://doi.org/10.23919/FUSION45008.2020.9190282>
- Boutros, F., Damer, N., Raja, K., Ramachandra, R., Kirchbuchner, F., & Kuijper, A. (2020b). Iris and periocular biometrics for head mounted displays: Segmentation, recognition, and synthetic data generation. *Image and Vision Computing*, 104. <https://doi.org/10.1016/j.imavis.2020.104007>
- Boutros, F., Damer, N., Raja, K., Ramachandra, R., Kirchbuchner, F., & Kuijper, A. (2020c). Periocular Biometrics in Head-Mounted Displays: A Sample Selection Approach for Better Recognition. *2020 8th International Workshop on Biometrics and Forensics, IWBF 2020 - Proceedings*.
<https://doi.org/10.1109/IWBF49977.2020.9107939>
- Cascone, L. (2021). Periocular features as a window on cognitive processing: From memory to understanding the semantic complexity of an image. *BioSMART 2021 - Proceedings: 4th International Conference on Bio-Engineering for Smart Technologies*.
<https://doi.org/10.1109/BioSMART54244.2021.9677786>
- Chen, H., Gao, M., Ricanek, K., Xu, W., & Fang, B. (2017). A Novel Race Classification Method Based on Periocular Features Fusion. *International Journal of Pattern Recognition and Artificial Intelligence*, 31(8). <https://doi.org/10.1142/S0218001417500264>
- Chen, Y., Wu, W., Xu, L., & Guo, S. (2023). Iris-periocular features-fused non-collaborative authentication. *Journal of Image and Graphics*, 28(5). <https://doi.org/10.11834/jig.220649>
- Cho, S. R., Nam, G. P., Shin, K. Y., Nguyen, D. T., Pham, T. D., Lee, E. C., & Park, K. R. (2017). Periocular-based biometrics robust to eye rotation based on polar coordinates. *Multimedia Tools and Applications*, 76(9). <https://doi.org/10.1007/s11042-015-3052-0>
- Dadi, H. S., & Mohan Pillutla, G. K. (2016). Improved Face Recognition Rate Using HOG Features and SVM Classifier. *IOSR Journal of Electronics and Communication Engineering*, 11(04).
<https://doi.org/10.9790/2834-1104013444>
- da Silva, E. P., Fambrini, F., & Saito, J. H. (2020). Convolutional Neural Networks and Periocular Region Image Recognition. *Communications in Computer and Information Science*, 1332.
https://doi.org/10.1007/978-3-030-63820-7_36
- Das, S., Kharbanda, K., M, S., Raman, R., & D, E. D. (2021). Deep learning architecture based on segmented fundus image features for classification of diabetic retinopathy. *Biomedical Signal Processing and Control*, 68. <https://doi.org/10.1016/j.bspc.2021.102600>
- Gangwar, A., & Joshi, A. (2016). DeepIrisNet: Deep iris representation with applications in iris recognition and cross-sensor iris recognition. *Proceedings - International Conference on Image Processing, ICIP, 2016-August*. <https://doi.org/10.1109/ICIP.2016.7532769>
- Han, N. Y., Seong, S. W., Ryu, J., Hwang, H., Joung, J., Lee, J., & Lee, E. C. (2021). Authentication of Facial Images with Masks Using Periocular Biometrics. *Lecture Notes in Computer Science (Including Subseries Lecture Notes in Artificial Intelligence and Lecture Notes in Bioinformatics)*, 12616 LNCS. https://doi.org/10.1007/978-3-030-68452-5_34
- Hernandez-Diaz, K., Alonso-Fernandez, F., & Bigun, J. (2020). Cross-spectral periocular recognition with conditional adversarial networks. *IJCB 2020 - IEEE/IAPR International Joint Conference on Biometrics*. <https://doi.org/10.1109/IJCB48548.2020.9304899>
- Hernandez V, J. J., Dejournett, R., Nannuri, U., Gwyn, T., Yuan, X., & Roy, K. (2022). Face Authentication from Masked Face Images Using Deep Learning on Periocular Biometrics. *Lecture Notes in Computer Science (Including Subseries Lecture Notes in Artificial Intelligence and Lecture Notes in Bioinformatics)*, 13343 LNAI. https://doi.org/10.1007/978-3-031-08530-7_38
- Hollingsworth, K., Clark, S., Thompson, J., Flynn, P. J., & Bowyer, K. W. (2013). Eyebrow segmentation using active shape models. *Biometric and Surveillance Technology for Human and Activity Identification X*, 8712. <https://doi.org/10.1117/12.2017646>
- Ipe, V. M., & Thomas, T. (2021). Periocular Recognition Under Unconstrained Image Capture Distances. *Communications in Computer and Information Science*, 1365. https://doi.org/10.1007/978-981-16-0425-6_14
- Joshi, A., Gangwar, A., Sharma, R., Singh, A., & Saquib, Z. (2014). Periocular recognition based on Gabor and Parzen PNN. *2014 IEEE International Conference on Image Processing, ICIP 2014*.
<https://doi.org/10.1109/ICIP.2014.7026008>
- Kaur, B. (2023). Iris and Periocular Recognition using Shape Descriptors and Local Invariant Features.

- Kaur, P., & Kumar, N. (2023). Enhanced Biometric Cryptosystem Using Ear & Iris Modality Based On Binary Robust Independent Elementary Feature. *2023 6th International Conference on Information Systems and Computer Networks, ISCON 2023*.
<https://doi.org/10.1109/ISCON57294.2023.10112197>
- Khellat-Kihel, S., Muhammad, J., Sun, Z., & Tistarelli, M. (2022). Gender and ethnicity recognition based on visual attention-driven deep architectures. *Journal of Visual Communication and Image Representation*, 88. <https://doi.org/10.1016/j.jvcir.2022.103627>
- Kirchgasser, S., Debiasi, L., Schraml, R., Hofbauer, H., Uhl, A., Boyle, J., & Ferryman, J. (2020). Template Protection on Multiple Facial Biometrics in the Signal Domain under Visible and Near-Infrared Light. *2020 8th International Workshop on Biometrics and Forensics, IWBF 2020 - Proceedings*. <https://doi.org/10.1109/IWBF49977.2020.9107964>
- K. M, S. K. (2021). Recognition of Masked Face Using Convolutional Neural Network Algorithm. *International Journal for Research in Applied Science and Engineering Technology*, 9(VII).
<https://doi.org/10.22214/ijraset.2021.37051>
- Kumar, G., Bakshi, S., Sa, P. K., & Majhi, B. (2021). Non-overlapped blockwise interpolated local binary pattern as periocular feature. *Multimedia Tools and Applications*, 80(11).
<https://doi.org/10.1007/s11042-020-08708-w>
- Kumari, P., & R, S. K. (2020). Periocular Biometrics for Non-ideal Images Using Deep Convolutional Neural Networks. *Advances in Intelligent Systems and Computing*, 1034.
https://doi.org/10.1007/978-981-15-1084-7_15
- Kumari, P., & Seeja, K. R. (2020). Periocular Biometrics for non-ideal images: With off-the-shelf Deep CNN & Transfer Learning approach. *Procedia Computer Science*, 167.
<https://doi.org/10.1016/j.procs.2020.03.234>
- Kumari, P., & Seeja, K. R. (2021). A novel periocular biometrics solution for authentication during Covid-19 pandemic situation. *Journal of Ambient Intelligence and Humanized Computing*, 12(11).
<https://doi.org/10.1007/s12652-020-02814-1>
- Kumari, P., & Seeja, K. R. (2022). Periocular biometrics: A survey. In *Journal of King Saud University - Computer and Information Sciences* (Vol. 34, Issue 4). <https://doi.org/10.1016/j.jksuci.2019.06.003>
- Lee, M. B., Kang, J. K., Yoon, H. S., & Park, K. R. (2021). Enhanced Iris Recognition Method by Generative Adversarial Network-Based Image Reconstruction. *IEEE Access*, 9.
<https://doi.org/10.1109/ACCESS.2021.3050788>
- Lee, Y. W., Kim, J. S., & Park, K. R. (2022). Ocular Biometrics with Low-Resolution Images Based on Ocular Super-Resolution CycleGAN. *Mathematics*, 10(20). <https://doi.org/10.3390/math10203818>
- Le, T. H. N., Prabhu, U., & Savvides, M. (2014). A novel eyebrow segmentation and eyebrow shape-based identification. *IJCB 2014 - 2014 IEEE/IAPR International Joint Conference on Biometrics*.
<https://doi.org/10.1109/BTAS.2014.6996262>
- Lionnie, R., Apronio, C., & Gunawan, D. (2022). Eyes versus Eyebrows: A Comprehensive Evaluation Using the Multiscale Analysis and Curvature-Based Combination Methods in Partial Face Recognition. *Algorithms*, 15(6). <https://doi.org/10.3390/a15060208>
- Liu, J., Hu, D., Ni, M., Zou, Y., Gu, Y., Han, Z., Li, J., He, Y., Zhang, Z., & Xu, X. (2022). Monolithic RGB-NIR Perovskite Photodetector for Fused Multispectral Sensing and Imaging. *Journal of Physical Chemistry Letters*, 13(16). <https://doi.org/10.1021/acs.jpclett.2c00701>
- Lohith, M. S., Manjunath, Y. S. K., & Eshwarappa, M. N. (2023). Multimodal Biometric Person Authentication Using Face, Ear and Periocular Region Based on Convolution Neural Networks. *International Journal of Image and Graphics*, 23(2). <https://doi.org/10.1142/S0219467823500195>
- Luo, Z., Li, J., & Zhu, Y. (2021). A Deep Feature Fusion Network Based on Multiple Attention Mechanisms for Joint Iris-Periocular Biometric Recognition. *IEEE Signal Processing Letters*, 28.
<https://doi.org/10.1109/LSP.2021.3079850>
- Ma, J., Zhao, J., Tian, J., Tu, Z., & Yuille, A. L. (2013). Robust estimation of nonrigid transformation for point set registration. *Proceedings of the IEEE Computer Society Conference on Computer Vision and Pattern Recognition*. <https://doi.org/10.1109/CVPR.2013.279>
- Mon, C. S., Hussin, A. A. A., Sin, T. K., & Mon, C. S. (2020). Analyzing the periocular biometric-based access control systems. *Journal of Physics: Conference Series*, 1529(3).

- <https://doi.org/10.1088/1742-6596/1529/3/032024>
- Morris, C., Abegaz, T. T., & Payne, B. R. (2022). Effectiveness of Periocular Biometric Recognition Under Face Mask Restrictions. In *Breakthroughs in Digital Biometrics and Forensics*.
https://doi.org/10.1007/978-3-031-10706-1_11
- Nascimeno, L. F., & Souza, J. M. de. (2023). *Deep Learning Utilized for Person Recognition Based on the Biometric Features of the Periocular Region*. <https://doi.org/10.5753/sibgrapi.est.2022.23270>
- Ogawa, K., & Kameyama, K. (2021). Adaptive Selection of Classifiers for Person Recognition by Iris Pattern and Periocular Image. *Lecture Notes in Computer Science (Including Subseries Lecture Notes in Artificial Intelligence and Lecture Notes in Bioinformatics)*, 13111 LNCS.
https://doi.org/10.1007/978-3-030-92273-3_54
- Park, S., Moon, B., Ko, S., Yu, S., & Paik, J. (2017). Low-light image restoration using bright channel prior-based variational Retinex model. *Eurasip Journal on Image and Video Processing*, 2017(1).
<https://doi.org/10.1186/s13640-017-0192-3>
- Phillips, S., & Karakaya, M. (2022). Effects of Distance and Gaze Angle on CNN-based Standoff Iris Recognition. *Conference Proceedings - IEEE SOUTHEASTCON, 2022-March*.
<https://doi.org/10.1109/SoutheastCon48659.2022.9764014>
- Prasanth, N., Kiran, C. U. S., Nethi, S., Ketineni, T., Srinivasu, N., & Pradeepini, G. (2023). Fusion of Iris and Periocular Biometrics Authentication using CNN. *Proceedings - 7th International Conference on Computing Methodologies and Communication, ICCMC 2023*.
<https://doi.org/10.1109/ICCMC56507.2023.10083982>
- Rahmad, C., Asmara, R. A., Putra, D. R. H., Dharma, I., Darmono, H., & Muhiqqin, I. (2020). Comparison of Viola-Jones Haar Cascade Classifier and Histogram of Oriented Gradients (HOG) for face detection. *IOP Conference Series: Materials Science and Engineering*, 732(1).
<https://doi.org/10.1088/1757-899X/732/1/012038>
- Ramachandra, S., & Ramachandran, S. (2022). Region specific and subimage based neighbour gradient feature extraction for robust periocular recognition. *Journal of King Saud University - Computer and Information Sciences*, 34(10). <https://doi.org/10.1016/j.jksuci.2022.07.013>
- Ramaraj, P. (2021). A Neural Network in Convolution with Constant Error Carousel Based Long Short Term Memory for Better Face Recognition. *Turkish Journal of Computer and Mathematics Education (TURCOMAT)*, 12(2). <https://doi.org/10.1776/turcomat.v12i2.1808>
- Rao, M. G., Priyanka, H., Pawar, S., Reddy, K. H. K., & Divakarla, U. (2022). Novel approach of Using Periocular and Iris Biometric Recognition in the Authentication of ITS. *2022 4th International Conference on Cognitive Computing and Information Processing, CCIP 2022*.
<https://doi.org/10.1109/CCIP57447.2022.10058656>
- Reddy, N., & Derakhshani, R. (2020). Emotion Detection using Periocular Region: A Cross-Dataset Study. *Proceedings of the International Joint Conference on Neural Networks*.
<https://doi.org/10.1109/IJCNN48605.2020.9207542>
- Rot, P., Vitek, M., Grm, K., Emeršič, Ž., Peer, P., & Štruc, V. (2020). Deep Sclera Segmentation and Recognition. In *Advances in Computer Vision and Pattern Recognition*.
https://doi.org/10.1007/978-3-030-27731-4_13
- Saad Shakeel, M., & Lam, K. M. (2022). Deep low-rank feature learning and encoding for cross-age face recognition. *Journal of Visual Communication and Image Representation*, 82.
<https://doi.org/10.1016/j.jvcir.2021.103423>
- Seha, S. N. A., Hatzinakos, D., Zandi, A. S., & Comeau, F. J. E. (2021). Improving eye movement biometrics in low frame rate eye-tracking devices using periocular and eye blinking features. *Image and Vision Computing*, 108. <https://doi.org/10.1016/j.imavis.2021.104124>
- Shao, H., Li, J., Zhang, J., Yu, H., & Sun, J. (2021). Eye-based Recognition for User Identification on Mobile Devices. *ACM Transactions on Multimedia Computing, Communications and Applications*, 16(4). <https://doi.org/10.1145/3399659>
- Srivika, S., Gayathri, L., Nivetha, B., Sri Devi, N., & Sujatha, R. (2023). Biometric Verification using Periocular Features based on Convolutional Neural Network. *2nd International Conference on Sustainable Computing and Data Communication Systems, ICSCDS 2023 - Proceedings*.
<https://doi.org/10.1109/ICSCDS56580.2023.10104783>
- Sujanthy, S., Bowshika, A., Dharaneesh, S. K., & Jai Sivadharsini, A. (2023). Iris Liveness Detection using Deep Learning Networks. *7th International Conference on Trends in Electronics and*

- Informatics, ICOEI 2023 - Proceedings.* <https://doi.org/10.1109/ICOEI56765.2023.10125665>
- Toledo Ferraz, C., Barcellos, W., Pereira Junior, O., Trevisan Negri Borges, T., Garcia Manzato, M., Gonzaga, A., & Hiroki Saito, J. (2021). A comparison among keyframe extraction techniques for CNN classification based on video periocular images. *Multimedia Tools and Applications*, 80(8). <https://doi.org/10.1007/s11042-020-10384-9>
- Tripathi, R. K., & Jalal, A. S. (2021). Novel local feature extraction for age invariant face recognition. *Expert Systems with Applications*, 175. <https://doi.org/10.1016/j.eswa.2021.114786>
- Tripathi, R. K., & Jalal, A. S. (2022). A robust approach based on local feature extraction for age invariant face recognition. *Multimedia Tools and Applications*, 81(15). <https://doi.org/10.1007/s11042-022-12783-6>
- Umer, S., Sardar, A., Rout, R. K., Tanveer, M., & Razzak, I. (2023). IoT-Enabled Multimodal Biometric Recognition System in Secure Environment. *IEEE Internet of Things Journal*. <https://doi.org/10.1109/JIOT.2023.3299465>
- Vitek, M., Rot, P., Štruc, V., & Peer, P. (2020). A comprehensive investigation into sclera biometrics: a novel dataset and performance study. *Neural Computing and Applications*, 32(24). <https://doi.org/10.1007/s00521-020-04782-1>
- Vyas, R., Kanumuri, T., Sheoran, G., & Dubey, P. (2020). Towards ocular recognition through local image descriptors. *Communications in Computer and Information Science*, 1147 CCIS. https://doi.org/10.1007/978-981-15-4015-8_1
- Wang, Y., Lei, S., Li, Y., Liu, B., & Zuo, H. (2022). Score Level Fusion for Iris and Periocular Biometrics Recognition Based on Deep Learning. *International Journal of Advanced Network, Monitoring and Controls*, 7(4). <https://doi.org/10.2478/ijanmc-2022-0033>
- Wazirali, R., & Ahmed, R. (2022). Hybrid feature extractions and CNN for enhanced periocular identification during Covid-19. *Computer Systems Science and Engineering*, 41(1). <https://doi.org/10.32604/csse.2022.020504>
- Zabin, A., & Bourlai, T. (2020). A Deep Learning Based Approach to Iris Sensor Identification. *Proceedings of the 2020 IEEE/ACM International Conference on Advances in Social Networks Analysis and Mining, ASONAM 2020*. <https://doi.org/10.1109/ASONAM49781.2020.9381354>
- Zanlorensi, L. A., Lucio, D. R., de Souza Britto Junior, A., Proença, H., & Menotti, D. (2020). Deep representations for cross-spectral ocular biometrics. *IET Biometrics*, 9(2). <https://doi.org/10.1049/iet-bmt.2019.0116>

